NUMERICAL INVESTIGATION OF SINKHOLE STABILITY IN UNDRAINED CLAY

A thesis submitted by

MOHAMMAD MIRZA HASSAN, BEng

For the award of

Master of Engineering (Research)

2019

Abstract

The stability of the soil that overlies a cavity is often of concern when it comes to the risk of sinkhole occurrence. Current sinkhole studies have been centred on the use of geophysical techniques to detect underground cavity sizes and associated depths. With measured information, it is possible to theoretically predict the extent of ground surface collapse.

The aim of the research is to numerically study the soil stability and its associated ground surface failure extent of an undrained cohesive cover over a collapsible sinkhole. The shear strength reduction method is utilised to explore two- and three-dimensional failure mechanisms of a trapdoor by using the finite difference programs. The problem solution is formulated by using two popular methods in geotechnical engineering i.e. Taylor's stability chart method and Broms and Bennerrmark's stability number. Stability results are compared with those using finite element limit analysis and other published literatures. Several practical examples are provided to demonstrate the use of design charts and tables.

Current study of soil arching development and ground surface failure extent in three-dimensional spaces provide useful engineering information, which may assist in decision making by practical engineers. Together with the use of geophysical tools, an early warning system shall be developed in the future to save lives and prevent billions in property losses.

Certification of Thesis

This Thesis is entirely the work of Mohammad Mirza Hassan except where otherwise acknowledged. The work is original and has not previously been submitted for any other award, except where acknowledged.

Principal Supervisor: Dr Jim Shiau

Associate Supervisor: Dr Ali Mirzaghorbanali

Student and supervisors signatures of endorsement are held at the University.

Acknowledgements

I am thankful for the path I have taken, and more importantly for the people who made this journey possible. The Research Training Scheme (RTS) provided by Australian Commonwealth Government through USQ is much appreciated.

First and foremost, I would like to thank my supervisor, Dr Jim Shaiu, for his continuous technical expertise and support, encouragement, availability and enthusiasm. The greatest challenges offered by Dr. Shiau in other roles such as teaching assistance, assistance in conference organisation, and the recent position as a research assistant for an industry project are much appreciated. The *FISH* programs used throughout this thesis is Dr Shaiu's development which has been modified as required for this study. This thesis would not have been possible without all the above support.

Secondly I would like to thank all my colleges at Dr. Shiau's Underground Tunnelling Research Laboratory at USQ. I am thankful to Mathew Sams, Fadhil Al-Asadi, Ji-Sung Lee, Fan Lin, and Xiang Yang for their friendship during this journey. I am also thankful to my co-supervisor Dr. Ali Mirzaghorbanali for his support whenever needed.

Last but not least, I would like to thank my family for their much needed encouragement and moral support. To my wife and my parents, thank you for providing me with just enough crazy to make me believe I can do anything and the confidence to do so with my head held high. To mum and dad, I am grateful for supportive parents which have been positively in my side through this period. I could never have stayed the course were it not for the love and support of my wife. Bahar, you never failed me when I needed the support. It is to my parents, wife and to my children Daran and Diana that I dedicate this thesis.

TABLE OF CONTENTS

List of Figures

List of Tables

List of Notation

The following is a list of the more important symbols used in text.

c	Soil cohesion
E	Surface failure extent
FDM	Finite difference method
$FELA$	Finite element limit analysis
FoS	Factor of Safety
H	Trapdoor height
L	Trapdoor length
N	Stability number
N_C	Critical stability number
OPR	Overburden pressure ratio
S_{max}	Maximum surface settlement
S_x	Surface Settlement
SPR	Supporting pressure ratio
SSR	Shear strength ratio
$SSRM$	Shear strength reduction method
$S_{u,}$	Undrained shear strength
W	Trapdoor opening width
x	Horizontal distance from the tunnel centreline
β	slope angle
γ	Unit weight of the soil
θ	Failure angle
σ_s	Soil surcharge load,
σ_t	Supporting pressure;
σ_v	Vertical stress
ϕ	Friction angle
ϕ'_u	Effective stress friction angle

1. INTRODUCTION

1.1. Background

There seems to be an increase in sinkhole occurrences across the world in recent years, which has led researchers to study the issue and investigate possible solutions to minimise fatalities and economic impact due to sinkholes.

Sinkholes are defined by Augurd et al. (2003) as depression at the soil surface due to a change in the soil or rock beneath. Sinkholes can form naturally or artificially (manmade) and present in varying shapes and sizes , such as a couple of metres in a suburban backyard or covering distances in kilometres, like the Qattara Depression in Egypt. However, regardless of the shape and size, they can be deadly and destructive (Olick 2013).

There are many causes that trigger a sinkhole formation. These may include limestone dissolution (Gutierrez et al. 2014, Poyiadji et al. 2010, Heydari et al. 2011), tensile failure of soil (Tharp 2002), and underground water system leakage (Guarino et al. 2018, Oh et al. 2015). Drumm et al. (2009) suggest that sinkholes are more common in karst terrain. The karst landscape develops in areas where the bedrock comprises a high volume of soluble elements, such as gypsum, limestone and dolomite. Figure 1.1 shows the distribution of karst around the world. Note that the map also represents potential sinkhole areas.

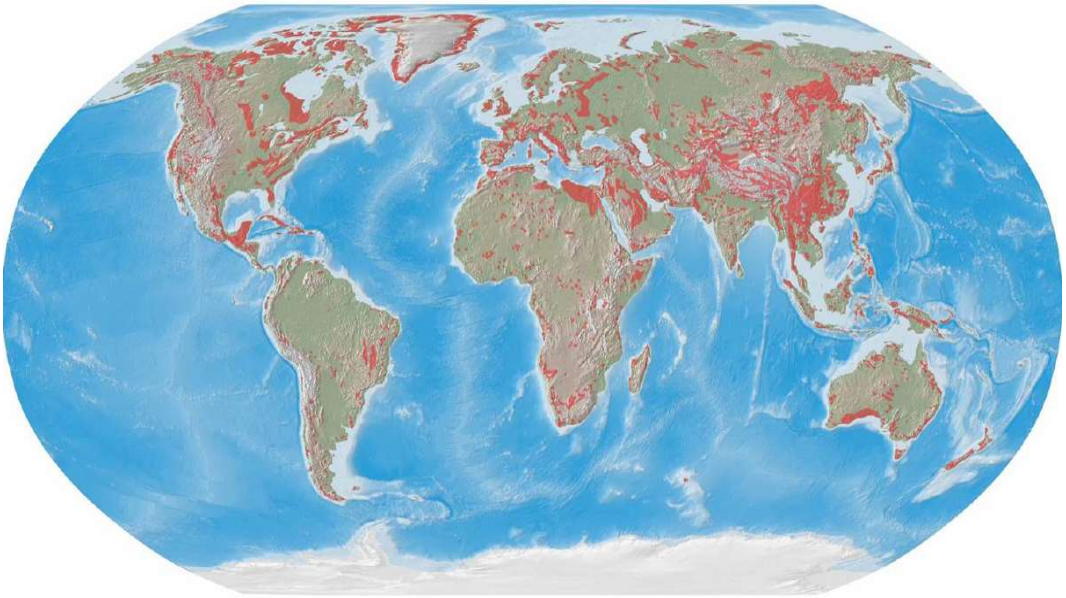

Figure 1. 1 Distribution of the karst around the world (Ford & Williams 2013)

The natural process of change in the piezometric level of underground water, due to the drought or percolation of surface water would cause the erosion in limestone as shown in figure 1.2. Erosion forms a void in limestone and can cause a failure in the cavity due to overburdened soil pressure or surcharge load, which may apply externally on the surface of the soil.

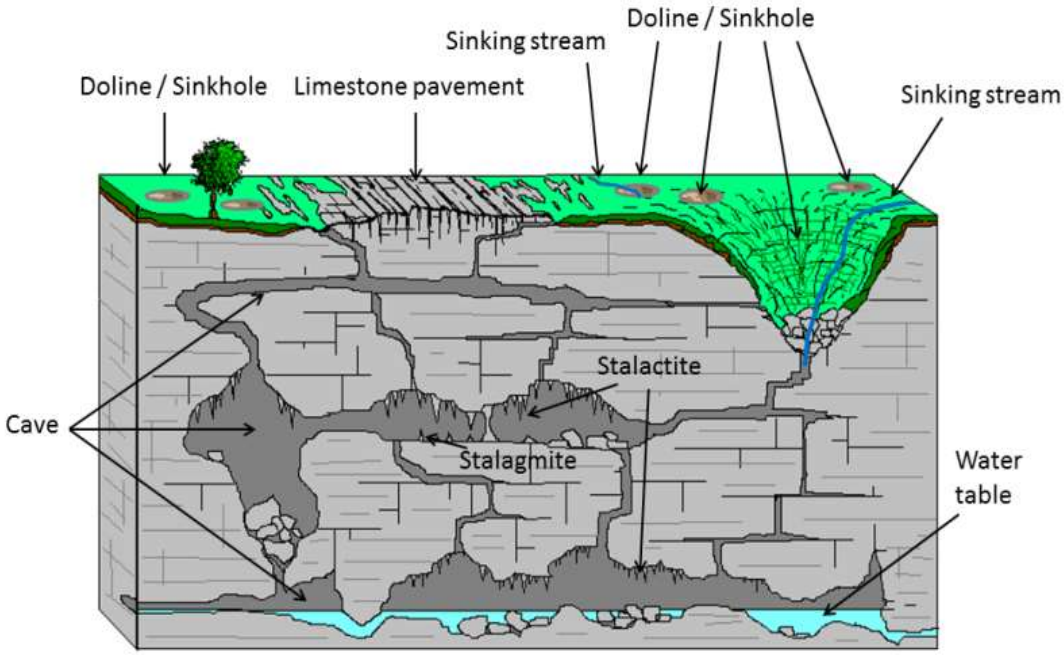

Figure 1. 2 Natural process of sinkhole formation (Geological survey, 2018)

The Umpherston sinkhole, shown in figure 1.3, located in Mount Gambier in SA, is an example of a naturally made sinkhole. The famous sinkhole, called cave garden, became a natural beauty and has become a big tourist attraction in the city despite the possibility of further evolution. That region of the south coast of South Australia where Mount Gambier is located is principally covered in limestone. When carbon dioxide dissolves into surface water, it produces light acid rain.

Figure 1. 3 Mount Gambier Sinkhole (Point 2017)

Scientists believe that the combination of precipitation of acid rain on the region and high natural permeability and porosity of the limestone created a cavity and a gradual increase in the size of the cavity caused the ceiling rock to fall beneath and create the famous Umpherston sinkhole (Point 2017).

Satarugsa (2011) suggests that human activities can activate or accelerate sinkhole failure. Activities and interventions, such as mining, tunnelling, extracting oil, gas, broken pipes, runoff drainage and over pumping underground water are types of activity which could trigger a collapse. Once a cavity occurs in soil, the overburden pressure can cause the gradual collapse of the ground. The Fukuoka sinkhole is an example of a human made sinkhole. This giant sinkhole occurred in the middle of

the business district in the Japanese city of Fukuoka. Experts suggested that the sinkhole commenced by nearby construction of a subway tunnel, which caused the instability of the soil and resulted in the collapse of the overburdened soil. Figure 1.4 shows a bird-eye view of Fukuoka sinkhole (Levy 2016).

Figure 1. 4 Fukuoka sinkhole (Levy 2016)

There has been an increase in sinkhole occurrences over the past two decades, particularly in urban areas. Human activities, such as mining, piping and underground construction have contributed to this increase in sinkhole occurrences. Although the exact number of all sinkholes occurrence around the world has not been stated, the US geological survey organisation reported that: 'Sinkhole damages over the last 15 years cost on average at least $300 million per year. Since there is no national tracking of sinkhole damage costs, this estimate is probably much lower than the actual cost' (USGS 2018a).

Therefore, the catastrophic impact of a sinkhole persuades scientists and researchers to study the characteristics and failure mechanisms to reduce the damage caused by sinkholes.

Types of Sinkholes

Irrespective of the formation type, sinkhole propagation is dominated by the characteristic of the rock beneath and overlying soil. Therefore, geologists classify sinkholes into three main groups (USGS 2018b).

Dissolution sinkholes

Dissolution sinkholes form naturally, where there is a process of change in the piezometric level of underground water due to drought or percolation of the surface water causing erosion in limestone as shown in figure 1.5.

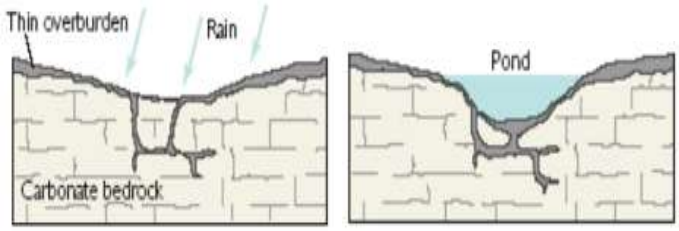

Figure 1. 5 Ideal dissolute sinkhole formation (USGS 2018b)

Erosion forms a void in limestone and it can cause the failure of a cavity due to the overburden of soil pressure or surcharge load, which may apply externally on the surface of the soil.

Cover subsidence sinkholes

Cover subsidence sinkholes as shown in figure 1.6, progress steadily where the covering sediment is permeable and contains sand. In areas where a thick layer of clay covers the carbonate rocks, the cover subsidence sinkholes are either uncommon or very small.

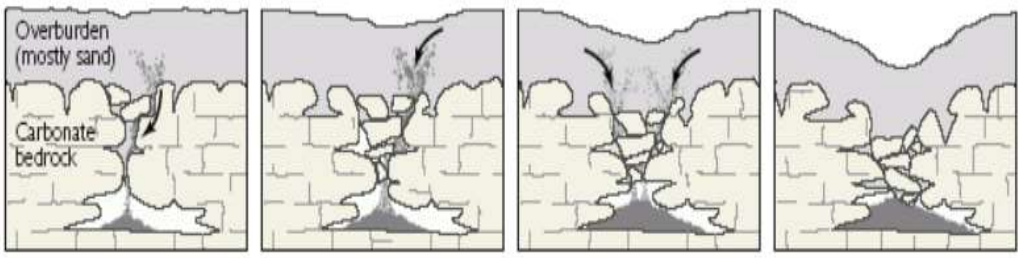

Figure 1. 6 Ideal cover subsidence sinkhole formation (USGS 2018b)

Cover collapse sinkholes

The most catastrophic type of sinkhole is a cover collapse sinkhole, where the failure is sudden. These types of sinkholes occur mainly in areas where the clay is the main soil type creating the cover.

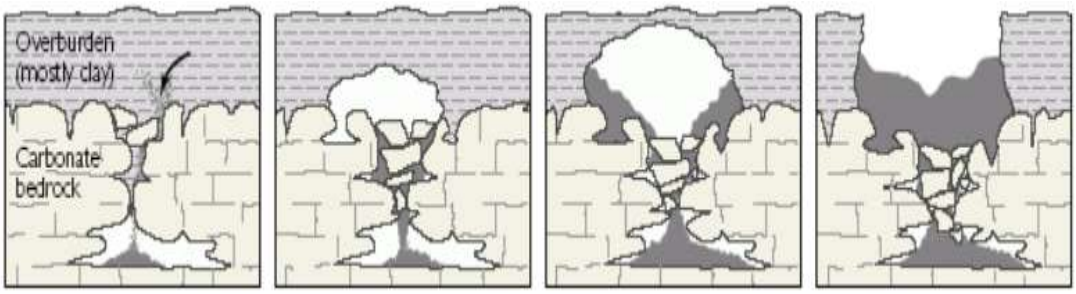

Figure 1. 7 Ideal cover collapse sinkhole formation (USGS 2018b)

Gradually, the cover soil deposits into the underground cavity and the cavity tends to move toward the surface till the internal pressure or arching cannot withstand the overburden pressure and sudden failure occurs as shown in figure 1.7.

Recent increases in sinkhole activity have highlighted the need for an enhanced understanding and prediction of the problem. Sinkholes can occur anytime, and experts simply cannot specify the time of the occurrence. It is a very challenging task for experts and engineers to study the cause and mechanism of a sinkhole after it occurs (Lei et al. 2005). Researchers have been trying to link current studies with recent techniques, such as geophysics mapping techniques and interferometric synthetic aperture radar (*InSAR*), to predict the cavity and opening in the sub-surface soil.

1.2. Aim & Objective

The primary objective of this thesis is to develop a numerical model that can be used to simulate the stability of the soil above a cavity and to estimate the associated extent of ground surface failure in the event of cavity failure.

To investigate stability, the problem is defined by using two different approaches that will capture the most possible situations. Firstly, the problem follows the Taylor approach to accommodate the greenfield conditions, such as military hand dug tunnels, natural sinkholes and the longwall mining goaf collapse, where there is no

surcharge pressure. This approach was followed by Broms and Bennerrmark's stability number approach where they defined underground stability, allowing for a surcharge load. This method particularly is useful for cases where the surcharge load exists, such as artificial sinkholes in urban areas etc.

In addition, the study investigates the surface extent of cavity collapse. Note that there is currently no standard procedure for determining the subsidence profile of the soil over the cavities. Through the study of surface failure, this research also investigates the shape of the affected area. In a broader sense, this study contributed to our understanding by offering valuable insight into the sinkhole failure mechanism and arching development, particularly in 3D sinkhole analysis. Furthermore, the charts and equation linking to geophysics tools could act as an early warning system, which might help government agencies and engineers predict the affected area and take all necessary actions to save lives and assets.

1.3. Scope of the work

The horizontal trapdoor problems are studied by undertaking the parametric study using dimensionless ratios that describes the soil parameters and trapdoor's geometry. Using the Tresca soil model, a two and three-dimensional finite difference analysis is conducted by utilising the shear strength reduction method in undrained homogeneous cohesive soil.

The problem can be defined following two popular methods in geotechnical engineering. Firstly, the problem can be expressed following the Taylor stability charts, where it assumes the greenfield condition. Secondly, it can be defined following the popular Broms and Bennerrmark's stability analysis method, which accommodates the surcharge and supporting pressure. The results of these investigations are presented in terms of safety factors and the stability number. Moreover, this research investigated the extent of ground surface failure by examining the vertical velocity output and briefly discussed the effect of the arching phenomenon on the extent of failure. The comprehensive results of stability analysis and failure extent are presented in form of dimensionless design charts and equations.

To ensure the reliability of the solutions, numerical results of this study will be compared with published literatures and the finite element limit analysis technique. Several practical examples are also provided to outline some of the potential uses of the design charts.

1.4. Thesis outline

This thesis is primarily focused on investigating the stability and surface failure extent of the sinkhole by undertaking parametric studies for various associated variables.

Chapter 2 - Literature review

Chapter two presents the relevant literature review, which involved sinkhole problem development and outlines previous studies on the sinkhole stability. It also reviewed the current geophysical technics, their theories and application in predicting the underground cavity and measurement of the soil surface settlement.

Chapter 3 - Numerical modelling

This chapter describes the common types of numerical analysis in geotechnical engineering and presents an overview of *ITASCA* software. This is followed by in-depth discussion about the *FLAC* software and the shear strength reduction method, which has been used in this research.

Chapter 4 – Two-dimensional analysis of undrained sinkhole in greenfield condition

This chapter investigates the stability of the trapdoor in an idealistic two-dimensional plane strain conditions with no external pressures. This is known as the unsupported greenfield condition. The parametric study was conducted for different depth and strength ratios.

Chapter 5 – Three-dimensional analysis of undrained sinkhole in greenfield condition

This chapter advances the previous chapter by adding a shape parameter of opening ratio, and the parametric study was undertaken in three dimensions. This chapter

also investigates the effect of opening ratio on the shape of the surface failure by discussing the transformation of ground surface circles.

Chapter 6 – Two-dimensional analysis of sinkhole problem using Broms and Bennermark's approach

This chapter investigates the stability of the trapdoor problem in a two-dimensional plane strain analysis for collapse and blowout failure by considering the existence of surcharge pressure and supporting pressure. Along with the stability investigation, the failure extent, due to collapse and blowout, has also been discussed.

Chapter 7 – Three-dimensional analysis of sinkhole problem using Broms and Bennermark's approach

This chapter furthers the study of chapter 6 by considering a more realistic three dimenisoanl problem. This chapter discusses the stability of the trapdoor associated with the surcharge and supporting pressure in three-dimensional model. It also discusses the effect of the arching phenomenon on the failure extent and compares the three-dimensional failure extent with the two-dimensional one.

Chapter 8 – Conclusion

This chapter summarises the outcome and discusses the key elements achieved in this research. Further, the future work and recommendation to improve results have been discussed, followed by some general closing comments on the justification of the conducted research.

1.5. Publications during the research

The following papers have been published or submitted over the duration of the degree.

- Shiau, J & Hassan, MM 2017, 'Numerical investigation of 2D trapdoor stability', in Proceedings of 3rd International Conference on Science, Engineering & Environment (SEE), The GEOMATE international society, Brisbane, Australia, pp.354-359.

- Shiau, J, Hassan, MM & Hossein, Z 2018, 'Stability charts for unsupported square tunnels in homogeneous undrained clay', International Journal of Geomate, vol. 15, no. 48, pp. 195-201.
- Shiau, J, Sams, M, Al-Asadi, F & Hassan, MM 2018, 'Stability charts for unsupported plane strain tunnel headings in homogeneous undrained clay', International Journal of Geomate, vol. 14, no. 41, pp. 19-26.
- Hassan, M and Shiau, J 2019, 'Stability charts for two-dimensional trapdoor problems' Journal of Recent Trends in Geotechnical and Geo-environmental Engineering and Education (Submitted and accepted; to be published in March 2019).
- Shiau, J & Hassan, M 2019, 'Three-Dimensional Analysis of Undrained Sinkhole', Geotechnique (Submitted on 26 October 2018).
- Shiau, J & Hassan, M 2019, 'Broms and Bennermark's Stability Number for Active and Passive Trapdoor Problems', Acta Geotechnica (Submitted on 11 December 2018).
- Shiau, J & Hassan, M 2019, 'Three-dimensional Broms and Bennermark's Stability Number for trapdoor problems', Computers and Geotechnics (Submitted on 9 January 2019).

2. LITERATURE REVIEW

2.1. Introduction

Recent growth in the number of sinkhole occurrences due to human activities, such as urbanisation, mining and agricultural activity has highlighted the need for a better understanding and prediction of the predicament. Sinkholes present environmental risks through subsidence or sudden ground collapse, leading to a great loss of life and infrastructure.

Lei et al. (2005) explains that a sinkhole collapse is an immediate occurrence; therefore, it is difficult to investigate the causes after the event. Like any natural disaster, early detection, prevention and mitigation of a sinkhole problem is a key element in sinkhole investigation. This includes detecting the physical location of a trapdoor, investigation of stability and finally, examination of failure extent in cases of collapse. Knowing this measure will allow authorities to issue the correct procedures to deter the loss of lives and minimise economic cost. The current study of the trapdoor problem is focal in two categories. Firstly, it relies on geophysical techniques centred on locating potential sinkholes. The second category concentrates on the stability of the trapdoor problem. Sower (1996) outlined a sub-profile of the karst soil and the process where a sinkhole is generated in karst. The conceptual nature of sinkhole formation is related to the interaction between the underlying limestone rock and groundwater, which causes deformations. In limestone areas, the gradual dissolution of rock at a depth influenced by the passing

of underground water, leads to subsidence of overburden of remaining and deposited soil resulting in a saucer-shape depression. Field investigation studies suggested that the underground voids created naturally or induced by humans, initiates in cracks between the underground rocks (Newton 1976 & Sower 1996). However, as it indicated by Tharp (2003), the initial size of a cavity does not reflect the size of the trapdoor. The initial cavity, due to internal erosion, grows and this increase in size creates the reverse funnel shape. When the cavity grows, the size of the neck gets smaller, which is a good indication of cover collapse failure. Moreover, Tharp (2003), stated that even small steady-pore pressure gradients can cause a large sinkhole over a period. Consequently, the geophysical tools are suitable to detect a cavity before it collapses.

2.2. Geophysics

Most recently, with the development of computer technology, there has been a greater focus placed upon geophysical tools. A large and growing body of literature has utilised geophysical mapping and radar imaging to predict and study the physical location of sinkholes before subsiding.

Geophysical tools can measure some physical subsurface properties, such as density, electrical resistivity and magnetic susceptibility to measure the surface movement. Some common geophysical techniques, which are used to locate the cavities in the subsurface are listed below:

Ground penetration radar

The ground penetration radar (*GPR*) or ground probing radar, is a geophysical method, which can be exercised to scan the shallow subsurface to detect a fracture, cave systems and sinkholes. The *GPR* technique sends electromagnetic waves to the ground. Those electromagnetic waves usually have a frequency of 25 MHZ to 1000 MHz. The energy of the waves reflect to the surface and a receiver measures the strength of the reflected waves. That data can be used to scan the underground soil profile (Griffin & Pippett 2002).

Figure 2.1 shows the profile of a *GPR*, which was collected in central Florida, obtained by using a 200 MHZ antenna.

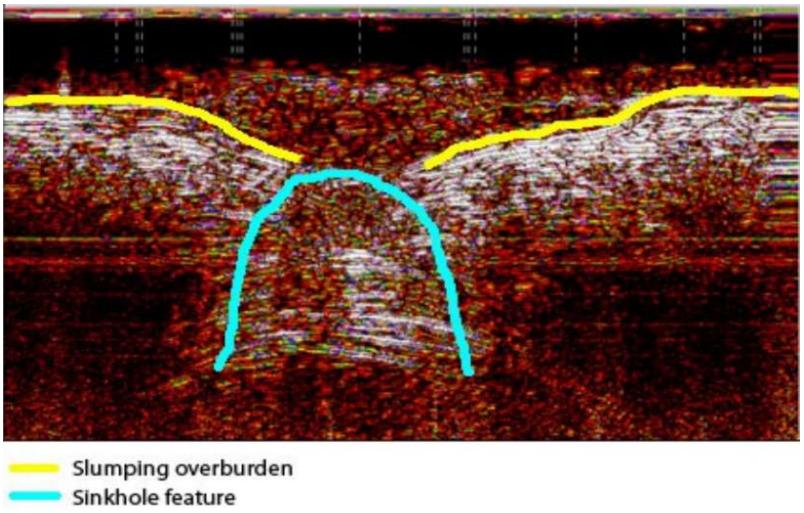

Figure 2. 1 GPR scan in central Florida with an antenna 200 MHz (Alpha Geofisica 2017)

Microgravity

This technique operates on the bulk density of the subsurface. Microgravity will detect the areas of contrast density via measuring the earth's gravity field to prepare the anomaly map.

Electric resistivity imaging

This technic uses the difference in the electrical property of the subsurface layers to scan underground soil. In this technique, the electrodes will transmit the current to the subsurface as shown in figure 2.2. A difference between two additional electrodes, known as potential electrodes, will be used to measure the voltage of the system. The received voltage then will be converted to resistance and the measured resistances will be used to model the underground.

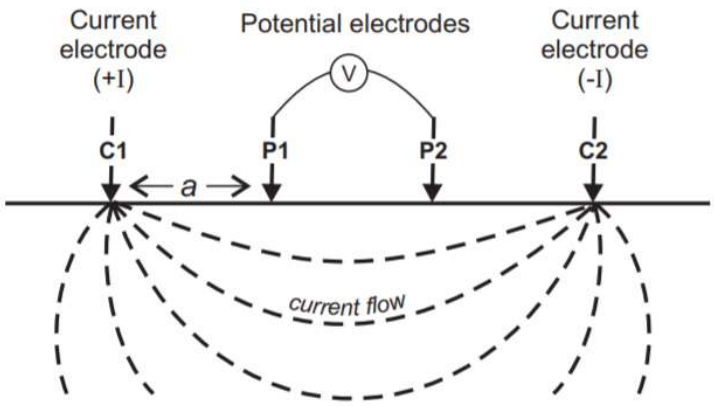

Figure 2. 2 Typical resistivity imaging process (Tuckwell 2017)

This technique unlike the *GPR* can be used to detect deep buried cavities (Benson 1995).

Induced polarisation imaging

Induced polarisation imaging is another geophysical technique that can be used to locate fissures and faults in rocks, or to uncover old mineshafts, cave systems and buried sinkholes. Like *ERI*, induced polarisation imaging (*IPI*) is based on electric resistivity. However, *IPI* measures subsurface material based on its capacity to store the electrical current. It is important to note that while two materials might have the same resistivity, they can have different chargeability (Tuckwell 2017).

Interferometric synthetic aperture radar (InSAR)

Interferometric synthetic aperture radar (*InSAR*) is a technique able to detect the movement of surface soil. The system can identify a surface movement of milometer to centimetre scale with high spatial resolution, which can be particularly beneficial in identifying surface subsidence. *InSAR* uses a number of images from the same area, captured by a synthetic aperture radar over time. If the distance between the satellite and surface varies between images, the satellite can detect the surface subsidence.

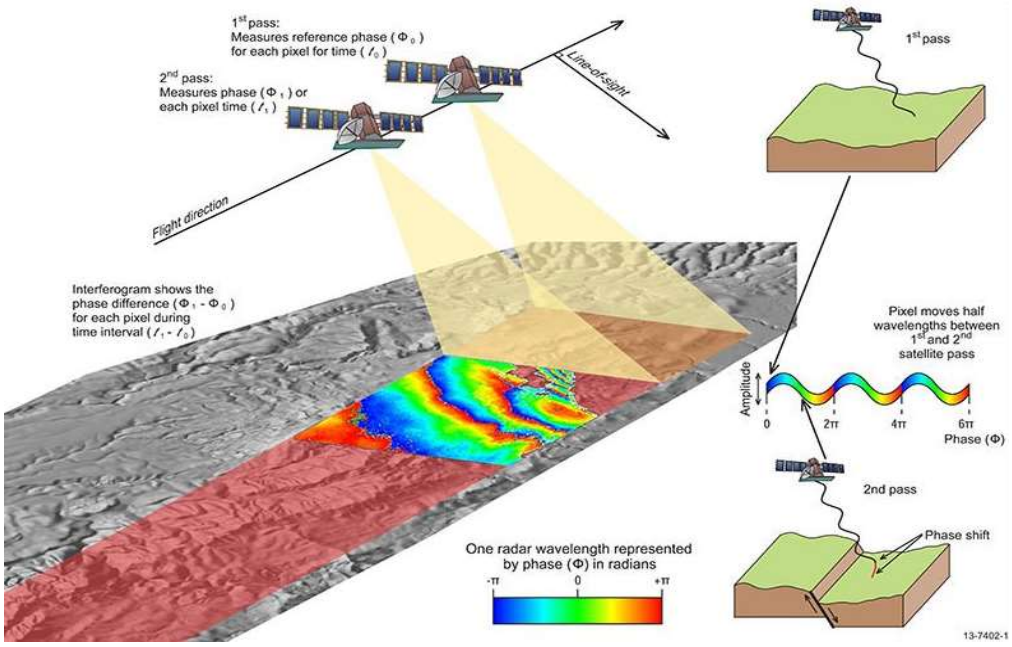

Figure 2. 3 SAR images of the same area are acquired at different times (Geoscience 2018)

Figure 2.4 is an example of ground surface movement, which did not show any signs of failure, however, it was detected by *InSAR* imaging map spanning.

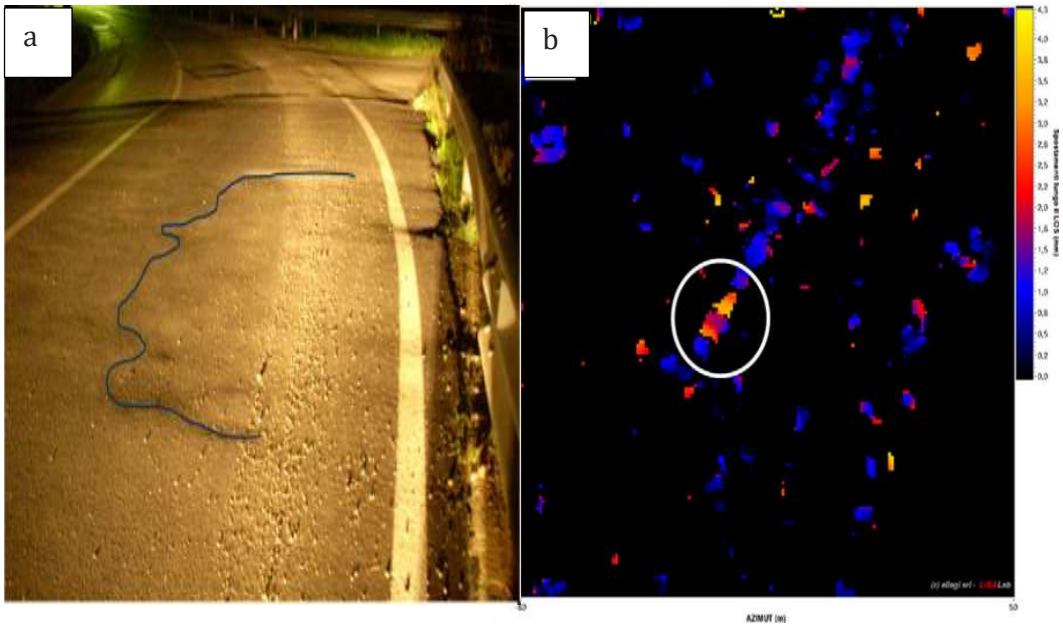

Figure 2. 4 (a) Depression on 25 November 2013 highlighted by the blue line (b) Displacement map spanning from 29 October to 25 November 2013 for same location (Intrieri et al. 2015)

With the measured information, such as cavity size, soil properties, and associated depths, it is possible to theoretically predict the extent of ground surface collapse.

Buis & Harrington (2014) described that NASA's Uninhabited Airborne Vehicle Synthetic Aperture Radar was able to detect large sinkhole in Bayou Corne Louisiana. By using the interformic synthetic aperture radar imagery. The report suggested that, if such radar data collected routinely from airborne systems or satellites, we could foresee sinkholes. Later, Jones et al. (2015) used interferometry to measure both surfaces horizontal and vertical displacement. Based on data analysis, it found that over time, sinkholes expand in all directions. Recent evidence suggests that Electrical Resistivity Imaging or Tomography (*RESTOM*) techniques are capable of distinguishing between a mature and a developing sinkhole. These techniques can measure conductivity by distinguishing if the cavity is filled with water or air (Van Schoor 2002).

Wilson and Garman (2016) selected three different case studies of sinkhole development across a period of time, with the geophysics mapping method, such as the ground penetration radar (*GPR*) and electrical resistivity (*ERI*) and detected a couple of buried sinkholes under roads and suggested the relocation of the road before construction as shown in figure 2.5.

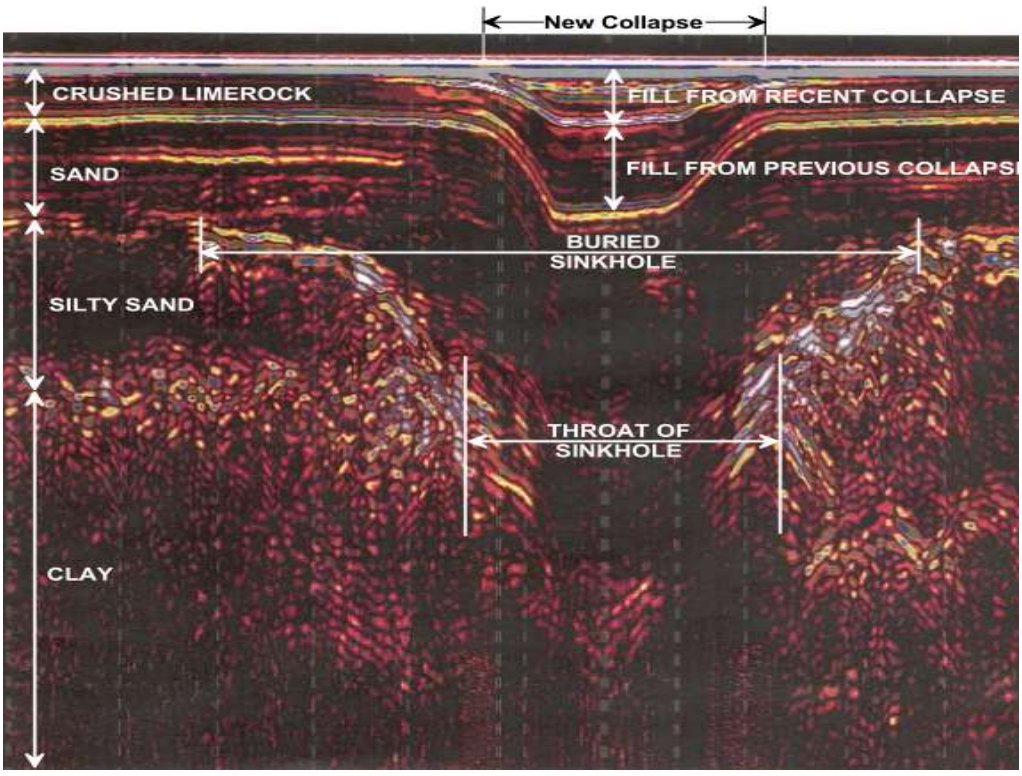

Figure 2. 5 *GPR* profile of the buried sinkhole (Wilson & Garman, 2016)

Intrieri et al. (2015) monitored and detected the sinkhole by a ground based interferometric synthetic aperture radar (*GB-InSAR*), which uses microwave signals to produce images. This system successfully predicted a 2.5 m cavity.

In a study which set out to determine the feasibility of satellite radar interferometry to detect subsidence, Chang and Hanssen (2014) compared and analysed satellite data during past 18 years to detect the growth in a cavity, which led to the instability of the foundations under a shopping complex. The results of this investigation is shown in figure 2.6.

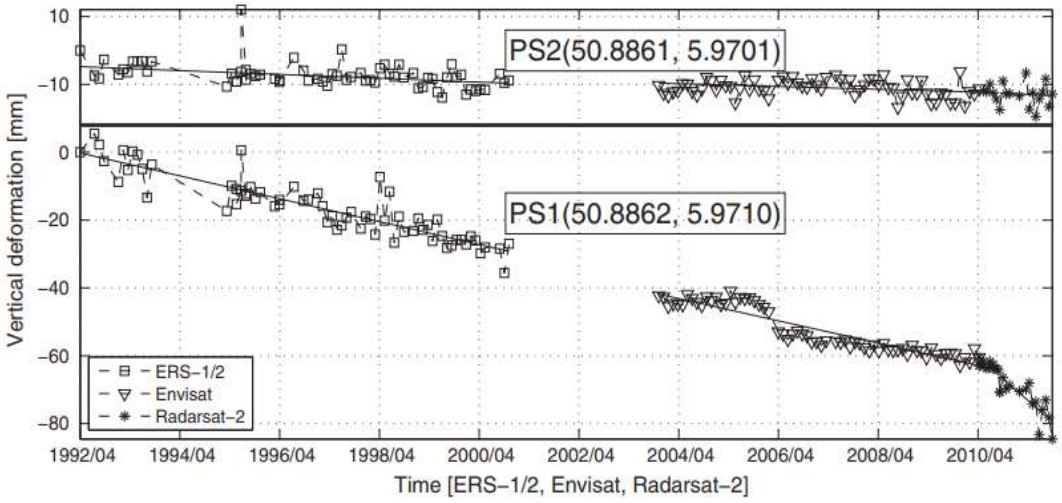

Figure 2. 6 Distribution of radar acquisitions and deformation time series of the building during the 18 years (Chang and Hanssen 2014)

The study considered two sections of the structure known as PS1 and PS2. The PS1 referred to the unstable section of the building and PS2 was the stable section. Chang and Hanssen (2014) noted that the average deformation rate of PS2 was 3.3 mm/year compared to 0.6 mm/year for PS1. The study recommended the automatic detection scanner radar over popular sinkhole areas.

A review of the current practice models of the geophysics tool reveals that the current mechanism is the best to locate the cavity and detect the subsidence, however, other tools and measures are required to examine the stability and predict the surface failure.

2.3. Stability analysis

The stability of the trapdoor was initiated by Terzaghi (1936), who experimentally investigated the effect of the distributed stress in sand and defined the active and passive trapdoor failure. He described the active mode as surcharge or overburden pressure, and passive mode as an uplifting force, such as an anchor. In principle, there are two key elements that stimulate an underground cavity's failure, one being the overburden pressure (γH) and the other the surcharge load (σ_s). It is not unusual in geotechnical engineering analysis and design, to consider a greenfield condition ($\sigma_s = 0$), with some examples being in Taylor's original slope stability charts (Taylor 1937). Without considering weathering effects, a failure may occur due to

overburden pressure (γH) above a cavity in the ground, which is a typical condition in the analysis of natural sinkholes and longwall mining.

Taylor's stability charts are one of the principal tools used in analysing slope stability problems, and they are still popular with engineers in the field. Using the limit equilibrium method, the stability of slopes is a function of the slope height (H), slope angle (β), and soil properties, such as the unit weight (γ) and undrained soil shear strength (S_u) (McCarthy 2002, Baker 2003). The undrained stability number introduced by Taylor is presented in equation 2.1, which can be used to investigate the stability of soil overlying a cavity.

$$N_s = \frac{S_u}{\gamma H \times FoS} \tag{2.1}$$

Experimental investigations on the stability of underground openings emerged in the 1970s. Broms and Bennermark (1967), through laboratory experiments and field data collection, studied the plastic flow of undrained clay in vertical openings as shown in figure 2.7. The stability number equation is presented in equation (2.2).

$$N = \frac{\sigma_s - \sigma_t + \gamma H}{S_u} \tag{2.2}$$

Where (σ_s) is the soil surcharge load, (σ_t) is the supporting pressure; (S_u) and (γ) are the undrained shear strength and unit weight of the soil respectively. The stability number (N) is independent of the depth ratio (C/D), where the C is the opening cover and D is the opening diameter. It is further noted that (σ_t/S_u) represents the supporting pressure, and ($\sigma_s+\gamma H)/S_u$ the overburden pressure.

Brom and Bennermark (1967) concluded that for a vertical opening in retaining wall, failure occurs when total overburden pressure ($\sigma_s+\gamma H$) is six to eight times greater than undrained shear strength of the soil. The value of six to eight would depend on the shape of the opening and the roughness of the wall.

Broms and Bennermark's work was continued by many other researchers, such as Mair (1979), Craig (1990), Abdulla et al. (1996) and more recently by Jacobsz (2016) and Shiau and Al-Asadi (2018) using limit analysis with lower and upper bound theorems.

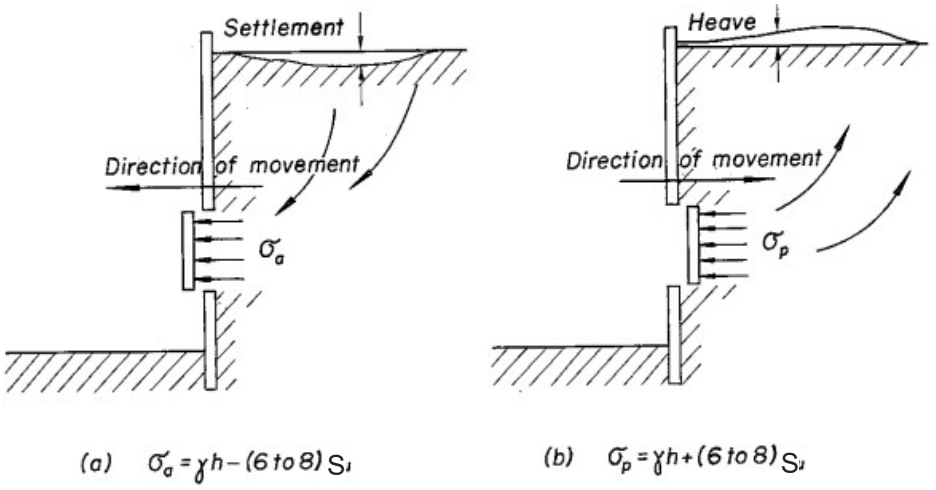

Figure 2. 7 Vertical wall stability model of Broms and Bennermark (1967)

Atkinson and Potts (1977) from Cambridge University, used the bound theory and experimental method to investigate the stability of shallow circular tunnels in cohesionless soil under plain strain conditions. The centrifugal experimental investigation consisted of small-scale models.

The study concluded that the theoretical solutions developed using FELA lower and upper bound have a high degree of accuracy and match the experimental centrifugal solutions. This approach was later followed and expanded by other researchers, such as Mair (1979), Davis et al. (1980), Muhlhaus (1985), and Leca et al. (1990) to investigate various types of underground openings.

One of the most influential studies of stability comes from Davis et al. (1980), who used the limit analysis theorem to determine the upper bound and lower bound solution of the problem. In his approach, unlike the original Brom and Bennermark (1967) approach, the parameters have been presented independently, so the stability pressure ratio has become the function of the strength ($\gamma D/S_u$) and depth ratios (C/D), as indicated in the following equation.

$$N = \frac{\sigma_s - \sigma_t}{S_u} = f\left(\frac{\gamma D}{S_u}, \frac{C}{D}\right) \tag{2.3}$$

The undrained shear strength (S_u) and the unit weight (γ) are soil properties, while the tunnel has a height (D) and cover depth (C) above its crown.

Numerical analysis of the trap door problem was also used by Koutsabeloulis and Griffiths (1989) to investigate the active and passive mode displacement of the soil. Koutsabeloulis and Griffiths (1989) used *FEM* to model the trapdoor numerically, to investigate the displacement of the soil in active and passive mode and presented the results in the form of empirical equations.

Craig (1990) employed a large centrifuge model to investigate the critical stability of a circular cavity. In this investigation, Craig (1990) used the lower and upper bond technique to estimate the stability of a shallow trapdoor (between 0.5-1.5) and concluded that, for a depth ratio greater than 1, the theoretical results are not valid. This approach to the problem has been continued and expanded in the finite element limit analysis (*FELA*) research by Yang et al. (2002), Auguard et al. (2003), Drumm et al. (2009), Martin (2009) and most recently by Keawsawvong et al. (2017).

In a major study, Sloan et al. (1990) implemented the numerical linear program. The program was based on the limit theory of plasticity and finite element, to examine the undrained stability of the trapdoor using rigorous upper bound and lower bound to obtain the exact value of the collapse load. Sloan et al. (1990) stated that the stability number (*N*) is a function of *H/B* and that it was based theoretically on a factor safety of 1. Figure 2.8 defines the Sloan et al. (1990) trapdoor problem.

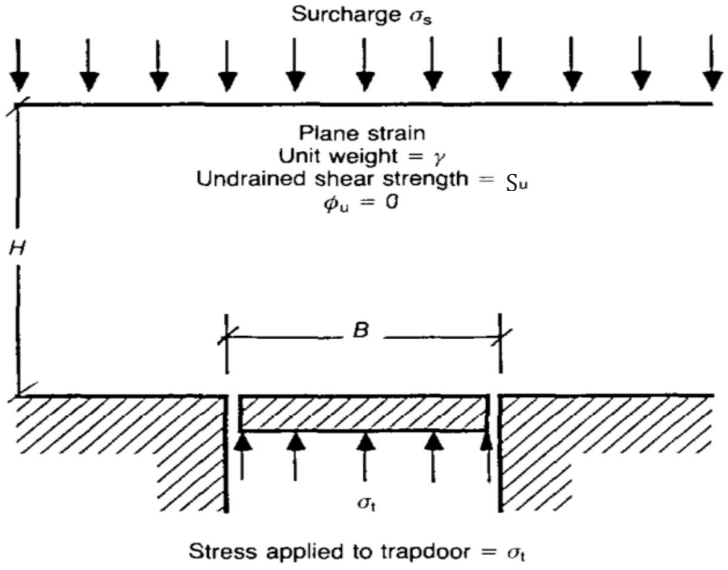

Figure 2. 8 The trapdoor model (Sloan et al. 1990)

Sloan et al. (1990) results were derived from the numerical formulation of limit theorems, enabling the exact solution to bracket down within 10% or better for the range of trapdoor geometries. This approach uses finite elements to discretise the problem domain but using limit analysis to solve two optimisation problems. The first is based on the principle of finding the highest loaded scenario that is still statically admissible – this will be lower bound. The second is to find the lowest loaded scenario that is still kinematically admissible – this will be the upper bound

Drum et al. (1990) used classical plasticity theory to examine the stability of cohesive-frictional soils with a cylindrical opening. The study concluded that "for a given overburden thickness, small cavities are more stable than large cavities. However, for a given cavity diameter, large overburden thicknesses are shown to be more stable than small thicknesses." (Drum et al. 1990)

Tharp (1999) introduced a hemispherical model to examine the upward propagation of a cover collapse sinkhole. The study examined the failure of the cavity walls of soil, void by compression due to crack propagation in which net tension is perpendicular to the wall of the cavity, produced by water pressure. Tharp (1999) concluded that formation of sinkholes is associated with the lowering of the ground water table and can be minimised by slow lowering of the water table.

Augarde et al. (2003) built upon the earlier definition of stability number (N) and used a finite element limit analysing technique to numerically model the stability of undrained submerged cavities subjected to surcharge load and internal vertical pressure as shown in figure 2.9, where C is depth of the cover soil and D is the diameter of spherical trapdoor opening. The study considered symmetrical technique to develop the spherical trapdoor model.

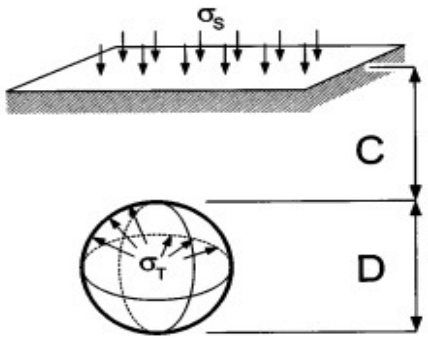

Figure 2. 9 Spherical sinkhole cavity (Augurd et al. 2003)

Augurd et al. (2003) defined a stability number as a pressure ratio $(\sigma_s-\sigma_t)/S_u$ and simplified it by setting the σ_s to zero. With this measure, the study proposed various stability charts for undrained cavity collapse.

Yang et al. (2002) used numerical analysis to develop the stability charts for the collapse of residual soil in karst. The shear strength reduction method was used to investigate the effect of soil friction angle in the stability design. Drumm et al. (2009) also developed dimensionless stability charts that can be used to evaluate the stability of soil in karst.

In another important study, Martin (2009) projected the plastic collapse of a horizontal trapdoor in homogeneous clay. Using upper and lower bound solution. Martin (2009) analytically introduced the new slip line solution for shallow trapdoors by correcting the stability factors (N_c) for various cover ratios (H/B). The study concluded that the corresponding stability factor N_c is 1.956 times the cover ratio H/B. the extensive investigation was carried out, the small cover ratio (H/B=2) has been a serious limitation in his study.

Recent studies have been conducted using a shear strength reduction method by Shiau et al. (2018), to investigate tunnel heading stability in homogeneous cohesive soil. What was notable about this study is that the strength ratio defined following Taylor's (1937) stability approach, so the factor of safety became the function of the depth ratio (H/W) and the soil strength ratio ($S_u/\gamma W$).

Experimental tests have played essential roles in trapdoor stability. Much of the 3D trapdoor stability research focused on the laboratory and centrifugal experiments. Vardoulakis et al. (1981) experimentally studied the trapdoor forces and introduced the ultimate and residual state solutions for the active and passive trapdoor. In a significant approach, Leca and Dormieux (1990) used a 3D failure mechanism in limit analysis and the centrifuge model in the framework of the kinematical method, to drive three upper bound solutions of supporting the pressure of the face tunnel in the frictional material.

Abdulla et al. (1996) conducted a series of centrifuge model tests to determine the stability of the sinkhole in weakly cemented sand. Their results indicated that the relative depths in terms of the opening of the cavity plays a major role in the stability of the cavity. The study concluded that for an inadequately cemented sand layer over

the cavity, the failure occurs in the range where H_c/D is greater or equal to 0.25 (where D is the opening diameter and H_c is the thickness of the soil).

Later, Mollon et al. (2009) improved the solution of the collapse pressure by using a kinematical approach which introduced earlier by Leca and Dormieux (1990). The numerical results of the study showed that a multiblock mechanism composed of three blocks is a good compromise between computation time and results accuracy.

Guan et al. (2017) built upon Subrin and Wong (2002) study and proposed an analytical solution for the 3D failure mode of a cavity by utilising the bound theorem in the finite limit analysis. Ibrahim et al. (2015) extended the Mollan et al. (2009) study by investigating the failure mechanism of the multi layered frictional soil. Yang and Huang (2013) extend on the 2D analysis by Fraldi and Guarracino (2009) and developed a three-dimensional failure mechanism for the rock over the deep cavity roof, deriving the analytical solution of the surface equation, which could determine the shape of collapsing block.

2.4. Subsidence study

Subsidence, because of the underground cavity collapse particularly in urban areas, can cause great risk to human lives, however, surface subsidence prediction due to trapdoor failure has been given less attention than trapdoor stability investigations. Recent studies have focused on tunnelling and longwall coal mining subsidence. Currently, there are no standard procedures for determining the subsidence profile of the soil over the cavities. In fact, in practice, it is difficult to obtain the exact magnitude of surface failure extent.

However, researchers have developed the various methods to estimate the surface deformation. Murayama (1969) studied the relations between land subsidence and withdrawal of groundwater. The study of the land subsidence was followed by many other researchers, such as Holzer (1984), Sheorey et al. (2000) Shen et al. (2006), Fattah et al. (2013) and Shiau et al. (2018) who investigated the surface failure extent due to tunnel heading collapse.

The earlier studies of subsidence used an empirical method. In 1958, Martos suggested that the Gaussian distribution curve would fit the deeply excavated

mining settlement. Following this important finding, Peck (1969) analysed the data of the number of tunnels and proposed an empirical equation.

$$S_x = S_{\max} \exp\left(-\frac{x^2}{2i^2}\right) \tag{2.4}$$

Where as shown in figure 2.10, S_x is a settlement, S_{max} is the maximum surface settlement, x is the horizontal distance from the tunnel centreline and i is the horizontal distance from the centreline to the point of inflection on the surface settlement. D is diameter of circular tunnel opening and Z_0 is a height from surface to the centreline of the circular tunnel.

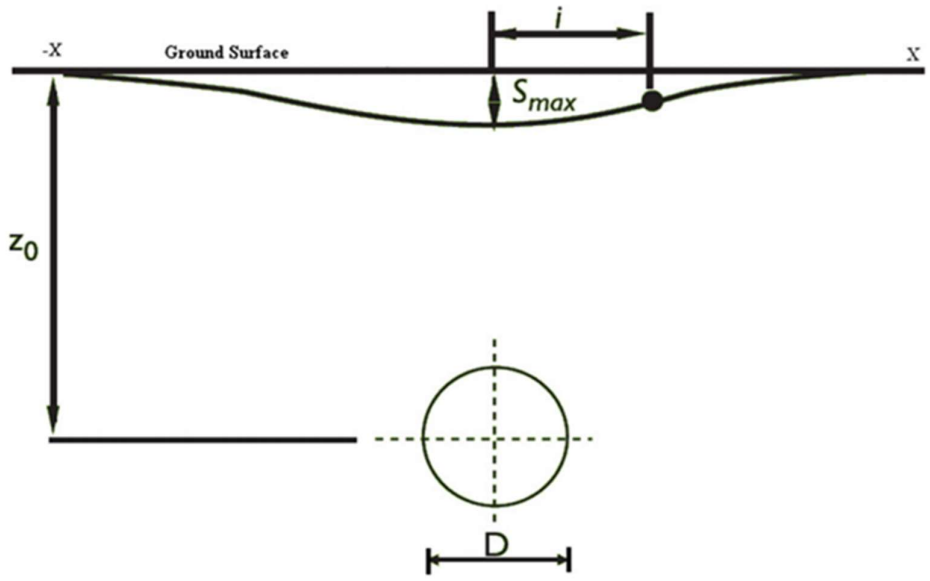

Figure 2. 10 Typical settlement generated by circular opening (Peck 1969)

In 1983, Mair used a similar approach and proposed a new equation to calculate the maximum surface settlement (S_{max}).

$$S_{\max} = \frac{V_S}{\sqrt{2\pi i}} = 1.252\frac{V_L R^2}{i} \tag{2.5}$$

Where V_s is the volume loss, V_L is the percentage (%) of volume loss ratio of the lost material to the area of the circular tunnel opening and R is the circular tunnel radius.

Subsequently, researchers, such as Clough and Schmidt (1981), O'Reilly and New (1982), Attewell et al. (1986) and Dimmock and Mair (2007), have associated volume loss (V_L) with stability number (N).

Influenced by Peck's work, The National Coal Board (*NCB*) in 1975, utilised the profile function and proposed the graphical method to estimate the subsidence due to long wall coal mining (Chrzanowski et al. 1998).

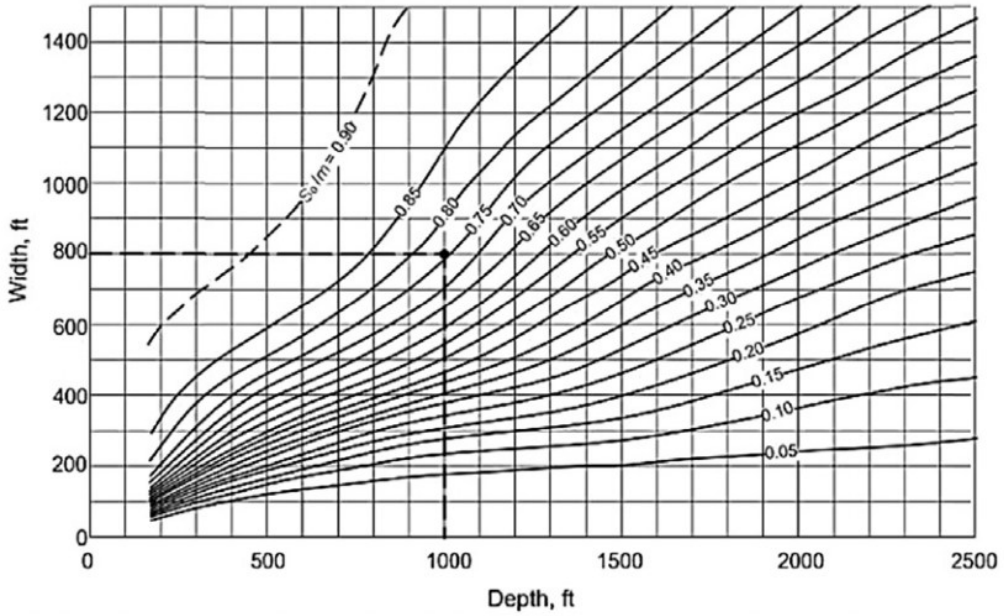

Figure 2. 11 Subsidence monograph (Chrzanowski et al. 1998)

The monograph proposed by the *NCB* shown in figure 2.11, enabled the user to estimate the subsidence based on the width and depth of the coal mine. However, since the monograph would not consider other parameters, such as mechanical property, the application of the chart only covers geological areas that have similar properties to locations where plot data has been collected (Chrzanowski et al. 1998).

In a recent study, Thongprapha et al. (2015) used a trapdoor apparatus for physical model testing. The experiment tested a series of various opening sizes to measure gravel subsidence. Experimental results were presented in terms of failure angle and maximum subsidence. The study concluded that for shallow depths, the subsidence will decrease as the opening size increases. This finding was different from the concept which was proposed earlier by Peck (1969). The large size gravel used for this experiment could be the reason for the variation.

2.5. Outstanding issues in trapdoor's problem

Despite the extensive studies of the trapdoor problems over the year, some issues related to sinkhole stability and its failure mechanism remains unsolved.

- The majority of studies considered specific geological regions. There is a lack of research using dimensionless ratio to address the problem.
- The greater part of the laboratory studies and numerical analyses used very limited opening sizes or depth ratios. Due to the dynamic nature and unpredictable behaviour of sinkholes, a comprehensive study (large depth and opening range) is required to understand the mechanism of the failure.
- The majority of surface failure studies were conducted on sand models.
- Although there is a limited number of studies that have addressed the problem in the three-dimensional aspect, the vast majority of the trapdoor stability studies relied on two-dimensional analysis.
- The shape of the ground surface failure is not studied previously.
- The margin between two- and three-dimensional trapdoor stability analyses has not been investigated. In addition, the effect of the arching particularly in three-dimensional analysis needs to be addressed.

This study aims to use finite difference method to undertake numerical study of two- and three-dimensional sinkhole stability problems. It is expected that the outcome of the study would provide useful engineering information and better understanding of the problem, which may assist in decision making by practical engineers.

3. NUMERICAL MODELLING

3.1. Introduction

The limitation of the human mind and the need for quick and accurate solutions of complex geotechnical analysis, advanced computer technology has paved the way for the development of fast and accurate numerical analysis. The numerical analysis requires a model and a set of the parameters to approximate the solution of any complicated problem that is difficult to solve in the real world. Therefore, many designers use numerical modelling to examine their problem with certain assumptions and uncertainties. In recent years, numerical analysis has been used as an alternative method for verification of other conventional analysis. Additionally, it opens a new window for researchers to carry out comprehensive studies of various geotechnical stability and settlement problems.

This chapter will briefly outline the development of numerical methods. It will be followed by a review of the software published by *ITASCA*, including the *FLAC* software that is the key analysis tool used in this thesis.

3.2. Review of current finite element techniques

Some of the popular finite element techniques in geotechnical numerical analysis will be introduced in this section. As the purpose of this section is to briefly describe the capability of those methods, the detailed descriptions and mathematical

approaches of each method can be found in more relevant books and published papers.

3.2.1. Finite element method

In the finite element method, the problem will be segregated into different elements connected at their nodal points. The *FEM* uses a set of equations that link unknown parameters to known parameters in the global stiffness matrix system to solve the problem. In that way, the problem can be solved by directly using known quantities. This process of relating the unknown to known parameters and solving the problem is referred to as implicit technique. A complete description of the method and the mathematical development has been described by Dhatt et al. (2012).

3.2.2. Finite difference method

The finite difference method is one of the oldest techniques used in numerical studies because of its simplicity and capability. This approach particularly applies to dynamic problems. The principle of the finite difference method is close to the numerical schemes used to solve ordinary differential equations. It entails approximating the differential operator by replacing the derivatives in the equation using differential equations. The finite difference method considers the time in numerical solution. This ability enables the user to observe the solution at each time step. Unlike the finite element method, the *FDM* isn't required to generate the global matrices, therefore, improves the efficiency of computation. The full method description has been explained by Narasimhan et al. (1976).

3.2.3. Finite element limit analysis

The finite element limit analysis and finite element method both use discrete formation by utilising the elements. However, theoretically the finite element limit analysis approach is very different to the conventional finite element method. The finite element limit analysis (*FELA*) presents the solution in terms of the lower bound and upper bound. In this approach, the upper bound solution outlines the kinematic admissible velocity field, which will provide an unsafe solution, while the lower bound represents a statically admissible stress field of stability number.

Initially, this method followed the bound theorem by Drucker et al. (1952) and was developed into linear and nonlinear programs by e.g. Sloan (1988, 1989), Lyamin et al. (2002a, 2002b) and Krabbenhoft et al. (2005). The complete development and description of *FELA* can be found in Sloan (2013).

3.2.4. Boundary element method (BEM)

This method, unlike others that consider the volume of the soil, only considers the boundaries. The *BEM* reduces the issue into a one-dimensional problem, suiting linear problems. Because the method looks at the surface (boundaries) only, the computational time of problem modelling, and solution processing is much less than the others. This ability is more advantageous in some lengthy 3D dimension models where only some of the solutions are required or in the problems where the domain is infinite. On the other hand, the *BEM* is not suited for thin structures, such as shell due to a large surface to volume ratio. Also, it is not suitable for analysing nonlinear problems because the interior elements might play a crucial role in the stability of the structure (Antes 2010).

The practicality and success of finite methods are associated with program availability and fast computers (Ural 1973). In past decades, developers, such as *ITASCA, PLAXIS, GEOSLOPE, ABAQUS* and others, utilised finite methods to develop a program that can be used to solve complicated geotechnical problems more accurately and efficiently.

3.3. ITASCA

ITASCA (2013) is a consulting group that was founded first by the members of the Civil and Mineral engineering department of the University of Minnesota to provide the consulting service in numerical modelling, rock mechanics and underground spacing. Since then, the group has developed numbers of geotechnical related software, such as *FLAC* 2D and 3D, *PFC* 2D and 3D, *X* site and *UDEC*.

Due to availability of the licence, *ITASCA FLAC* 2D and 3D are the tools that will be used to undertake the numerical investigation of this study.

3.4. FLAC

FLAC (Fast Lagrangian Analysis of Continua) is a two-and three-dimensional explicit finite difference program associated with geotechnical and geomechanic engineering. *FLAC* utilises Lagrangian analysis, dynamic equation of motion and numbers of built in constitutive models to solve the problem. In *FLAC*, due to small time steps in the problem-solving process, the information would not physically transfer from one element to the other. Each element acts as a base on the linear or nonlinear stress/strain regulation to respond to the exerted force and boundary condition (Wang et al. 2011).

3.4.1. Numerical Modelling in FLAC

FLAC recommends the following steps to be undertaken to execute a successful two- and three-dimensional numerical analysis:

a) Defining the objective of the work: Defining the objective of the work will reduce or illuminate the complication of the work that may impact on the accuracy of the results.
b) Creating a conventional vision of the model: This will allow the user to approximate the model and results. The conceptual model also helps decide on the best tool and model structure.
c) Build and run an idealised model: Running the simple idealised model will help detect issues that might not be possible when dealing with complicated models. It also helps to understand the system and the structure of the physical model.
d) Determine problem specific data: The accuracy of the successful numerical model depends on the reliability of the input. Therefore, the geometric details, initial condition, external loads and material property need to be defined before analysing.
e) Prepare a series of detailed model runs: There are important elements, such as running time, which need to be considered for an effective and efficient parametric study. The computational processing time is particularly important when it comes to three dimensional models. Applying several

monitoring stages in a model would help in checking with the physical data, which is beneficial in terms of a better interpretation of the results.

f) Perform the model calculation: It is recommended to conduct a few individual detailed runs and once the results are confirmed, series of the runs can be performed.

g) Present results for interpretation: The final phase of successful modelling is to interpret the results. The results can best be presented graphically in the form of contours and vector plots.

FLAC is explicit, finite difference program that performs a Lagrange analysis. Finite difference method is oldest method used for solving set of differential equations. In *FDM* every derivative in set of governing equations is replaced directly by an algebraic expression which is written in term of stress, displacement or other field variables. Even though the *FLAC* produce static solution, the dynamic equations of motion are included in formulation. The general calculation sequence in *FLAC* is discussed in section 3.4.2 of this Thesis. *FLAC* uses and explicit time marching method. To avoid instability, in each loop known as timestep, *FDM*, re-generate algebraic equations to replace the actual field variables. It is important to know that, while each variable update in every timestep, the known field parameters which has been replaced by algebraic equation remains constant. *FDM* iterate until a solution is found with minimum unbalanced forces. (FLAC 2D 2003)

Since in explicit method the global stiffness matrix is not needed, updating the coordinates at each timestep in large-strain mode is not important. *FLAC* use the "Lagrangian formulation to add incremental displacement to the coordinates so that the grid deforms with the material it represents". (FLAC 2D 2003)

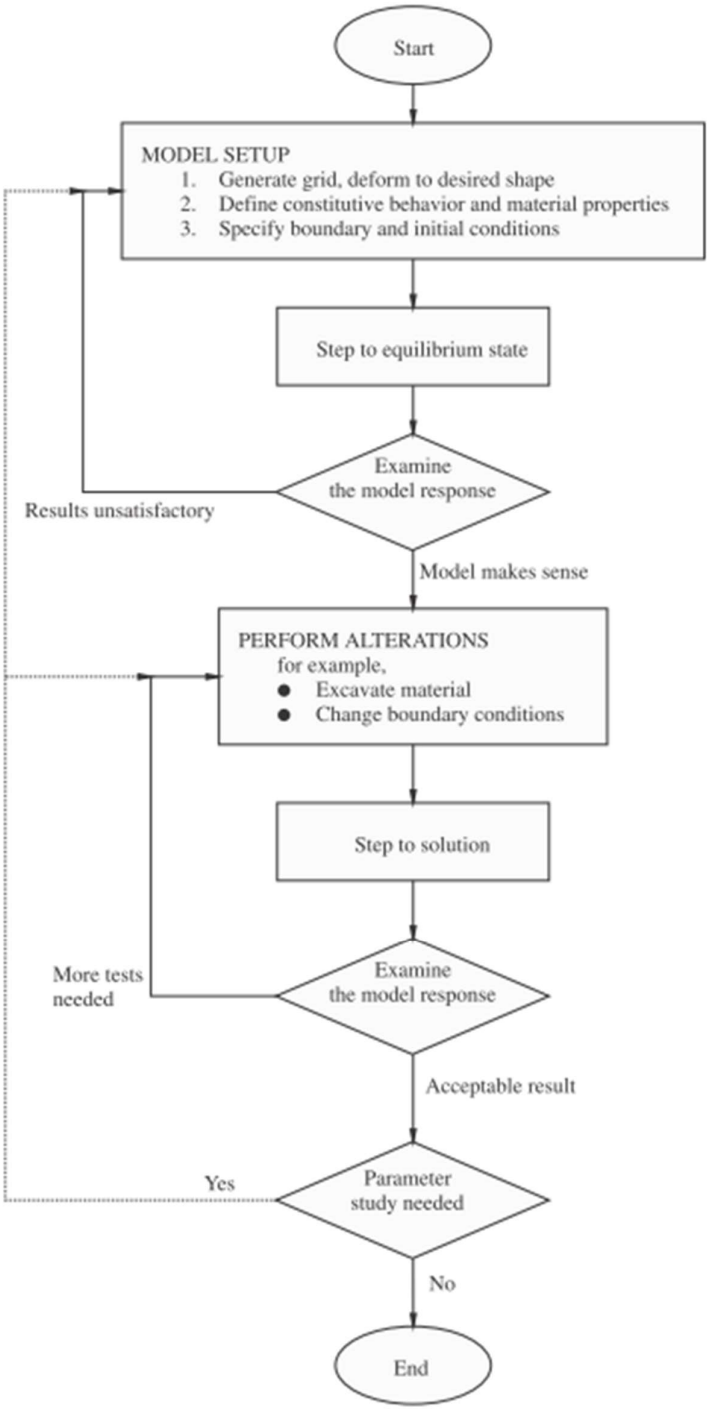

Figure 3. 1 Numerical modelling setup in *FLAC* (FLAC 2D 2003)

3.4.2. Explicit analysis process

The *FLAC* solution considers the dynamic equation of motion in its process of finding the static solution. This ability will ensure that the numerical system remains stable when the physical system is at an unstable condition. This is particularly important in nonlinear materials where there is always the possibility of high instability. In reality, some of the strain energy in the system will dissipate by converting into kinetic energy. To face this situation, *FLAC* models this process directly, because the inertial terms are included kinetic energy is generated and dissipated. In contrast, schemes that do not include inertial terms must use some numerical procedure to treat physical instabilities. Figure 3.2 illustrates the general progress of the explicit method, which has been implemented in *FLAC*. (FLAC 2D 2003)

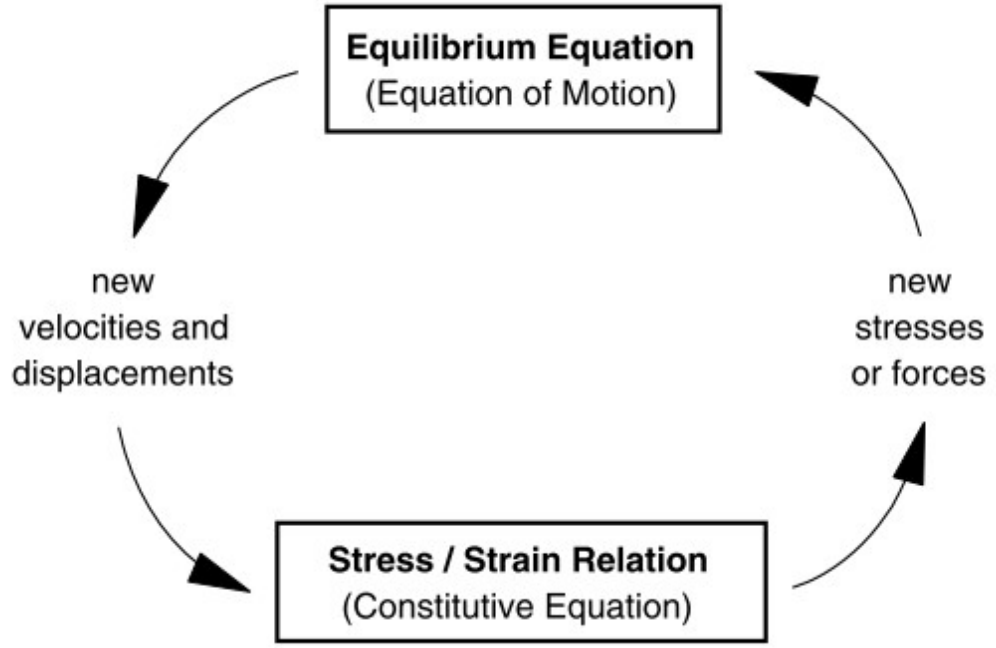

Figure 3. 2 General explicit calculation loop (FLAC 2D 2003)

The process starts with the equation of motion, which drives new displacement and velocity from stresses. The strain rate would be driven from velocity to form a new stress. The entire loop explained above would take place in one timestep. It should be noted that each box in the above figure will update the grid parameters from the known constant variables. For example, the "stress/strain relation" box would consider the new velocity, which has already been calculated to compute the new stress rates.

The explicit method has several advantages in comparison with the implicit technique mainly associated with the finite element method. Table 3.1 shows the comparison of explicit and implicit method.

Table 3. 1 Comparison of explicit and implicit methods.

Explicit	*Implicit*
Timestep must be smaller than a critical value for stability.	Timestep can be arbitrarily large, with unconditionally stable schemes.
Small amount of computational effort per timestep.	Large amount of computational effort per timestep.
No significant numerical damping introduced for dynamic solution.	Numerical damping dependent on timestep present with unconditionally stable schemes.
No iterations necessary to follow nonlinear constitutive law.	Iterative procedure necessary to follow nonlinear constitutive law.
Provided that the timestep criterion is always satisfied, nonlinear laws are always followed in a valid physical way.	Always necessary to demonstrate that the abovementioned procedure is (a) stable and (b) follows the physically correct path (for path-sensitive problems).
Matrices are never formed. Memory requirements are always at a minimum. No bandwidth limitations.	Stiffness matrices must be stored. Must find ways to overcome associated problems, such as bandwidth. Memory requirements tend to be large.
Since matrices are never formed, large displacements and strains are accommodated without additional computing effort.	Additional computing effort is needed to follow large displacements and strains.

In summary, the explicit method fits best for nonlinear, large strain and physically unstable systems.

3.4.3. Lagrangian analysis

The Lagrangian strategy uses a similar principle to the finite difference method by dividing the continuum material into a number of connected elements. Since *FLAC* does not need to form a global stiffness matrix, amending the coordinate's change at every time step became unimportant. Unlike the Eulerian method, the Lagrangian

equation, incremental displacement will be added to coordinates and the grid will distort to suit the material.

3.4.4. Grid generation

The model is discretised to a mesh comprised of quadrilateral elements. The solid body is divided by the user into a finite difference mesh composed of quadrilateral elements. Internally, FLAC subdivides each element into two overlaid sets of constant-strain triangular elements. Using the triangular elements would eliminate problems that may occur in constant strain finite elements. (FLAC 2D 2003)

FLAC separates these mesh elements into two overlaid constant-strain triangular elements. The triangles are illustrated as a, b, c and d in figure 3.3a.

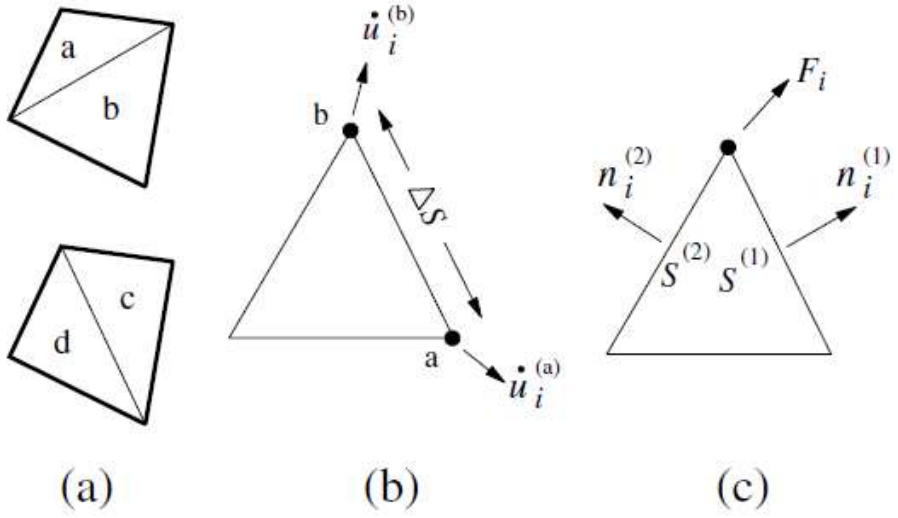

Figure 3. 3 (a) Overlaid quadrilateral elements used in FLAC, (b) Typical triangular element with velocity vectors, (c) Nodal force vector (FLAC 2D 2003)

The incompressibility of plastic flow is a major issue for some materials that experience yielding. Using of plane strain or axisymmetric condition initiates a kinematic restrain in out of plane direction, which will result in an excessive stiff element and will over predict the failure load. This condition has been explained by Nagtegaal et al. (1974).

FLAC uses the mixed discretisation method suggesting different discretisation for isotropic and deviatoric sections of materials stress and strain. The detail process was described by Marti and Cundall (1982). It should be noted that while deviatoric

is fixed, the volumetric strain would be an average of each pair of triangles. So, for triangle a and b in figure 3.3a, the strain rate would be the mean of both triangles as presented in equation 3.1.

$$e_m = \frac{e_{11}^a + e_{22}^a + e_{11}^b + e_{22}^b}{2} \tag{3.1}$$

The similar approach would be considered for triangle c and d. However, the preceding formulation is for plane-strain conditions only. In axisymmetry, all three direct strains are used to derive the mean stress, e_m. (FLAC 2D 2003)

Computational geomechanics faces challenges in applying constitutive models to those are physical instability and exhibit high non-linear stress-strain behaviour which is path dependency. The *FLAC* uses its explicit and dynamic problem-solving ability with the aid of the constitutive models ranging from linear elastic models to highly nonlinear plastic models to address this issue.

Currently, *FLAC* has fourteen constitutive models to represent the geomechanical properties of the soil such as Modulus of elasticity, comprehensive strength of the soil etc.

- Null model: to represent the excavated/removed material.
- Elastic, isotropic model: This model represents the homogeneous, continuous materials where stress-strain behaviour presents as a linear relationship.
- Elastic, transversely isotropic mode: The elastic, transversely isotropic mode allows software to simulate layered elastic materials.
- Drucker Prager model: This model is used for materials with a low frictional angle, such as soft clay.
- Mohr-Coulomb model: This is a common plastic model, which represents the shear failure of the soil and rocks.
- Ubiquitous joint model: This model represents the anisotropic plastic models, which includes weak planes enclosed in the Moher coulomb model.
- Strain softening/hardening model: This criterion will represent the nonlinear softening and hardening behaviour of the material base on the Moher Coulomb properties.

- Bilinear strain softening/hardening ubiquitous joint model: This model will represent the softening or hardening material behaviour of the weak plane-based material.
- Double yielded model: The double yielded failure criterion characterises the material that undergoes irreversible compaction.
- Modified cam clay model:
  This criterion will be used to represent the cases where the volume change, bulk property and shear resistivity requires consideration.
- Hoek Brown model: Hoek Brown characterises stress conditions, resulting in a failure in rocks.
- The modified Hoek Brown model: This model represents the post failure plastic behaviour in term of the dilation angle.
- Cysoil model: The cap-yield soil used to represent the nonlinear behaviour of the soil.
- Simplified cysoil model: Simplified cysoil uses hyperbolic model parameters, which are input by the user. It also uses the Moher coulomb failure envelope.

The software uses the above criteria to simulate the behaviour of the structures constructed of various materials, which reach the plasticity deformation when it reaches the yielding limit.

3.4.5. Shear strength reduction method (SSRM)

With the development of computer technology over the past decades, numerical modelling has become an essential tool in geotechnical engineering. Stability analysis can be performed by the calculation of factors of safety in *FLAC* using the shear strength reduction method (*SSRM*). The *SSRM* is commonly applied through the factor of safety calculation by gradually reducing the shear strength of the testing material to estimate the point where the system reaches a state of limiting equilibrium. This method is popular in the stability analysis of slopes, retaining walls and tunnels, however, it has rarely been used in stability analysis of sinkholes. This study uses the shear strength reduction method (*SSRM*) with the aid of the built-in program language, *FISH*, to analyse the trapdoor problem.

This method was utilised as early as 1975 by Zienkiewicz et al. (1975), followed by Naylor (1982), Matsui et al. (1992), Ugai et al. (1995), Griffiths et al. (1999), Michalowski (2002), Zheng et al. (2005) and numerous other researchers. The *SSRM* is coded in the finite difference software *FLAC* as well as many other computational tools, such as Plaxis (2011) and *OptumG2* (2018).

In the method of shear strength reduction, a factor of safety is defined as the ratio of the actual undrained shear strength and the critical undrained shear strength, as shown in equation (3.2).

$$FoS = \frac{S_u}{S_c} \tag{3.2}$$

Where (S_u) is the actual undrained shear strength of the soil and (S_c) is a critical shear strength at collapse. In practice, the factor of safety above one demonstrates a stable condition.

In this study, the soil body is defined as a homogeneous, undrained clay, following the Tresca material. The shear strength reduction method (*SSRM*) is usually applied to the conventional model of Mohr-Columb material.

With this method, *FLAC* first brackets down the results to "stable" and "unstable".

A series of simulations are made by using trial values of factor F^{trial} to reduce the cohesion, c, and friction angle ϕ until slope failure occurs.

$$c^{trial} = \frac{1}{F^{trial}} c \tag{3.3}$$

$$\phi^{trial} = \arctan\left(\frac{1}{F^{trial}} \tan\phi\right) \tag{3.4}$$

In the second stage, the solution gradually reduces between "stable" and "unstable" until the solution falls below the tolerance (FLAC 2D 2003). To determine the boundary between a stable and unstable model, a series of individual runs with different strength reduction factors will be performed to determine if the model is at equilibrium, or if the continuing plastic flow has already reached. The final failure point with the aid of successive bracketing of strength reduction factor, would identify the failure point (FLAC 2D 2003).

3.4.6. FISH

FISH is a programming language, embedded within the *FLAC*. The function extends the *FLAC*'s functionality by allowing the user to define the parameters. For this study, a *FISH* code has been developed to generate the mesh in the *FLAC* environment and solve the issue automatically. Using the code, parametric studies can be conducted efficiently and effectively with a quick change of input parameters.

```
;------------------------------------------------------------------
;               3D FoS Trapdoor Collapse/Blowout Clay
;               1/4 Mesh
;               Tresca material; Associated plastic flow-
;------------------------------------------------------------------
; Developed by Dr. Jim Shiau, PhD(Newcastle)
; @ University of Southern Queensalnd, Toowoomba, QLD, 4350, Australia
; 31 August 2017
;------------------------------------------------------------------
new
        set echo on
        set log on

def g_cons
;;;;;;;;CHANGE the following parameters to suit your need;;;;;;;;;;
; -----------Set up all the parameters of the model
; -----------This is the place you can change problem geometry
; ----------- and material property
        H = 18.0                ;  Soil cover
        W = 6.0                 ;  width (W=L i.e. square opening)
        L = 30.0                ;  Length (W=L i.e. square opening)

        SOIL_DEN = 1834.86      ; Soil density
        SOIL_COH = 80000        ; A small 5 Pa to improve numerical stability
        SOIL_FRI = 0            ; zero for clay
        SOIL_DIL = 0            ; ** watch this value very carefully**
        SOIL_TENS = 1e10        ; very limited soil tension(N/m2, Pa)
        SOIL_Young = 16E6       ; Youngs Modulus
        SOIL_poisson = 0.49     ; Poisson's ratio

; -----------surface pressure set to zero in most cases (in pascal, N/m2)------
        Set_grav = -1 * 9.81    ; centrifuge model - more g

        Sigma_s = 0.0           ; For soft cases, better set sigma_s=0
        Sigma_t = 0.0           ; supporting pressure
; --------------For strong cases, non-zero sigma_s is reuqired to fail the soil.
        XElementSize = 1.0      ; element size;divide equally with B W & H
        YElementSize = 1.0      ; element size;divide equally with B W & H
        ZElementSize = 1.0      ; element size;divide equally with B W & H

;;;;;;;;CHANGE the above parameters to suit your need;;;;;;;;;;
```

Figure 3. 4 Input section of the shear strength reduction method script for *FLAC 3D*

Figure 3.4 presents a typical sample of the developed *FISH* code. Together with the use of batch analyses, it allows users to conduct parametric study both efficiently and effectively. Unlike the *FLAC* graphical interface (*GIIC*), the developed *FISH* code would assist users to run hundreds of cases automatically without user interference.

4. TWO-DIMENSIONAL ANALYSIS OF UNDRAINED SINKHOLE IN GREENFIELD CONDITION

4.1. Introduction

This chapter discusses the stability of trapdoors in an idealistic condition known as "unsupported greenfield", which can be applied to natural sinkholes, old hand digs tunnels and longwall coal mining where the unsupported roof collapses into the open cavity. In this chapter, the failure of a cavity underlying homogeneous clay is examined. Shear strength reduction technique is utilized to study two-dimensional failure mechanisms of a horizontal trapdoor by using the finite difference method (*FDM*). Numerical results are presented in form of a factor of safety (*FoS*) for various depths in dimensionless forms that are similar to Taylor's slope stability charts and verified by the finite element limit analysis technique with upper and lower bound theorems. Some practical examples are provided to demonstrate the usefulness of the design charts and tables. These charts gives a good approximation of *FoS* and can be used by engineers in their preliminary designs.

4.2. Problem definition and modelling technique

Figure 4.1 presents the schematic plot of an idealised two-dimensional sinkhole problem. The opening of the cavity is assumed to be horizontal, with the width represented by (W) and the depth by (H). The soil follows the Mohr-Coulomb failure criteria. For the current study of undrained clay, the friction angle (ϕ) is assumed to be zero and the undrained shear strength is represented by (S_u). Practically, a basic soil investigation will determine the shear strength (S_u) and the soil unit weight (γ), while a more advanced approach such as ground-penetrating radar (*GPR*) or electrical resistivity imaging (*ERI*) is required to reveal the depth (H) and the opening size (W) of a sinkhole.

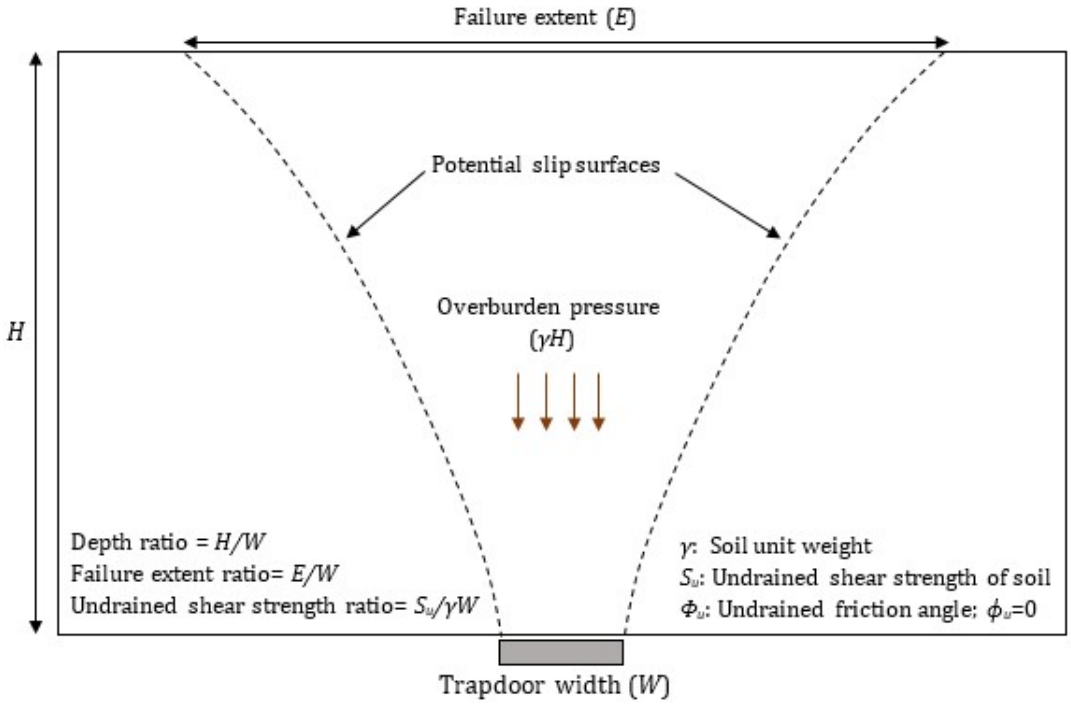

Figure 4. 1 Statement of the problem

A sinkhole with gradual formation has dynamic characteristics, meaning that the cavity size and shape may change over time. This complex behaviour would make the investigation impossible and it has been assumed that the cavity shape and size used in this study is an idealized two-dimensional horizontal trapdoor problem. To further simplify the study, both the surcharge load (σ_s) and the cavity's internal normal stress (σ_t) are not considered. The overlying soil is assumed to be homogeneous with constant unit weight (γ) and shear strength (S_u). The factor of

safety (*FoS*) therefore can be defined as a function of the depth ratio (*H/W*) and soil shear strength ratio ($S_u/\gamma W$).

$$FoS = f\left(\frac{H}{W}, \frac{S_u}{\gamma W}\right) \tag{4.1}$$

The finite difference software *FLAC* 2D (2003) and the shear strength reduction method (*SSRM*) were used to numerically examine 80 different cases in this study. A *FISH* script was developed to facilitate the automatic mesh generation and problem solving with a simple and direct input of problem parameters. The development provides an efficient tool for the current parametric study. A typical grid for simulating the trapdoor stability problem is shown in figure 4.2.

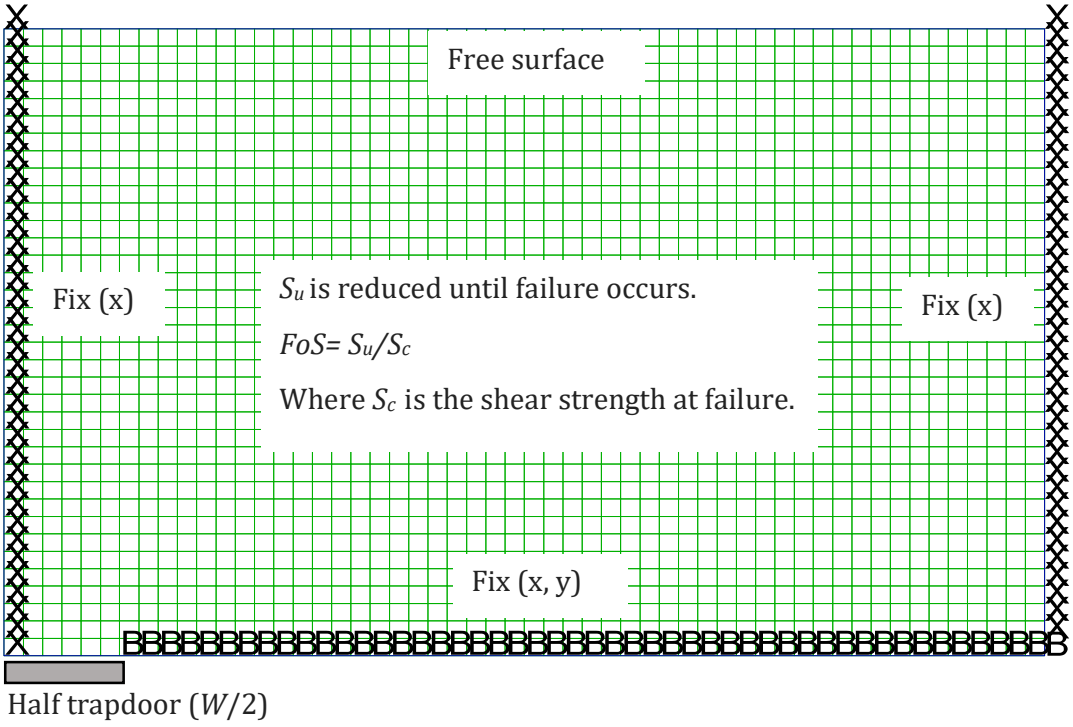

Figure 4. 2 Boundary condition and a typical half mesh with grids

A symmetrical boundary condition is utilised to minimize computational time. The symmetrical line has the boundary condition of "Fix (x)", which is the same as the right-hand side boundary condition. This "Fix (x)" condition allows vertical movement and represents a symmetrical boundary condition. The lower boundary grid points are restrained in both the vertical and horizontal directions, except

where the opening is located. The domain size is important when it comes to the right hand side boundary. It should be large enough to allow the displacement field to develop freely without giving any boundary constrains.

For a typical half mesh of H/W=3 with a total number of 648 elements, FLAC 2D requires CPU time of 4 minute using Optiplex 9020 desktop i7-4790 @ 3.60 GHz.

In this chapter, an extensive range of shear strength ratios ($S_u/\gamma W$ ranging from 0.2 ~ 2) and depth ratios (H/W = 1 ~ 10) were selected to complete the investigation. Design charts, tables and equation are presented throughout the study.

4.3. Results and discussions

Table 4.1 and 4.2 presents the (*FoS*) stability results for a horizontal opening in cohesive undrained soil.

Table 4. 1 *FoS* results obtained by using *SSRM* in *FDM* for *H/W*= 1 to 5

	FoS				
SSR	*H/W=1*	*H/W=2*	*H/W=3*	*H/W=4*	*H/W=5*
0.2	0.43	0.39	0.33	0.28	0.25
0.4	0.86	0.78	0.66	0.56	0.5
0.6	1.29	1.17	0.99	0.85	0.74
0.8	1.72	1.56	1.31	1.13	0.99
1	2.16	1.95	1.64	1.41	1.24
1.3	2.8	2.53	2.13	1.83	1.61
1.6	3.45	3.11	2.63	2.26	1.99
2	4.31	3.89	3.28	2.82	2.48

Table 4. 2 *FoS* results obtained by using *SSRM* in *FDM* for *H/W*= 6 to 10

	FoS				
SSR	*H/W=6*	*H/W=7*	*H/W=8*	*H/W=9*	*H/W=10*
0.2	0.22	0.2	0.19	0.17	0.16
0.4	0.44	0.4	0.37	0.34	0.31
0.6	0.67	0.6	0.55	0.51	0.47
0.8	0.89	0.8	0.74	0.68	0.63
1	1.11	1.01	0.92	0.85	0.79
1.3	1.44	1.31	1.19	1.1	1.03
1.6	1.76	1.61	1.47	1.36	1.26
2	2.22	2.01	1.84	1.7	1.58

SSR: Shear Strength Ratio ($S_u/\gamma W$)

What stands out from this table is the clear impact of shear strength ratio (*SSR* = $S_u/\gamma W$) and depth ratio (*H/W*) on the factor of safety (*FoS*). A graphical representation of the tables is also shown in figure 4.3.

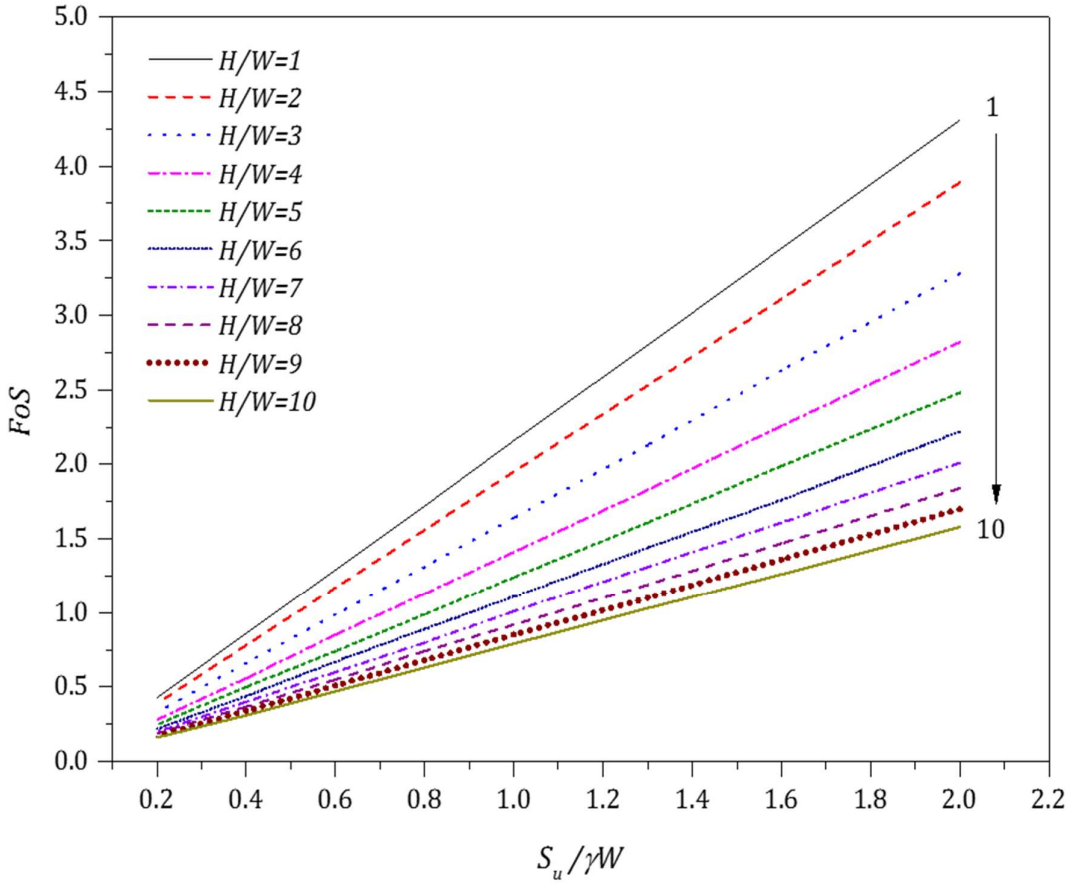

Figure 4. 3 *FoS* vs shear strength ratio *($S_u/\gamma W$)*

This figure shows a linear relationship between *FoS* and shear strength ratio ($S_u/\gamma W$) for various depth ratios (*H/W*), ranging from 1 to 10. A critical shear strength ratio $(S_u/\gamma W)_{critical}$ can therefore be defined as ($S_u/\gamma W FoS$) owing to its linear relationship.

Figure 4.4 highlights the effect of overburden pressure (γH) in cohesive soil. For a given strength ratio ($S_u/\gamma W$) and known depth ratio (*H/W*), the *FoS* can be obtained from the figure 4.4. Further investigation of figure 4.4 reveals the nonlinear relationship between *FoS* and depth ratio (*H/W*) for any given shear strength ratio ($S_u/\gamma W$).

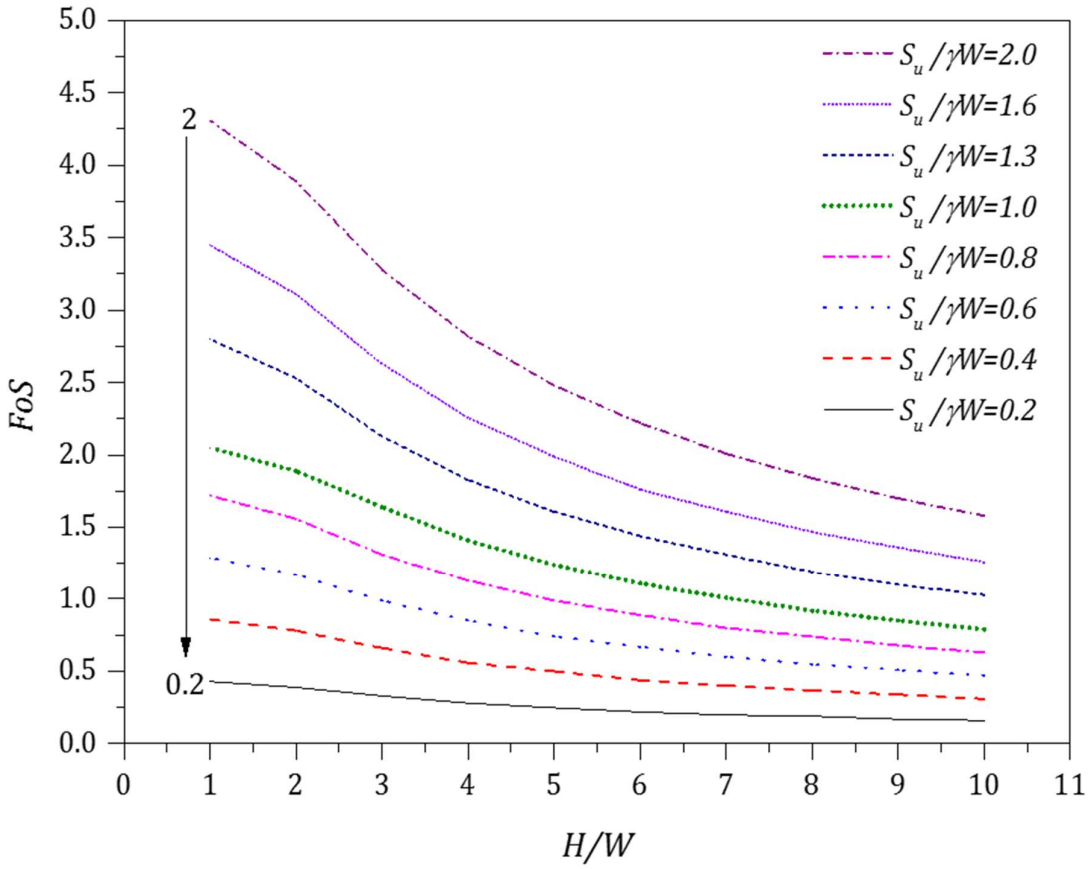

Figure 4. 4 *FoS* vs depth ratio (*H/W*)

As shown, the *FoS* value decreases nonlinearly as the depth ratio (H/W) increases. Indeed, for the homogeneous cohesive soil with a constant shear strength ratio, the increase of overburden pressure (γH) would reduce the stability, and thus the value of *FoS*. This suggests that none or very little arching support is developed for the current study of homogeneous cohesive soils with zero internal soil frictional angle (ϕ). For this cohesive material, the shear strength (τ) is not dependent on the normal stresses (σ) and the ($tan\phi$) in the Mohr-Coulomb model. The vertical stress above the cavity opening may experience a pressure that is close to the overburden pressure (γH). In addition to the "material" arching, the geometric arching is not sufficient to provide extra arching support for deep cases. A possible explanation for not experiencing the large magnitude of arching in this study is the idealised horizontal opening, which reduces the soil's ability to generate arching support. Stress distribution can be a good indicator to detect the arching. Figure 4.5 and 4.6 shows the principle stress plot for H/W=3 and 8 respectively.

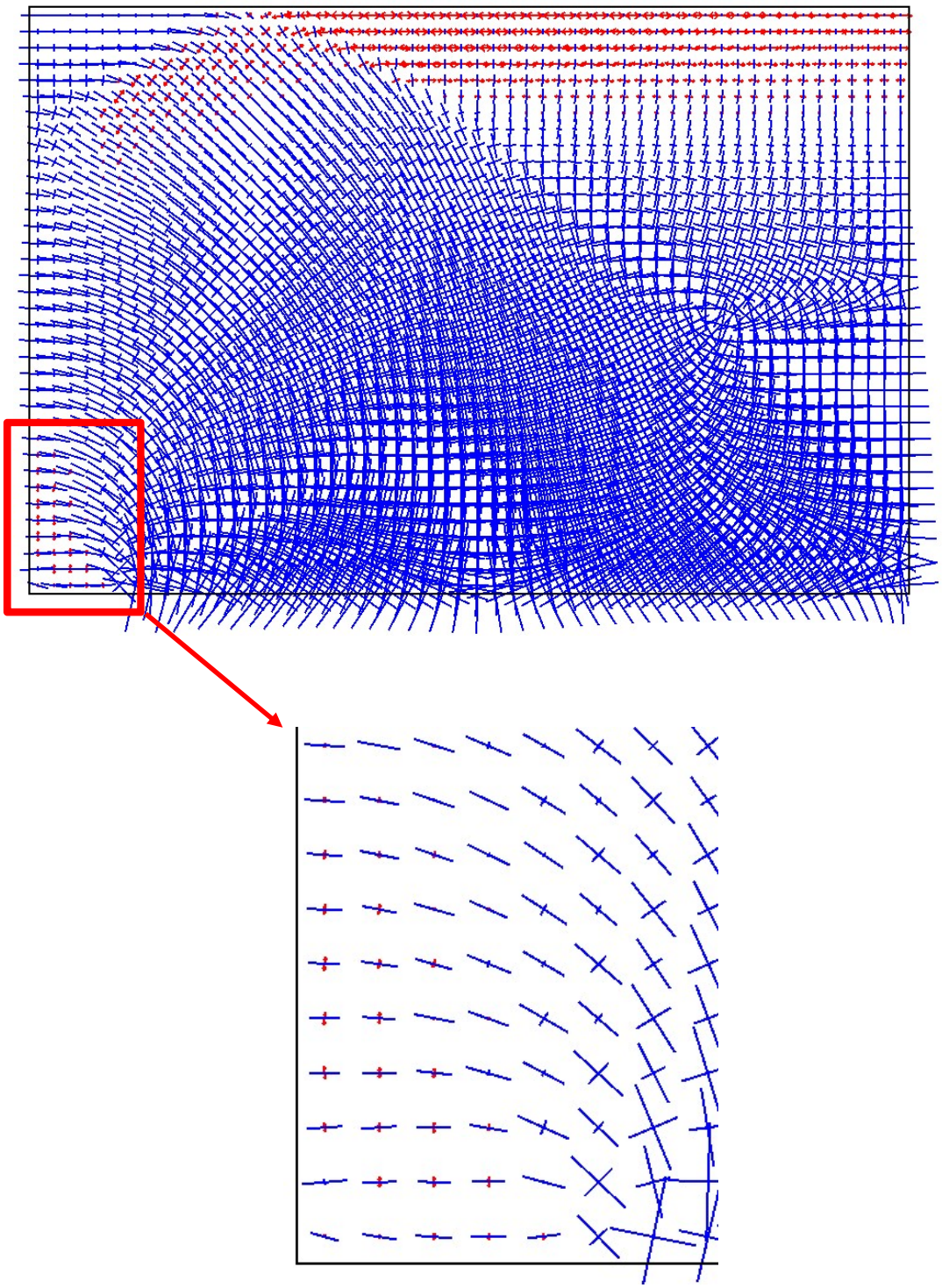

Figure 4. 5 Principle stress plot (H/W=3)

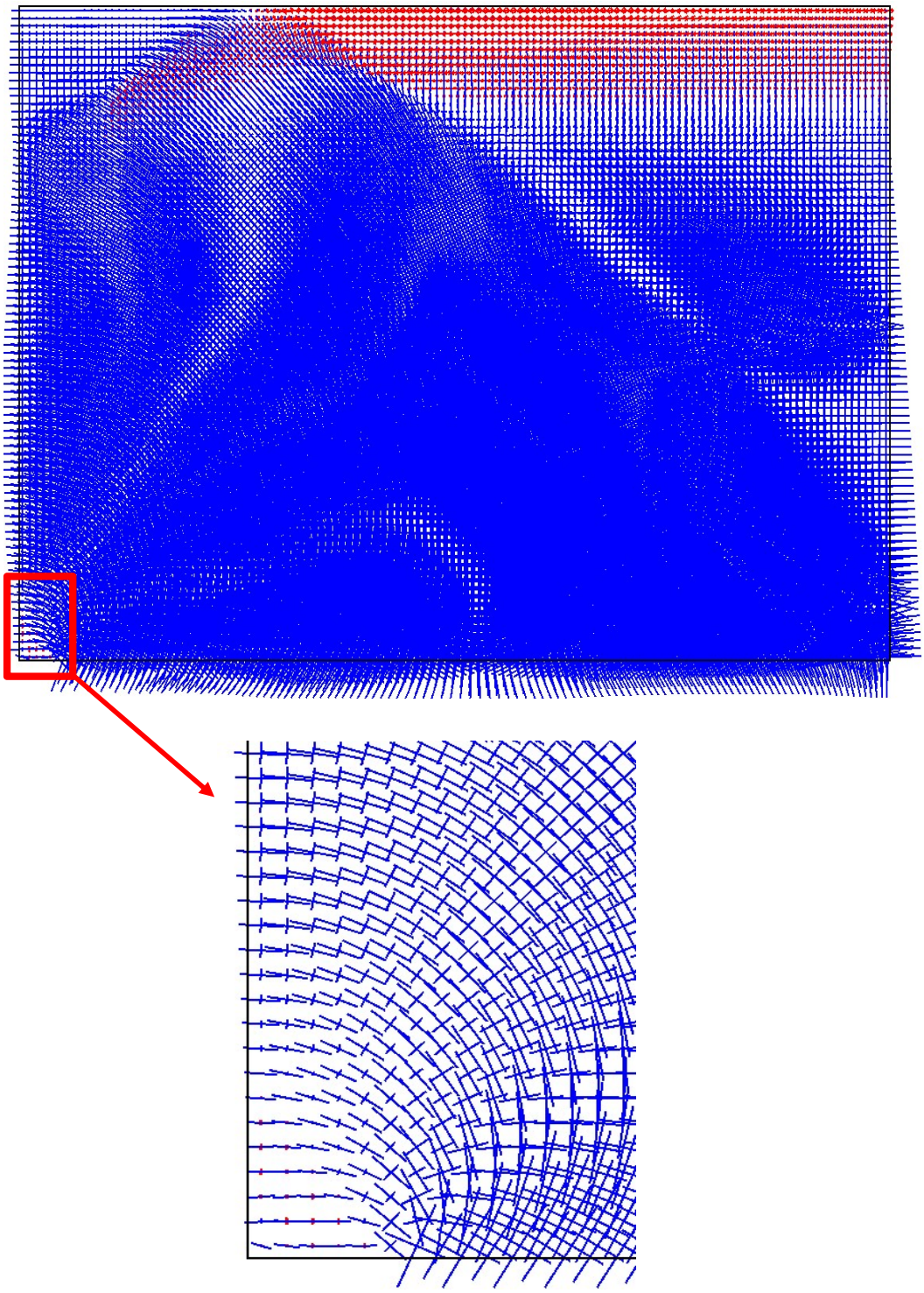

Figure 4. 6 Principle stress plot (H/W=8)

Closer inspection of the figures reveals that the stresses are being redistributed from the yielded soil particles (above the trapdoor opening) into the immediate adjacent soil particles in non-yielded part. The process creates the shearing resistance which resists the soil downward movement. This effect is more noticeable in deeper case.

Vermeer et al. (2002, 2003) suggested that more arching can be expected in three-dimensional analyses, and therefore, 3D solutions are always conservative when compared to two-dimensional ones.

Owning to linear relationship given in figure 4.3, the failure envelope can be determined to represent the parameters. The failure envelope represents the critical value of parameters when *FoS*=1. Table 4.3 represents the value of the failure envelope.

Table 4. 3 Data used for plotting figure 4.7

H/W	$S_u/(\gamma W\ FoS)$
1	0.46
2	0.51
3	0.61
4	0.71
5	0.81
6	0.90
7	1.00
8	1.08
9	1.18
10	1.27

Note that, as *H/W* increase the value of the failure envelope increase as well. This means that as depth increase, more support needed to keep the system in equilibrium. The results also highlights the effect of the overburden pressure on the stability of unsupported cavity.

Alternatively, failure envelope can be represented as in figure 4.7. It shows the relationship between the critical shear strength ratio ($S_u/\gamma W\ FoS$) and the depth ratio (*H/W*).

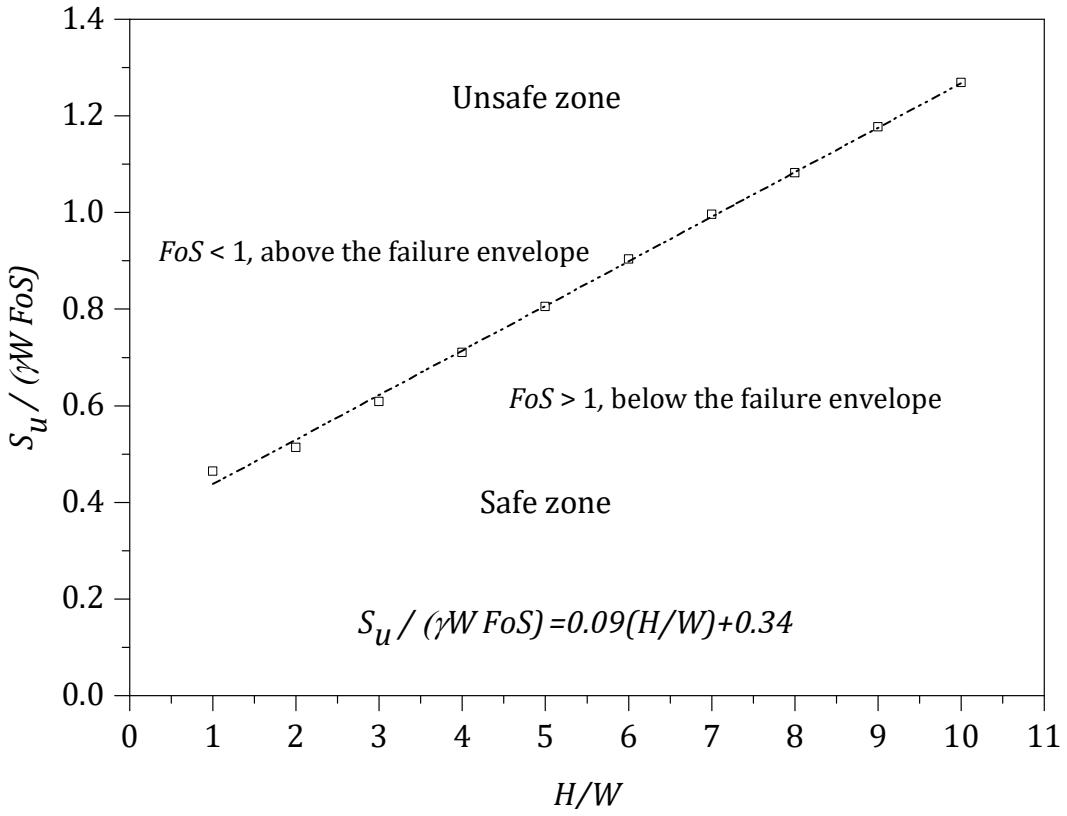

Figure 4. 7 Failure envelope for stability designs

The linear failure envelope separates the safe zone (*FoS* >1) with the unsafe one (*FoS* <1). This linear relationship is represented in equation 4.2 is obtained by linear curve fitting of the data with high accuracy of r^2=0.99. The equation 4.2 can be used to determine some of the critical design parameters such as depth (*H*), opening width (*W*), and undrained shear strength S_u.

$$\frac{S_u}{\gamma W FoS} = 0.09\left(\frac{H}{W}\right) + 0.34 \tag{4.2}$$

Equation (4.2) can be further transformed to equation (4.3) to calculate *FoS*. This equation is useful for practical engineers to determine the *FoS* during their preliminary design stage.

$$FoS = \frac{S_u}{[0.09(\frac{H}{W}) + 0.34]\gamma W} \tag{4.3}$$

4.3.1. Failure extent

Results of the failure extent (E) study are presented in table 4.4. The values of (E) were obtained by measuring the deformed surface of the non-zero plastic shear strain rate from program output plots.

Table 4. 4 Determination of failure extent

Depth ratio (H/W^*)	Actual depth, H (m)	Measured half surface failure extent, $E/2$ (m)	#Failure angle $\theta = \tan^{-1}(H/(E/2))$ in degree	Ratio of failure extent to trapdoor width (E/W) +
1	6	4.5	53.1	1.50
2	12	8.5	54.7	2.83
3	18	12.0	56.3	4.00
4	24	15.5	57.1	5.17
5	30	20.5	55.7	6.83
6	36	24.0	56.3	8.00
7	42	28.0	56.3	9.33
8	48	32.0	56.3	10.67
9	54	36.0	56.3	12.00
10	60	41.5	56.3	13.83

* Cavity width W = 6 (m)

Failure angle θ is defined as the arctangent of ($2H/E$). See figure 4.8 for details.

+Table 4.4 is for all values of strength ratio S_u/YW. For undrained clay, the failure extent is independent of S_u/YW.

The data in table 4.4 is also graphically shown in figure 4.8 where (E/W) is defined as the failure extent ratio and plotted against the depth ratio (H/W).

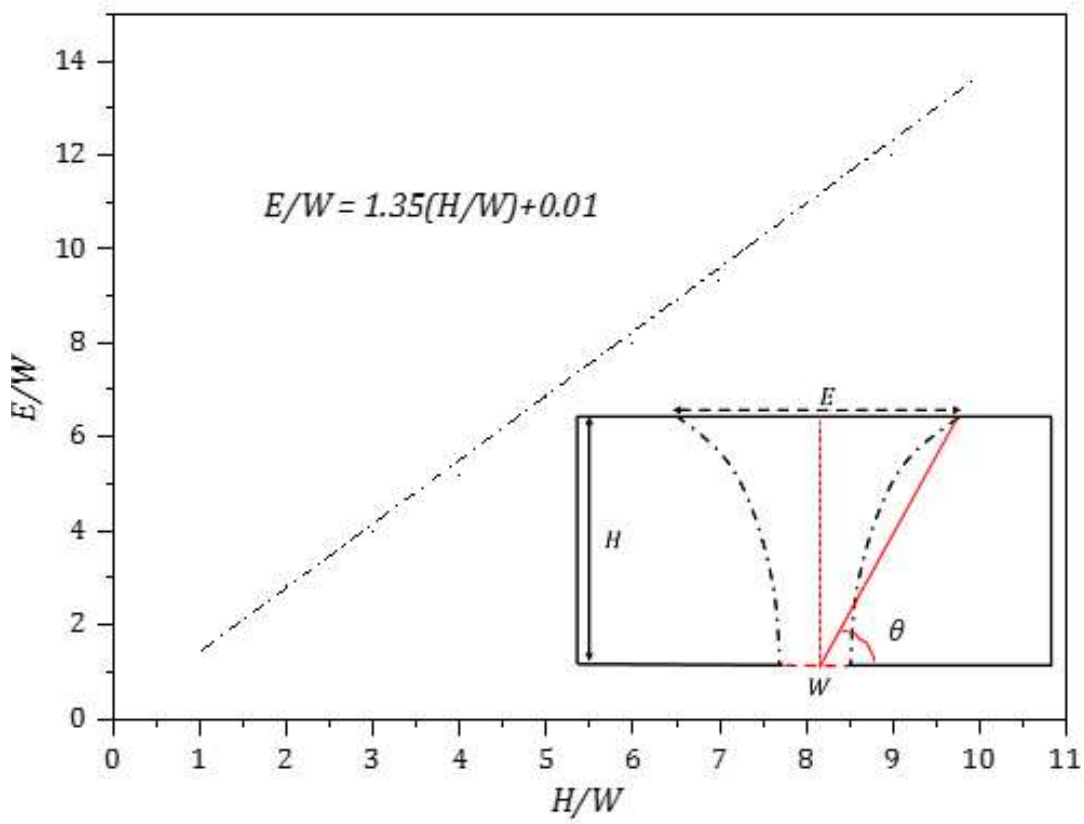

Figure 4. 8 Design chart for the determination of failure extent

Figure 4.8 suggests that the failure extent ratio (*E/W*) is associated directly with the depth ratio (*H/W*). It can be seen that (*E/W*) increases linearly with (*H/W*). A linear regression analysis gives equation 4.4.

$$\frac{E}{W} = 1.35\left(\frac{H}{W}\right) + 0.01 \tag{4.4}$$

By ignoring the *y* interceptor (0.01), a gradient of 1.35 for the linear line can be adopted, meaning that (*E/W*) is approximately 1.35 time larger than the depth ratio (*H/W*). A 56-degree line can therefore be drawn from the centre of the trapdoor to the ground surface to indicate the failure extent. Note that this result is for all values of shear strength ratios ($S_u/\gamma W$).

Figure 4.9 shows the non-zero shear strain rate plots of three selected cases ($S_u/\gamma W$ = 0.4, 1 and 2). The shear strain rate plot is normally used to display possible collapse mechanisms. It represents the zone of plastic deformation for a perfectly elastic-plastic soil model where the actual strain cannot be determined.

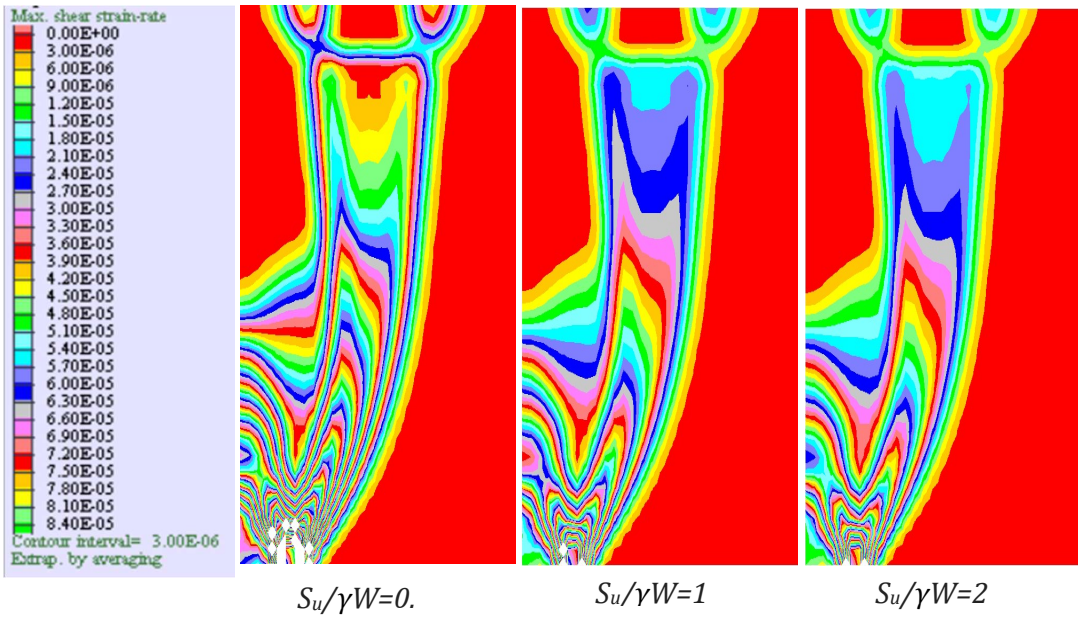

Figure 4. 9 Plots of shear strain rate (*H/W*=3 and values of $S_u/\gamma W$=0.4, 1and 2)

As shown in figure 4.9, no significant differences were found between the surface failure extents when the strength ratio $S_u/\gamma W$ is varied. This is due to the nature of the shear strength reduction technique for the undrained soil were no volume changes allowed during plastic shearing.

Figures 4.10 to 4.12 present the shear strength rate plots of three different depth ratios (*H/W*=1, 5 and 10).

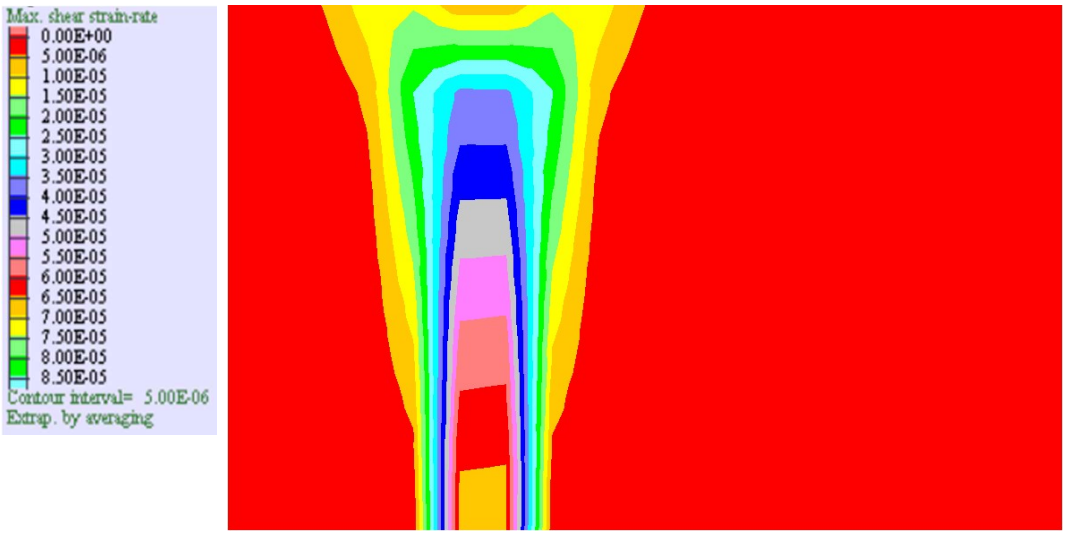

Figure 4. 10 Shear strain rate (*H/W*=1 and $S_u/\gamma W$=1)

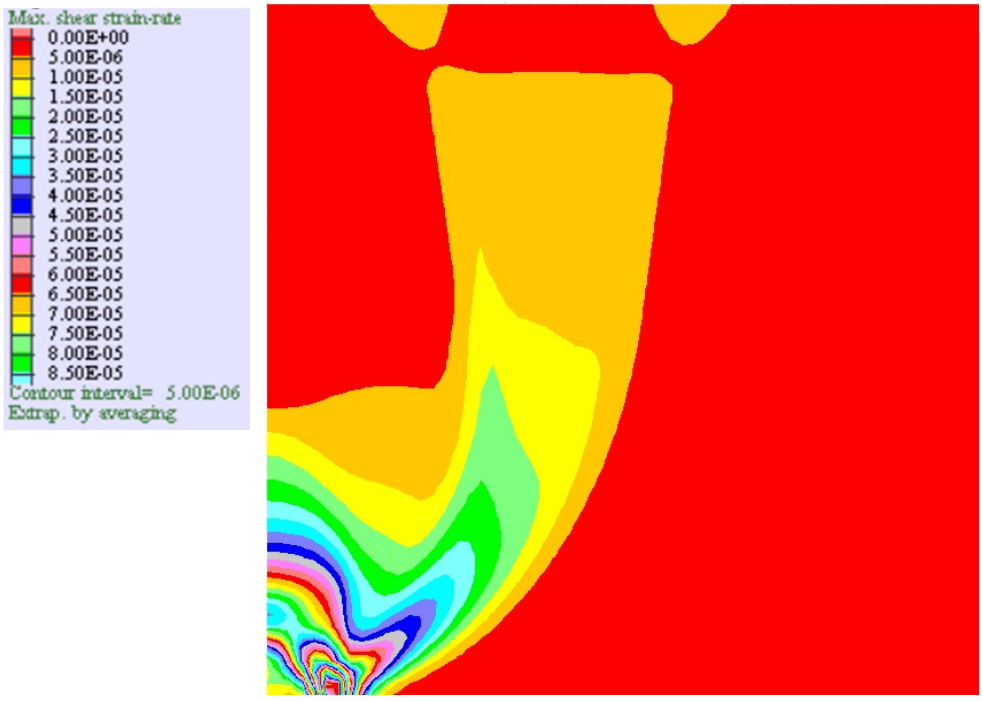

Figure 4. 11 Shear strain rate (H/W=5 and $S_u/\gamma W$=1)

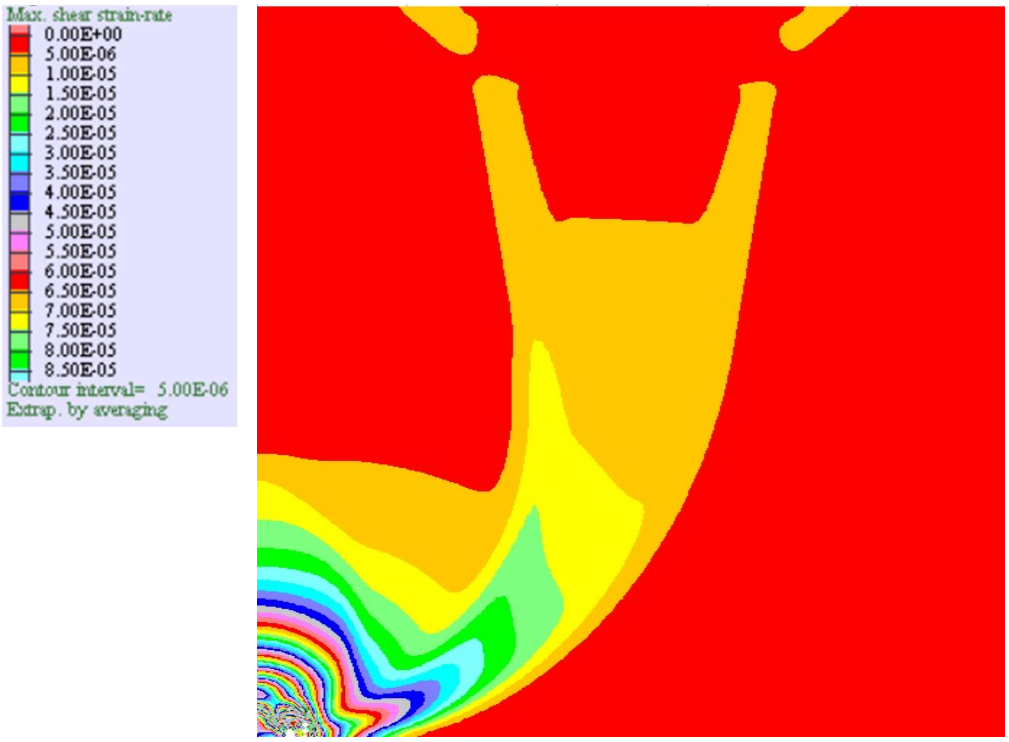

Figure 4. 12 Shear strain rate (H/W=10 and $S_u/\gamma W$=1)

Careful inspection of the failure mechanism in figures 4.10 to 4.12 suggests that, unlike the strength ratio, the depth ratio (*H/W*) does have certain effect on the extent of surface failure. As the depth ratio (*H/W*) increases, the failure extent also increased. The absolute values of the non-zero shear strain rates (*SSR*) are not important in a perfectly plastic material model and are therefore not in these figures.

Figures 4.13 to 4.15 present velocity vector plots of *H/W*=1, 5 and 10 respectively. Velocity vector indicates the movement of soil particles and can also be used to determine the overall failure mechanism.

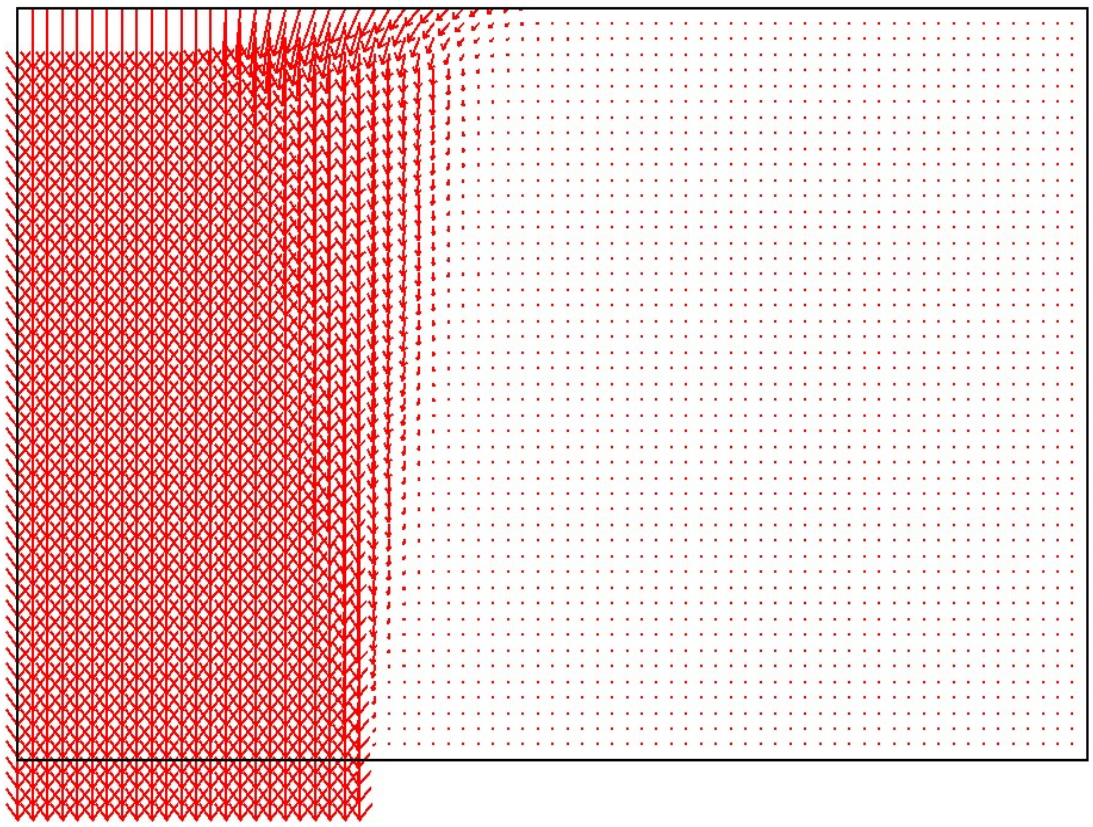

Figure 4. 13 Velocity vector plot (*H/W*=1 and all values of $S_u/\gamma W$=1)

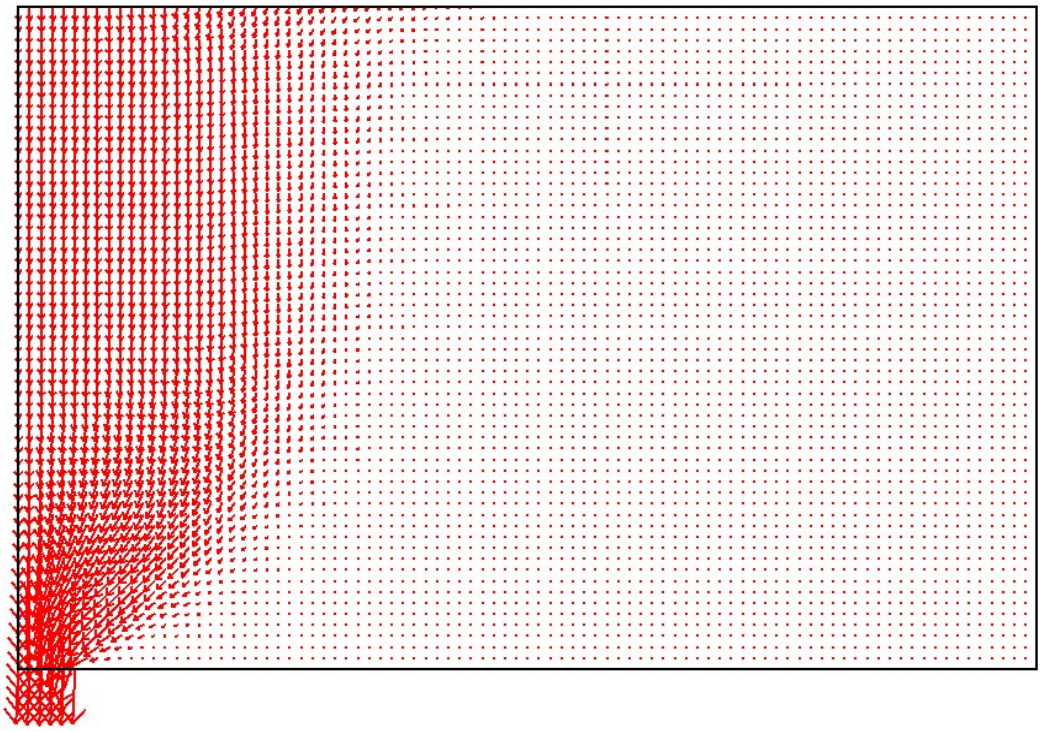

Figure 4. 14 Velocity vector plot (H/W=5 and all values of $S_u/\gamma W$=1)

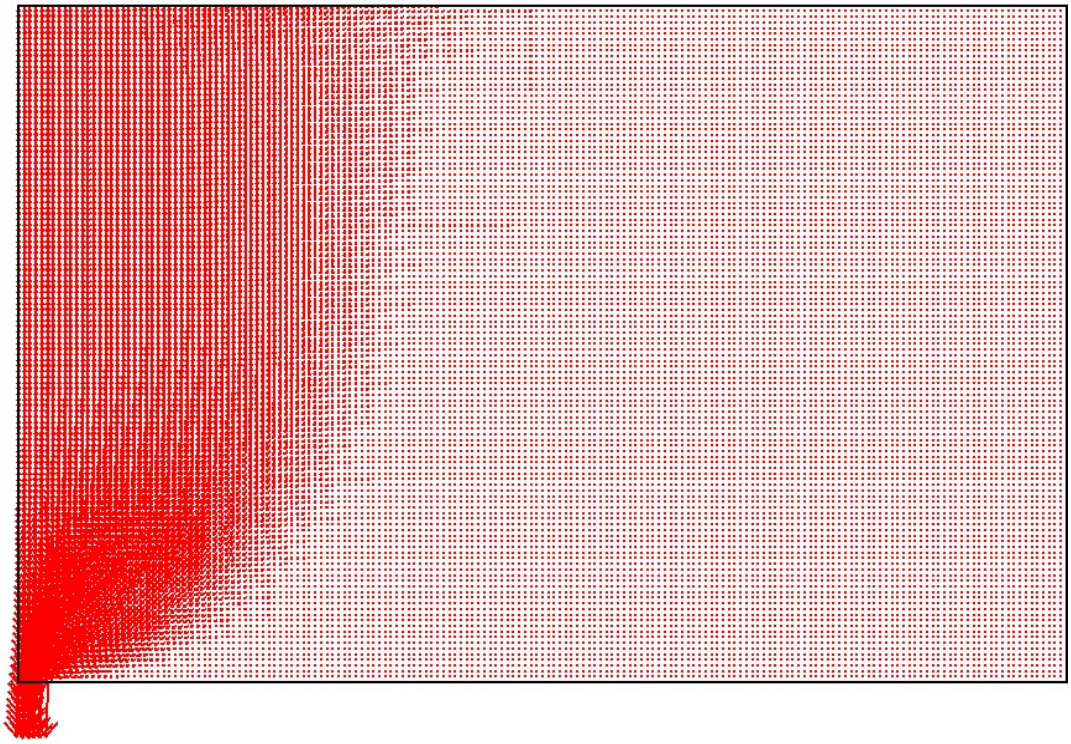

Figure 4. 15 Velocity vector plot (H/W=10 and all values of $S_u/\gamma W$=1)

A review of the velocity vector plots shown in figures 4.13 , 4.14 and 4.15 suggests that when the depth increases a larger part of the soil is being funnelled toward the trapdoor opening. The comparison of the plots confirms that the surface failure extent is directly associated with the depth, which means that as the depth increases the failure surface extent increases.

4.3.2. Comparison of results

The use of *SSRM* and *FoS* is prevalent in the analysis of slope stability. However, this process is uncommon when it comes to estimating the stability of an underground cavity. Hence, the author was not able to find any published literature to compare to the *FoS* results. The results obtained from finite difference method are compared with unpublished work of Shiau et al. (2019) which utilized the finite limit analysis method to obtain the solutions. Table 4.5 presents the results of *FDM* and the rigorous upper bound and lower bound solutions of Shiau et al. (2019) analysis.

Table 4. 5 *FoS* results of *FDM* and *FELA LB* and *UB* for ($S_u/\gamma W$=1)

	This study	Shiau et al. (2019)	
H/W	*FLAC*	*G2 UB*	*G2 LB*
1	2.16	1.98	1.92
2	1.95	1.85	1.80
3	1.64	1.59	1.55
4	1.41	1.38	1.34
5	1.24	1.21	1.19
6	1.11	1.09	1.06
7	1.01	0.99	0.96
8	0.92	0.91	0.88
9	0.85	0.84	0.81
10	0.79	0.78	0.75

In general, it found that the finite difference results are consistently higher than the upper bound results by approximately 3%. The comparison results also can be represented by the figure 4.16.

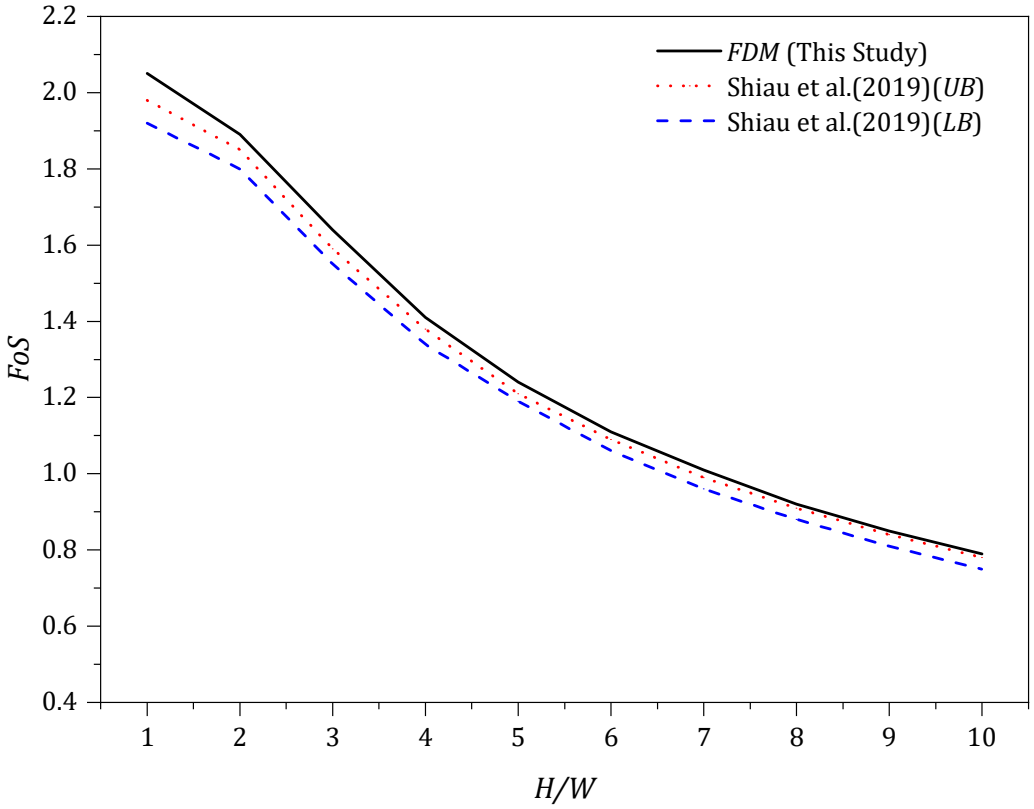

Figure 4. 16 *FoS* comparison – *FDM* vs *FELA* ($S_u/\gamma W=1$)

As shown in figure 4.16, the finite difference method results are in good agreement with those obtained from the upper and lower bound solutions. This comparison has greatly enhanced the confidence level in the current finite difference results.

4.3.3. Practical examples

In addition to equation 4.3, where *FoS* can be calculated with any input values of shear strength ratio ($S_u/\gamma W$) and (H/W), a design chart in the form of a contour map is also provided in figure 4.17.

This chart can be best demonstrated practically through a number of examples.

Example 1 - to determine the factor of safety (FoS)

The following data has been provided: H=10 m, W=2 m, γ= 18 kN/m^3 and S_u=50 kPa. It is required to determine the factor of safety.

1. Given $H/W=5$ and $S_u/\gamma W = 1.39$, figure 4.3 returns a *FoS* value of approximately 1.74.

2. Using equation 4.3, a value of *FoS* = 1.75 is obtained.
3. Using Figure 4.17, a value of *FoS* = 1.71 is approximately determined.
4. An actual computer analysis of this case using *FDM* gives *FoS* = 1.76.

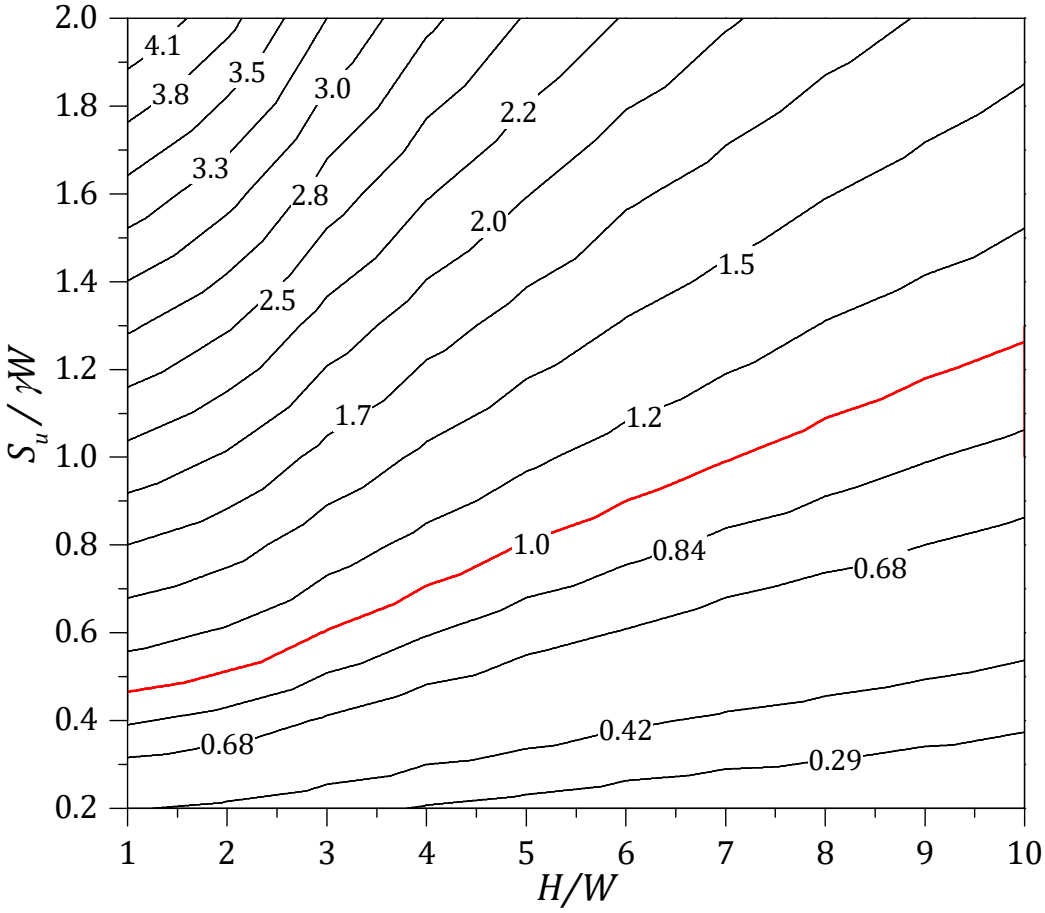

Figure 4. 17 Stability design chart – (*H/W, S_u/YW and FoS*)

Example 2 - to determine the critical depth ratio (H/W)

The client requires an estimation of the depth of an existing sinkhole. The following parameters are available: S_u= 54 kPa, W=3 m, γ= 18 kN/m^3 and *FoS* = 1.0

1. Equation 4.2 returns a value of H/W=7.33.
2. Figure 4.4 approximately give a value of H/W= 7.25.

Example 3 – to determine the failure extent (E)

To determine the extent of surface failure due to cavity collapse in cohesive undrained soil, where H = 20 m, W = 4 m, S_u = 28 kPa and γ = 18 kN/m^3.

1. Using H/W = 5, equation 4.4 gives E/W=6.76.

2. Using H/W = 5, figure 4.8 gives an approximate value of E/W=6.9.
3. The non-zero plastic shear strain rate and velocity vector plot from the actual finite difference analysis gives approximately E = 28.5 m. Written in dimensionless form, E/W=7.13.

4.4. Conclusion

The stability and extent of the surface failure of a plane strain opening in undrained clay in an unsupported greenfield condition, which is the case in sinkholes and coal longwall mining, are studied in this study. A *FISH* script has been developed to study 80 different cases by adopting a shear strength reduction method (*SSRM*) in the finite element difference method software *FLAC*. Following Taylor's slope stability approach, results are presented in the form of the factor of safety (*FoS*). Numerical solutions are then compared with a rigorous upper and lower bounds solution in the finite limit analysis, which showed the competency of the obtained results.

The results suggested that the *FoS* value decreases nonlinearly as the depth ratio (H/W) increases. This finding suggest that very little arching support is developed for the current study of homogeneous cohesive soils with zero internal soil frictional angle (ϕ). Additionally, the study of non-zero plastic shear strain rates and velocity vectors also suggested that the arching has minimal effect in the current plane strain study of undrained clay. The study showed that the failure extent ratio increases linearly with the depth ratio. It was concluded that the total surface failure extent (E) is approximately 1.35 times larger than the depth (H).

The *FoS* approach to sinkhole and longwall mining collapse provides a simple solution for the estimation of cavity failure. To assist designers, these numerical results are presented in the form of a dimensionless design chart just like a Taylor design chart (Taylor, 1937) and examples are demonstrated to show the use of the design charts. Recommendations for future work may include the investigation of three-dimensional responses, which is to be discussed in the next chapter.

5. THREE-DIMENSIONAL ANALYSIS OF UNDRAINED SINKHOLE IN GREENFIELD CONDITION

5.1. Introduction

Following Chapter 4, which has investigated the two-dimensional stability of unsupported greenfield, this chapter advances the study of cavity's stability underlying homogeneous clay in an unsupported greenfield condition in a realistic three-dimensional condition. In this chapter, shear strength reduction technique is utilised to study the three-dimensional failure mechanisms of a rectangular and square trapdoor by using the finite difference program, *FLAC*. The stability results are presented in the form of a factor of safety and a failure extent ratio for various dimensionless ratios and verified by using the finite element limit analysis technique with upper and lower bound theorems. In addition, the three dimensional numerical solutions used to estimate the failure surface extent.

The 3D numerical results are compared with 2D results which was obtained earlier in Chapter 4 as well as other available solutions. A number of practical examples are provided to demonstrate the use of design charts and tables.

5.2. Problem definition

The sinkhole propagation process is a complex procedure. It is not possible to predict the exact behaviour of sinkholes over the time. Hence, this study assumes an idealised three-dimensional horizontal trapdoor and assumes that the propagation process is at the last stage where the cavity is big enough to cause a collapse failure.

Figure 5.1 presents an idealised horizontal trapdoor problem underlying undrained homogeneous clay layer with constant unit weight (γ) and shear strength (S_u).

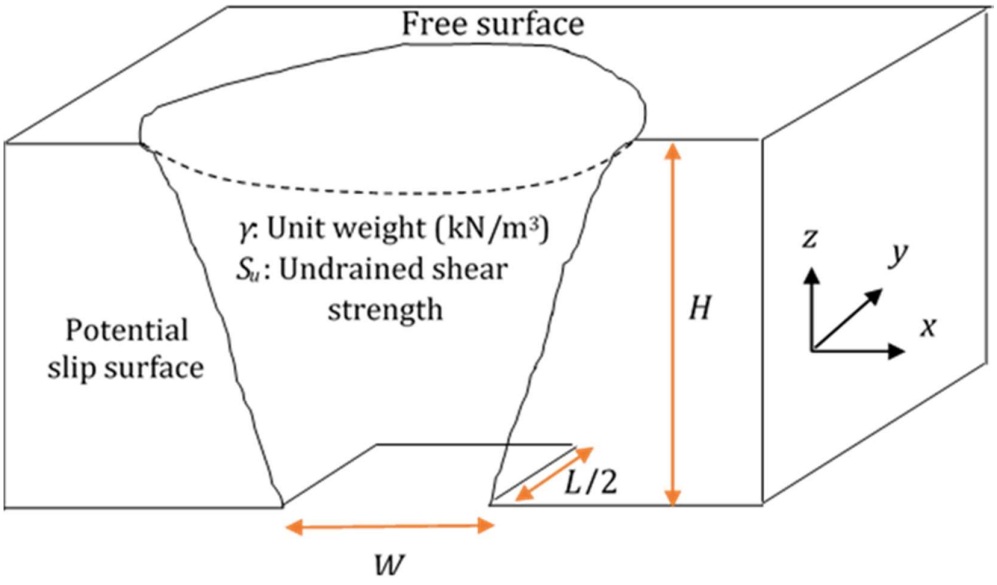

Figure 5. 1 An idealised sinkhole problem

The three-dimensional soil body is modelled as uniform Tresca material, which is the same as Mohr-Coulomb material when the soil friction angle (ϕ) is zero. The opening of the cavity is assumed to be horizontal, with the width represented by (W) in the x direction, the length (L) in the y direction and the height represented by (H) in the z direction.

To cover a wide range of practical parameters, an extensive range of depth ratios (H/W= 1 to 6), width ratios (L/W=1 to 10) and shear strength ratios ($S_u/\gamma W$= 0.2 to 2) were chosen for the parametric studies. Note that the shear strength ratio is defined following Taylor's method and the *FoS* can be defined as a function of the

shear strength ratio ($S_u/\gamma W$), the depth ratio (H/W) and the width ratio (L/W). This relationship is shown in equation 5.1.

$$FoS = f\left(\frac{S_u}{\gamma W}, \frac{H}{W}, \frac{L}{W}\right) \tag{5.1}$$

However, when the cavity length (L) is very large ($L/W = \infty$), the problem is considered as a two-dimensional plane strain. Consequently, the *FoS* is only a function of the strength ratio ($S_u/\gamma W$) and depth ratio (H/W), as shown in equation 5.2.

$$FoS = f\left(\frac{S_u}{\gamma W}, \frac{H}{W}\right) \tag{5.2}$$

5.3. Modelling technique

Both the two- and three-dimensional finite difference software and shear strength reduction method (*SSRM*) developed by *ITASCA* (2013) were employed to examine the trapdoor stability in undrained cohesive soil. Built-in *FISH* scripts were also developed for the problem to facilitate the auto mesh generation, and hence allow parametric studies to be conducted efficiently. For the purpose of validating the model, three different mesh types were established; the full, half and quarter meshes. Internal verification and model validation of the solution revealed that results from full, half or quarter meshes were almost identical. This has greatly enhanced the level of confidence in the current 3D development.

A typical half grid for simulating a trapdoor problem is shown in figure 5.2. Although the mesh shows perfect square cubes, *FLAC* 3D uses a mixed discretisation technique of various element shapes such as wedges, pyramids, bricks and tetrahedrons to form and solve the problem (Abbasi et al. 2013).

An important element in the numerical study which would influence the sensitivity and reliability of the results are the boundary conditions and domain size. For this study, a symmetrical boundary condition was employed to reduce the computational time. While the faces at the two sides and at the back of the model are restrained in x and y directions, the front face is only fixed in the y-direction,

allowing the soil particles to move in both x and z-directions. The lower boundary grid points are fixed in the x, y and z-directions except where the trapdoor openings are specified. The other important consideration for 3D numerical studies is the domain size, which could influence the sensitivity and reliability of the results. It is necessary to ensure that the velocity field is not affected by the finite domain size. In general, the output contour plot of the velocity field can estimate the required domain size. The domain size is particularly required more attention when it comes to the large values of *L/W*.

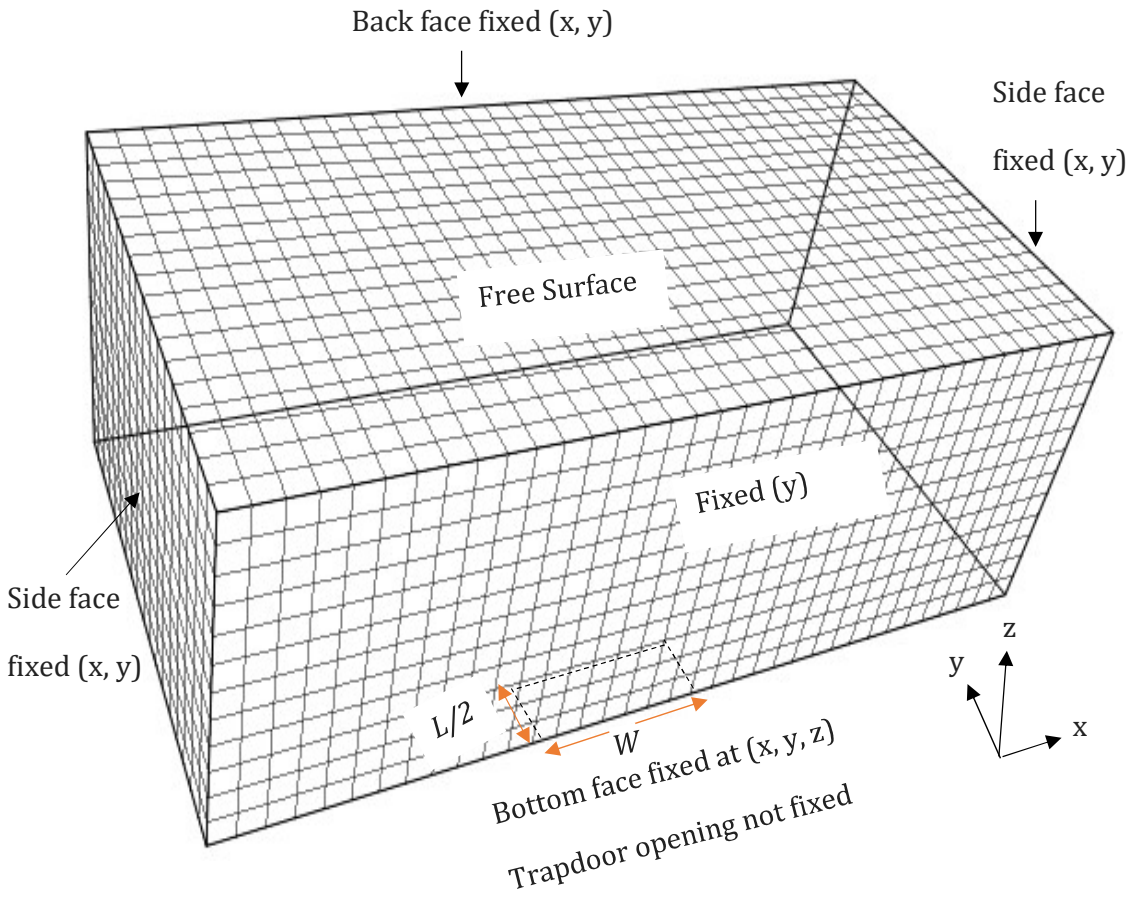

Figure 5. 2 Typical half mesh and boundary condition

For a typical half mesh of H/W=3 with a total number of 8747 elements, FLAC 3D requires CPU time of 38 minutes using Optiplex 9020 desktop i7-4790 @ 3.60 GHz.

This chapter adopts the shear strength reduction method (*SSRM*) for three-dimensional stability analysis of trapdoor problem in undrained homogeneous layer

of clay. Additionally, the vertical velocity plots of the finite difference method software employed to determine the surface subsidence due to collapse of the sinkhole. The results of this study then compared with available sources.

5.4. Results and discussion

A combination of wide range of depth ratio (*H/W*= 1-6), strength ratio ($S_u/\gamma W$) and opening ratio (*L/W*= 1-10) utilizes to investigate all possible situations associated with the trapdoor stability. The factor of safety (*FoS*) results obtained by utilizing the shear strength reduction method in 3D finite difference method software which discussed previously. The factor of safety results of this investigation are presents in tables 5.1 and 5.2.

Table 5. 1 *FoS* results for *H/W*=1 to 6, $S_u/\gamma W$=*0.2* to *2* and *L/W*=1 to 5

H/W	*Su/γW*	*FoS*				
		L/W=1	*L/W=2*	*L/W=3*	*L/W=4*	*L/W=5*
1	0.2	0.85	0.69	0.63	0.59	0.56
2	0.2	0.71	0.58	0.53	0.5	0.47
3	0.2	0.61	0.51	0.46	0.43	0.41
4	0.2	0.54	0.45	0.4	0.38	0.36
5	0.2	0.48	0.4	0.36	0.34	0.32
6	0.2	0.43	0.36	0.33	0.31	0.29
1	0.6	2.54	2.08	1.88	1.76	1.67
2	0.6	2.13	1.75	1.59	1.49	1.42
3	0.6	1.84	1.52	1.37	1.29	1.23
4	0.6	1.62	1.34	1.21	1.14	1.09
5	0.6	1.44	1.19	1.08	1.02	0.97
6	0.6	1.3	1.08	0.98	0.92	0.88
1	0.73	3.09	2.53	2.28	2.14	2.03
2	0.73	2.6	2.13	1.93	1.81	1.72
3	0.73	2.24	1.84	1.67	1.57	1.5
4	0.73	1.97	1.62	1.47	1.38	1.32
5	0.73	1.76	1.45	1.32	1.24	1.18
6	0.73	1.58	1.31	1.19	1.12	1.07

Continue Table 5.1

H/W	*Su/γW*	*FoS*				
		L/W=1	*L/W=2*	*L/W=3*	*L/W=4*	*L/W=5*
1	1	4.23	3.46	3.13	2.93	2.79
2	1	3.56	2.92	2.64	2.48	2.36
3	1	3.07	2.53	2.29	2.15	2.05
4	1	2.7	2.23	2.02	1.9	1.81
5	1	2.41	1.99	1.81	1.7	1.62
6	1	2.17	1.8	1.63	1.53	1.47
1	1.5	6.35	5.19	4.69	4.39	4.18
2	1.5	5.34	4.38	3.96	3.71	3.54
3	1.5	4.6	3.79	3.43	3.22	3.07
4	1.5	4.04	3.34	3.03	2.84	2.71
5	1.5	3.61	2.98	2.71	2.54	2.43
6	1.5	3.26	2.7	2.45	2.3	2.2
1	2	8.47	6.92	6.25	5.85	5.57
2	2	7.11	5.84	5.29	4.95	4.72
3	2	6.13	5.05	4.58	4.29	4.1
4	2	5.39	4.45	4.04	3.79	3.62
5	2	4.81	3.98	3.61	3.39	3.24
6	2	4.34	3.6	3.27	3.07	2.93

Table 5. 2 *FoS* results for *H/W*=1 to 6 and *L/W*=6 to 10

H/W	*Su/γW*	*FoS*				
		L/W=6	*L/W=7*	*L/W=8*	*L/W=9*	*L/W=10*
1	0.2	0.54	0.52	0.51	0.5	0.49
2	0.2	0.45	0.44	0.43	0.42	0.41
3	0.2	0.39	0.38	0.37	0.37	0.36
4	0.2	0.35	0.34	0.33	0.32	0.32
5	0.2	0.31	0.3	0.3	0.29	0.28
6	0.2	0.28	0.27	0.27	0.26	0.26

Continued Table 5.2

H/W	*Su/γW*	*FoS*				
		L/W=6	*L/W=7*	*L/W=8*	*L/W=9*	*L/W=10*
1	0.6	1.61	1.56	1.52	1.49	1.46
2	0.6	1.36	1.32	1.29	1.26	1.24
3	0.6	1.18	1.15	1.12	1.1	1.08
4	0.6	1.05	1.02	0.99	0.97	0.95
5	0.6	0.94	0.91	0.89	0.87	0.85
6	0.6	0.85	0.82	0.8	0.79	0.77
1	0.73	1.96	1.9	1.85	1.81	1.77
2	0.73	1.66	1.61	1.57	1.54	1.51
3	0.73	1.44	1.4	1.36	1.33	1.31
4	0.73	1.27	1.24	1.2	1.18	1.16
5	0.73	1.14	1.11	1.08	1.06	1.04
6	0.73	1.03	1	0.98	0.96	0.94
1	1	2.68	2.6	2.53	2.48	2.43
2	1	2.27	2.21	2.15	2.1	2.06
3	1	1.97	1.92	1.87	1.83	1.79
4	1	1.74	1.69	1.65	1.61	1.58
5	1	1.56	1.52	1.48	1.45	1.42
6	1	1.41	1.37	1.34	1.31	1.29
1	1.5	4.02	3.9	3.8	3.72	3.64
2	1.5	3.41	3.31	3.22	3.15	3.09
3	1.5	2.96	2.87	2.8	2.74	2.69
4	1.5	2.62	2.54	2.47	2.42	2.38
5	1.5	2.34	2.27	2.22	2.17	2.13
6	1.5	2.12	2.06	2.01	1.97	1.93
1	2	5.37	5.2	5.07	4.96	4.86
2	2	4.55	4.41	4.3	4.21	4.12
3	2	3.95	3.83	3.73	3.65	3.58
4	2	3.49	3.38	3.3	3.23	3.17
5	2	3.12	3.03	2.96	2.89	2.84
6	2	2.83	2.74	2.68	2.62	2.57

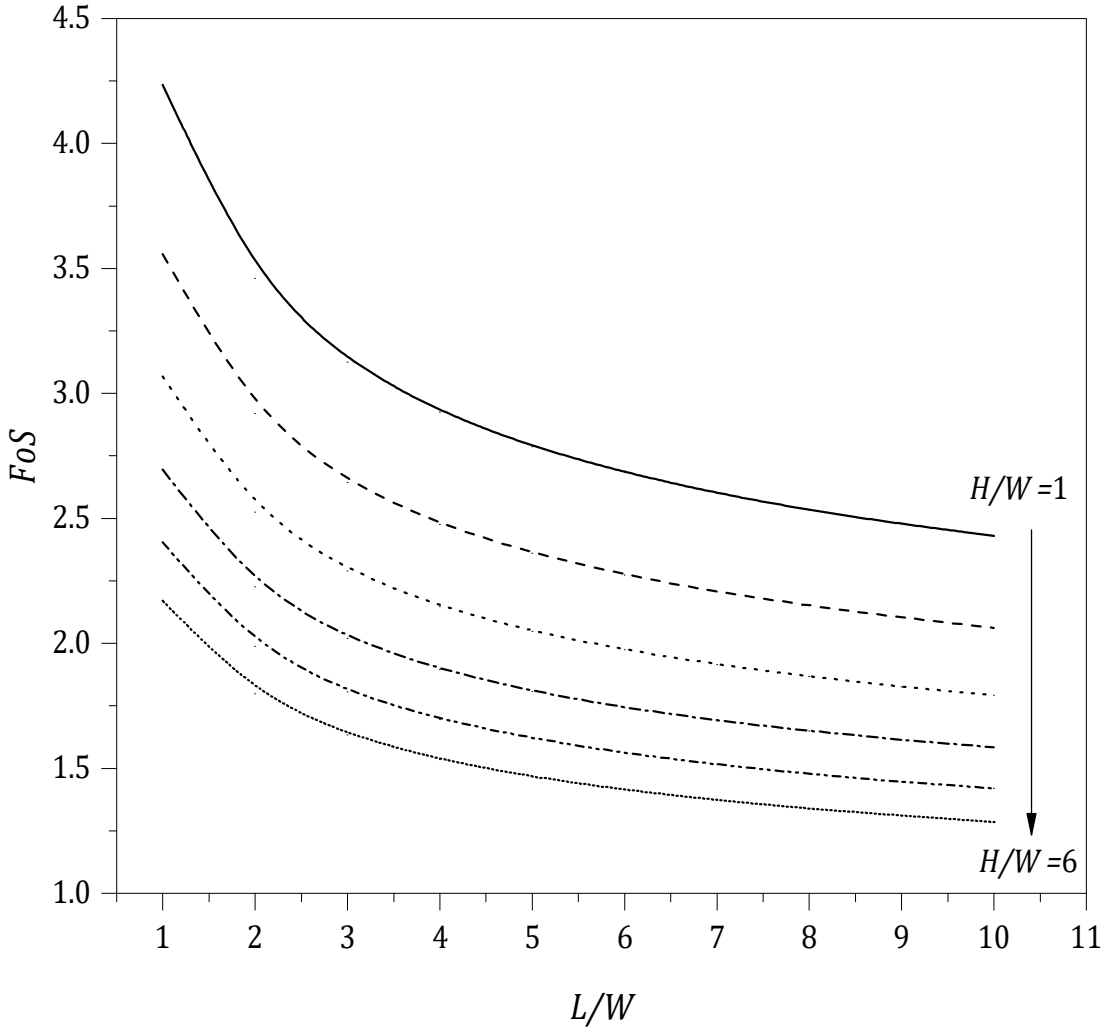

Figure 5. 3 Effect of *L/W* (*H/W*=1 to 6)

Figure 5.3 investigates the effect of the opening size (i.e. the width ratio *L/W*) on the stability of the trapdoor. It can be seen that, an increase in *L/W* results in a nonlinear decrease in the stability i.e. a decrease in *FoS*. Further observation reveals that, as *L/W* increases, the *FoS* approaches a constant value which is the result of a two-dimensional plane strain analysis (*L/W* = ∞). This observation is valid for all values of *H/W*.

Figure 5.4 shows the effect of shear strength rate ($S_u/\gamma W$) on factor of safety (*FoS*) with various opening size ratios (*L/W*). Note that the 2D results (*L/W* = ∞) were obtained from Chapter 4.

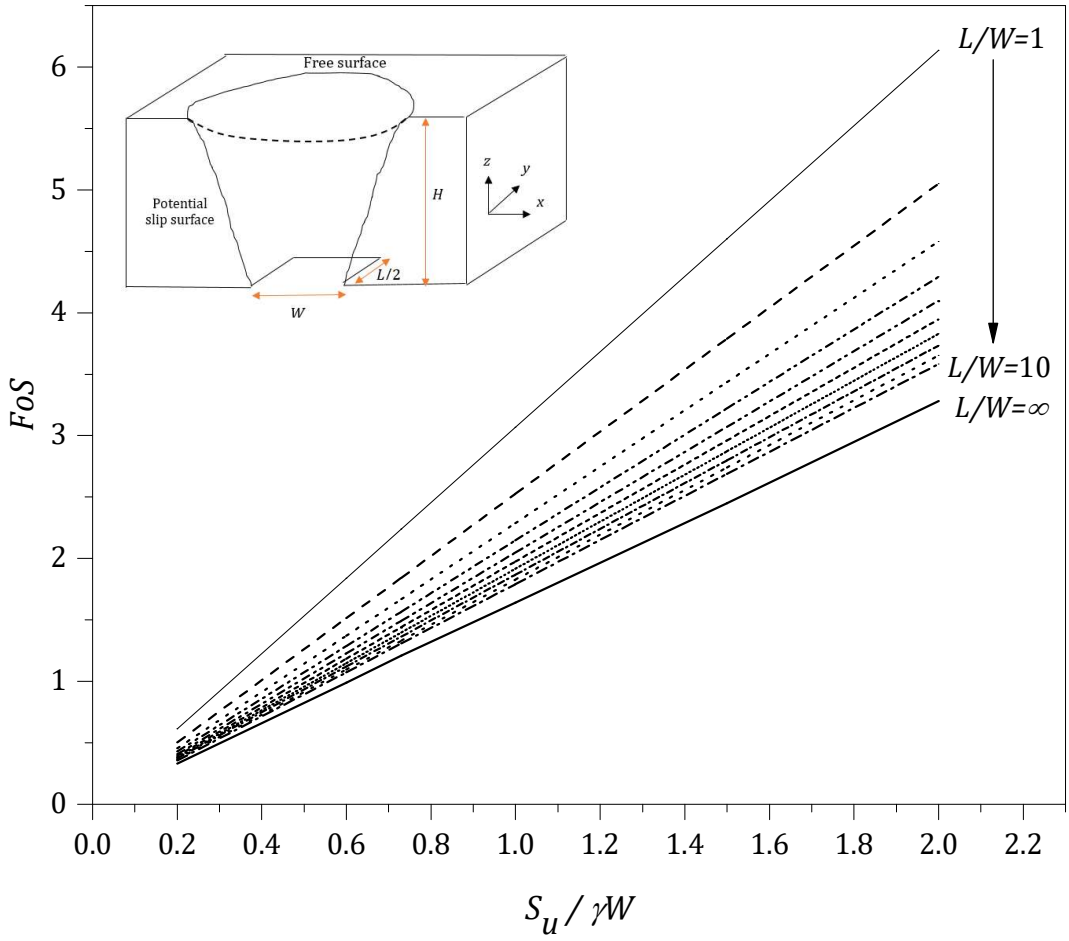

Figure 5. 4 Effect of $S_u/\gamma W$ (H/W=3)

This figure shows a linear correlation between *FoS* and shear strength ratio ($S_u/\gamma W$) for all values of *L/W*. As expected, *FoS* increases as the shear strength of the soils $S_u/\gamma W$ increases. Such a linear relationship between the *FoS* and $S_u/\gamma W$ was also reported in chapter 4 for a 2D plane strain sinkhole.

Given the linear relationship in figure 5.4, a failure envelope or critical strength ratio ($S_u/\gamma WFoS$) is presented in figure 5.5. The shear strength ratio is normalised with respect to *FoS*, and therefore represents a critical condition where the *FoS* =1. Figure 5.5 is particularly important for designers because it represents the critical value of each parameter. The values below each line indicate a safe working zone (*FoS >1*), while the values above indicate an unsafe zone (*FoS* <1). Closer inspection of the figure reveals that the value of ($S_u/\gamma W$ *FoS*) increases as both the depth ratio (*H/W*) and the width ratio (*L/W*) increase.

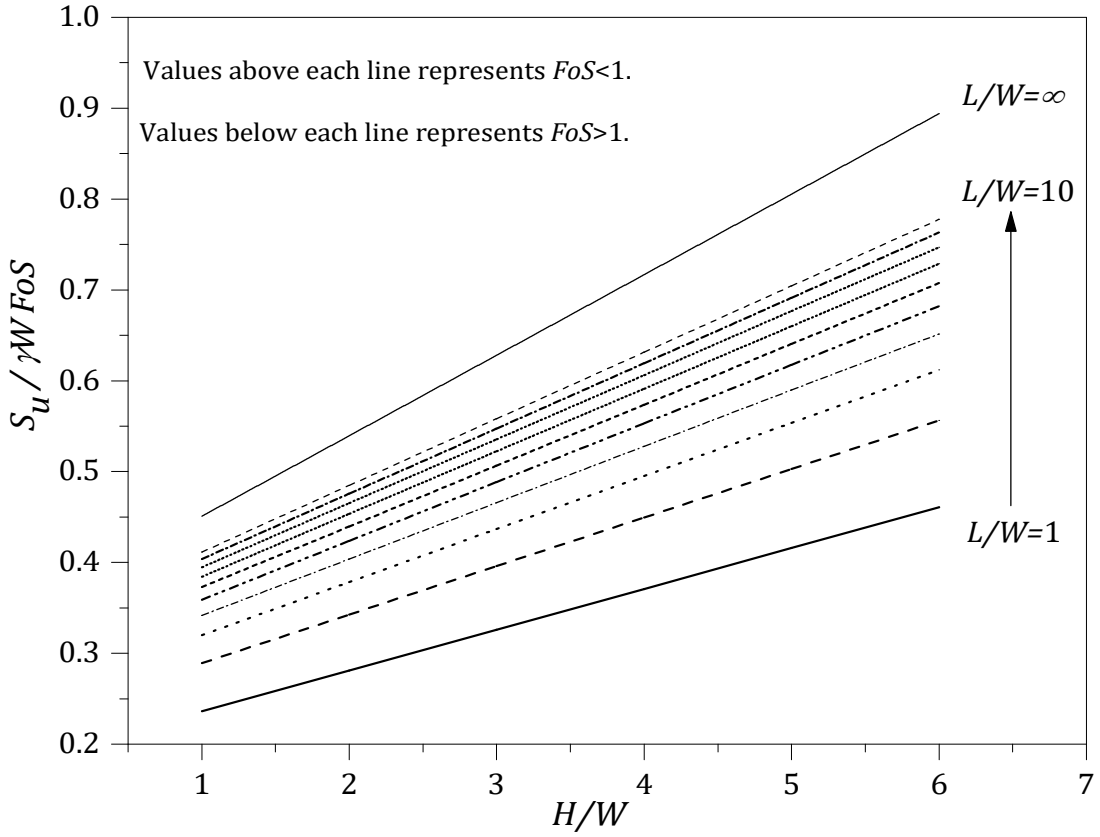

Figure 5. 5 Failure envelope (*L/W*=1 to *L/W*=∞)

A nonlinear double regression analysis was employed to develop a practical design equation covering both geometrical parameters *L/W* and *H/W*. The logarithmic function was chosen to yields an accurate curve-fitting of original *FoS* solutions with r^2 = 0.97.This is shown in equation 5.3.

$$\frac{S_u}{\gamma W \times FoS} = \left(\frac{0.045H}{W} + 0.191\right) + \left(\frac{0.012H}{W} + 0.064\right)\ln\frac{L}{W} \qquad (5.3)$$

Equation 5.3 can be used to obtain critical parameters such as undrained shear strength (S_u), depth (*H*), opening width (*W*), and in-plane depth (*L*).

Table 5. 3 Data used for plotting Figure 5.5.

L/W	*H/W*=1	*H/W*=2	*H/W*=3	*H/W*=4	*H/W*=5	*H/W*=6
	$S_u/(\gamma W\ FoS)$					
1	0.236	0.281	0.326	0.371	0.416	0.461
2	0.289	0.342	0.396	0.449	0.503	0.556
3	0.32	0.378	0.437	0.495	0.554	0.612
4	0.342	0.404	0.466	0.528	0.59	0.652
5	0.359	0.424	0.488	0.553	0.618	0.682
6	0.373	0.44	0.507	0.574	0.64	0.707
7	0.384	0.453	0.522	0.591	0.66	0.729
8	0.395	0.465	0.536	0.606	0.677	0.747
9	0.404	0.476	0.547	0.619	0.691	0.763
10	0.412	0.485	0.558	0.631	0.705	0.778

The data in Table 5.3 shows that the 2D plane strain (*L/W*=∞) prediction requires almost twice as much as 3D square opening (*L/W*=1) to maintain the stability. As suggested in Vermeer et al. (2002), the strong soil arching developed in 3D models yield realistic results.

5.5. Arching mechanism

Arching is a phenomenon of redistribution of the stresses from yielding soil particles into to non-yielded adjacent soil body. In general, the arching support can develop due to material property, geometrical shape or combination of both. In Mohr-Coulomb failure criterion, the shear stress (τ) is a function of normal stress (σ), the internal frictional angle (ϕ) and soil cohesion (c). Thus, the shear strength is represented by the following equation:

$$\tau = c + \sigma \tan\phi \tag{5.4}$$

For cohesive soils such as undrained clay where the friction angle (ϕ) is zero, the shear strength of the soil will be determined by soil cohesion (c) value. A better understanding of the arching support can be explained by studying the soil's failure

mechanism. Figure 5.6 presents vertical velocity contours for a shallow (H/W =2) and deep case (H/W =5).

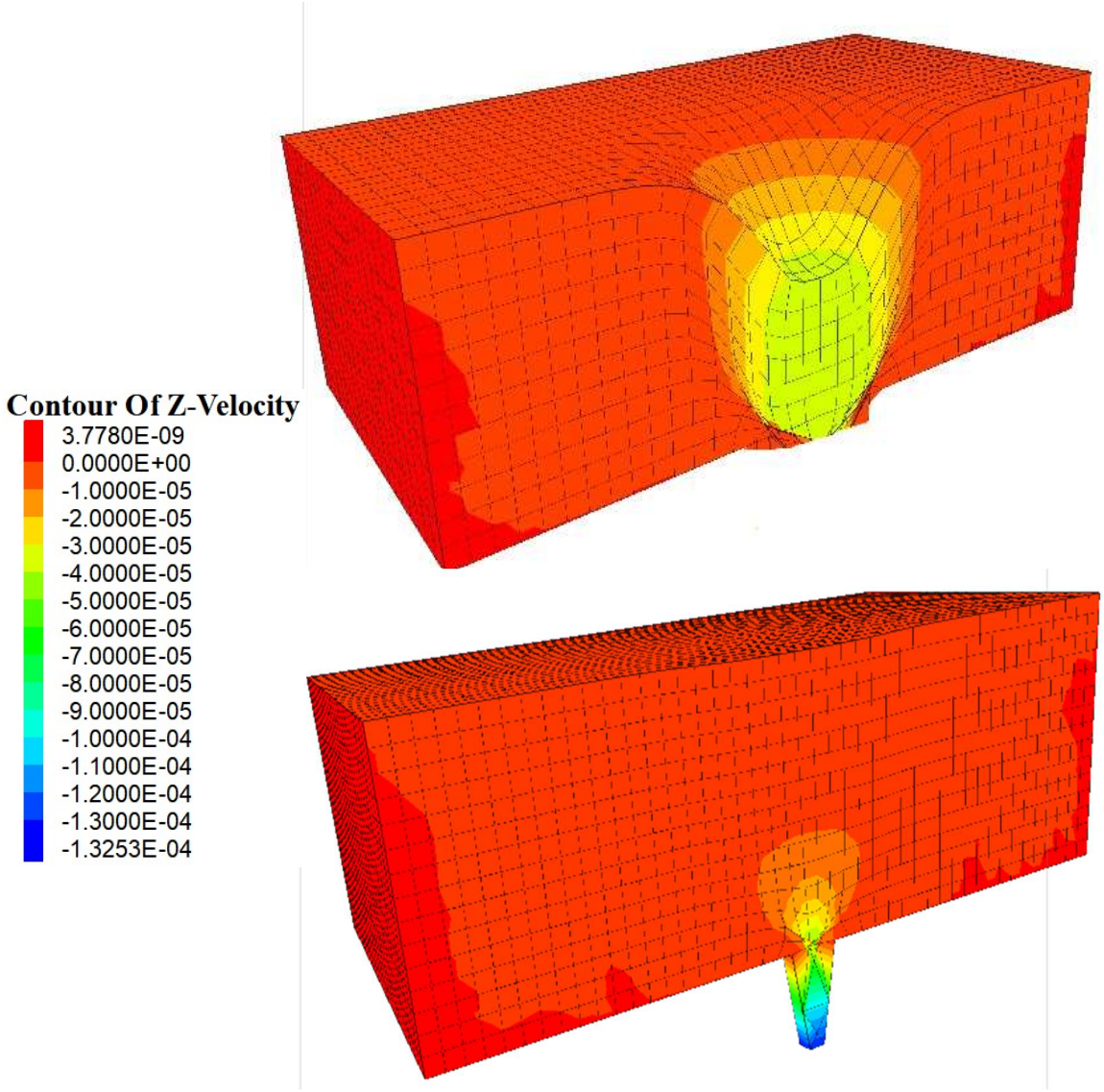

Figure 5. 6 Contour plots of the vertical velocity of H/W=2 (above) and H/W=5 (below) for L/W=1

As shown in the figure, for deeper case (H/W=5), the failure mechanism does not extend to the ground surface. This suggests that strong arching support is developed near the cavity in the deep case, resulting in a local failure.

The arching development also can be seen from the *FoS* results presented in Tables 5.1 and 5.2. It is noted that the rate of change of *FoS* starts to decrease for deeper cases. In addition, the stress distribution plot shown in figure 5.7, suggest that there is a change in vertical stress across the soil heights above the cavity.

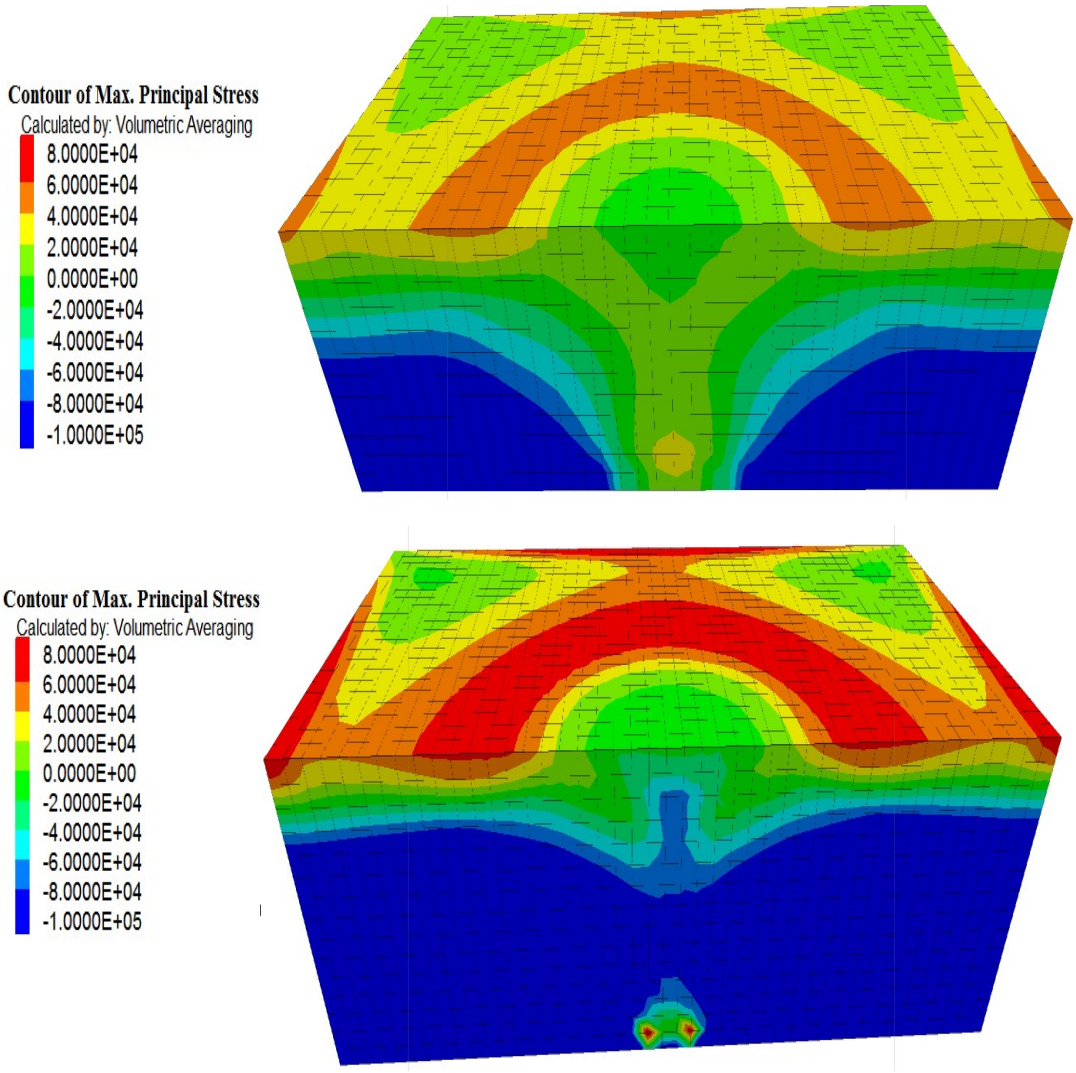

Figure 5. 7 Contour plots of principal stress of H/W=2 (above) and H/W=5 (below) for L/W=1

The transformation of compressive stress to tensile stress suggests that the vertical stress (σ_v) above the trapdoor is less than the total overburden pressure (γH) due to the load being redistributed in deeper case. This finding agrees with the observations in real engineering cases which assumes that the deeper tunnels are safer.

5.6. Failure extent

Results of the failure extent (E) study are presented in table 5.4. The values of (E) were obtained by measuring the deformed surface of the non-zero vertical velocity from program output plots.

Table 5. 4 Determination of failure extent for L/W=1 (for all values of $S_u/\gamma W$)

Depth ratio (H/W)	Actual depth(H) in meter	Measured surface half failure extent ($E/2$) in meter	Angle $\theta=H/(E/2)$ in degree	Ratio of failure extent to trapdoor width (E/W)
1	6	4.5	53.13	1.50
2	12	5.8	64.20	1.93
3	18	6.1	71.27	2.03
4	24	-	-	-
5	30	-	-	-
6	36	-	-	-

The results suggest that as the depth increases the angle theta (θ) (shown in figure 5.8) become larger which demonstrate that the surface failure extent (E) will become smaller.

Figure 5.8 displays the failure extent results for $L/W=1$ that were obtained from the preliminary analysis of z velocity vectors. The results are presented in the form of extent ratio (E/W) and depth ratio (H/W). The failure extent for all other investigated opening ratios (L/W=2 to10) are located within the area bounded by L/W=1 and L/W=∞ (refer to Chapter 4, figure 4.8).

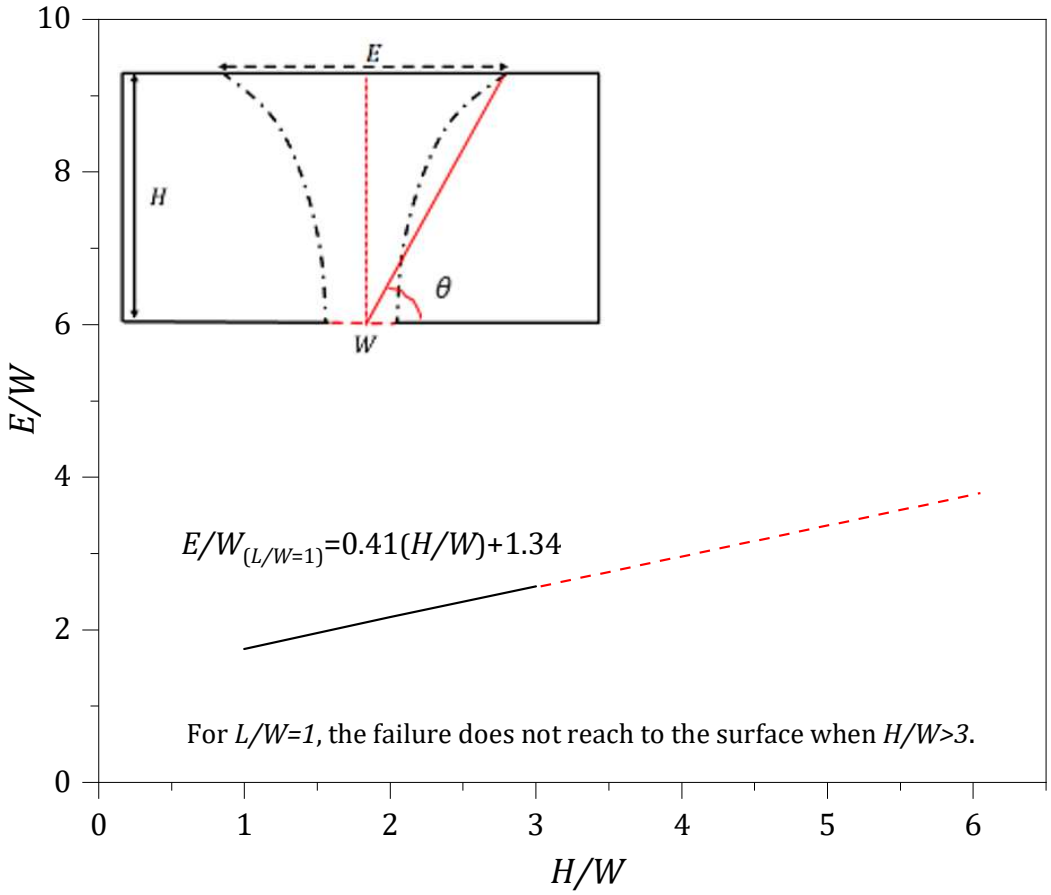

Figure 5. 8 Failure extent

Review of the plot reveals that while the failure extent increases linearly, unlike the 2D investigation, the failure extent cannot be obtained for $H/W>3$. It suggests that there is a strong arching development when $H/W=3$ or larger. The dash line in the plot is the "assumed" path of the failure, however, the numerical simulation was unable to find a solution for $H/W>3$. The affected surface area for square opening also can be estimated by using equation 5.5 which has been driven from the results in figure 5.8.

$$\left(\frac{E}{W}\right)_{L/W=1} = 0.41\frac{H}{W} + 1.34 \qquad (5.5)$$

It is important to note that equation 5.5 is not applicable for $H/W > 3$. Further study of the failure extent on the ground surface indicates a transformation from a perfect circle for $L/W=1$ to a shape of an ellipse when L/W increases, as shown in figure 5.9.

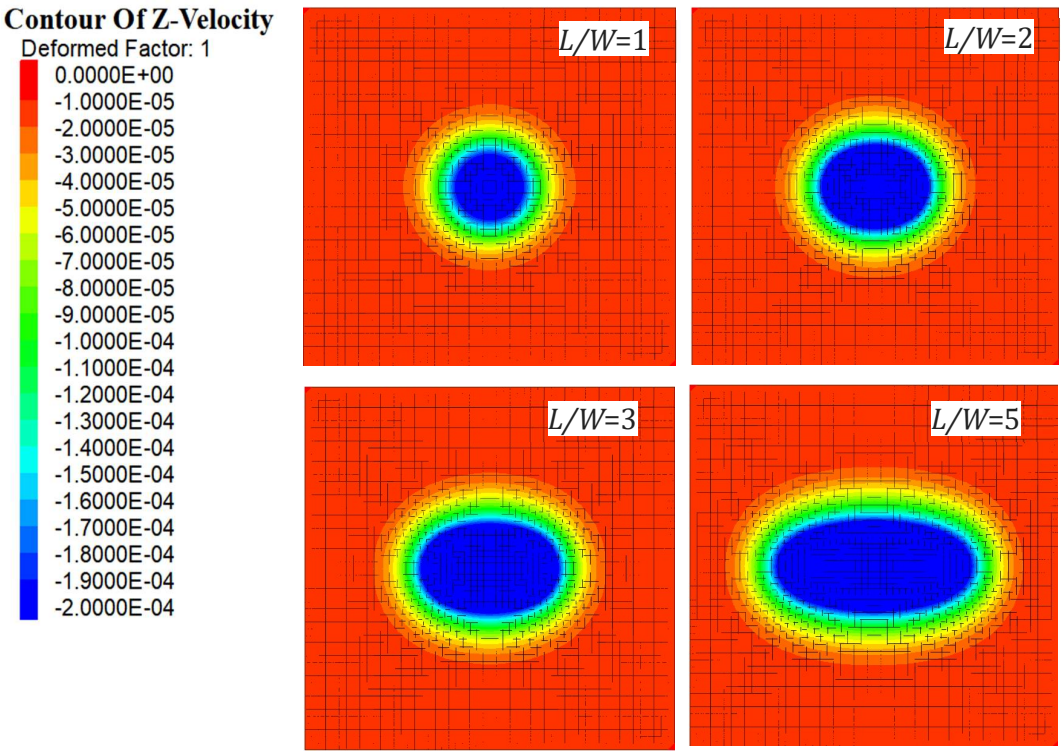

Figure 5. 9 Surface failure extent for H/W=3 and $S_u/\gamma W$=1(L/W=1, 2, 3 and 5)

A review of the existing natural sinkholes images suggest that the ground surface failure is often a circular shape. Given the same dimension of *m* and *n* (shown as *m* and *n* respectively in figure 5.10), it should be noted the opening ratio (L/W) has to be close to one, based on the study.

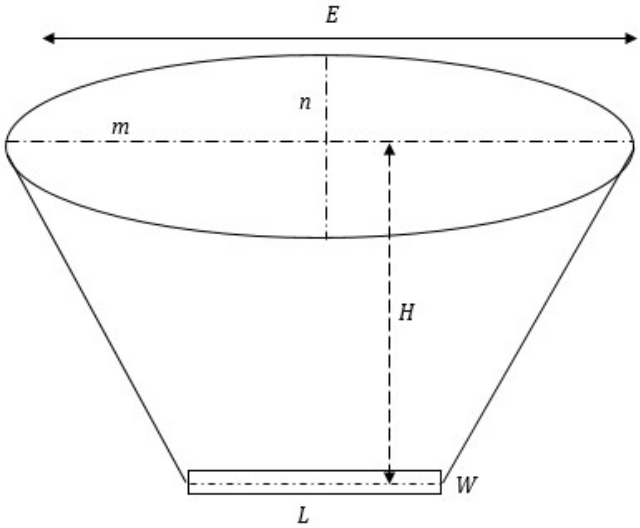

Figure 5. 10 Definition of surface failure

It should be noted that for L/W=1, the E represents the diameter of the surface failure shape (circle) and for L/W>1, the E represents the larger axis of the ellipse as it shown in figure 5.10. When the major axes of the ellipse (m) becomes larger, the results are gradually approach to 2D plane strain problem.

5.7. Results verification

The use of *SSRM* and *FoS* is prevalent in slope stability analyses, however, this process is uncommon when it comes to estimating the stability of underground cavities. Owing to the lack of published literature for comparison, it was decided that the current 3D results obtained are to be compared with 2D *FDM* which presented in Chapter 4 as well as 2D upper bound and lower bound solutions using the finite element limit analysis by Shiau et al. (2019). Figure 5.11 shows such a comparison.

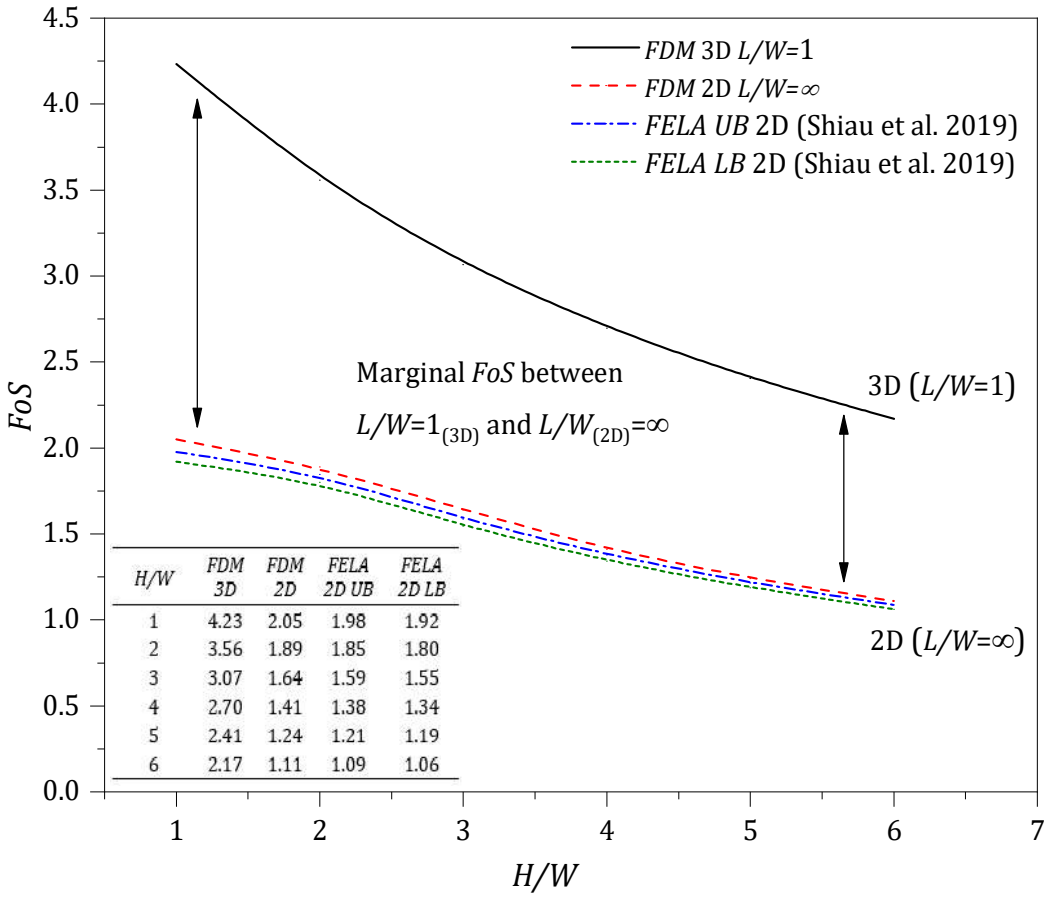

H/W	FDM 3D	FDM 2D	FELA 2D UB	FELA 2D LB
1	4.23	2.05	1.98	1.92
2	3.56	1.89	1.85	1.80
3	3.07	1.64	1.59	1.55
4	2.70	1.41	1.38	1.34
5	2.41	1.24	1.21	1.19
6	2.17	1.11	1.09	1.06

Figure 5. 11 Comparison of *FoS* results from 2D and 3D analyses (for $S_u/\gamma W$=1)

Figure 5.11 shows that there is significant variance between the 3D (L/W=1) and 2D results (L/W= ∞). Table 5.5 shows the values used to plot figure 5.11.

Table 5. 5 *FoS* results of *FLAC* 3D, *FLAC* 2D and *FELA UB* and *LB* for $S_u/\gamma W$=1

H/W	FDM_{3D}	FDM_{2D}	Shiau et al.(2019) *FELA LB*	Shiau et al. (2019) *FELA UB*
1	4.23	2.05	1.92	1.98
2	3.56	1.89	1.80	1.85
3	3.07	1.64	1.55	1.59
4	2.70	1.41	1.34	1.38
5	2.41	1.24	1.19	1.21
6	2.17	1.11	1.06	1.09

The results presented in table 5.5 shows that the *FoS* of 3D analyse is approximately two times higher than those 2D solutions. This is not particularly surprising, as a two-dimensional analysis will always yield conservative results when compared to a three-dimensional analysis. This finding can significantly reduce the estimation cost for practical purposes.

5.8. Design charts and equation

The factor of safety results can be best presented in the form of design charts and equation. A wide range of design charts for H/W=1-6 are presented in Figures 5.12 to 5.18.

Figure 5.12 presents al 3D surface plot of the horizontal trapdoor stability for H/W=6. For a given opening ratio (L/W) and strength ratio ($S_u/\gamma W$), figure 5.12 can be used to estimate the *FoS*. The figure 5.12 might not be suitable for practical use since it would be hard to locate the interception of three points in space and determine the precise *FoS* value. However, the plot is useful for the preliminary estimation of the *FoS*.

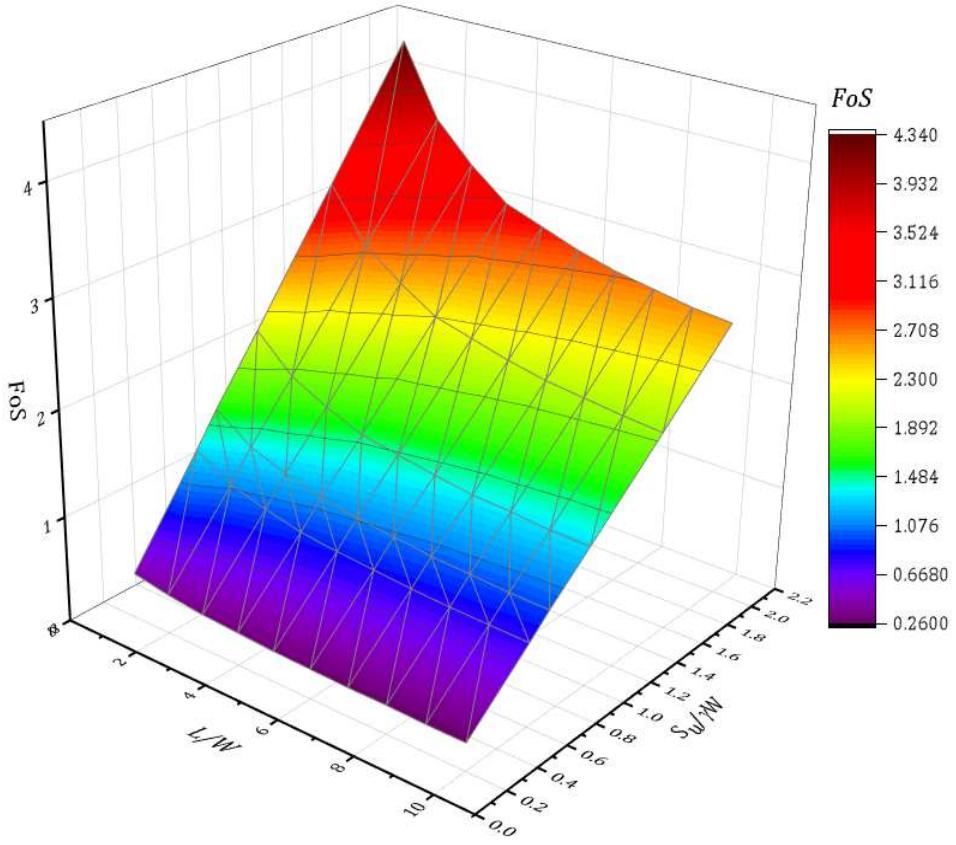

Figure 5. 12 3D Surface plot for trapdoor stability (*H/W*=6)

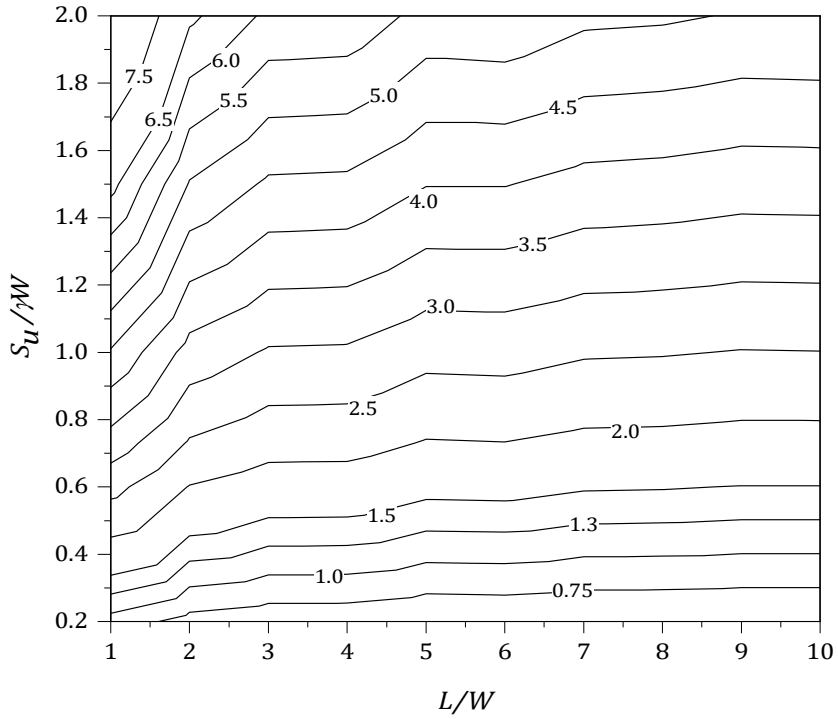

Figure 5. 13 Design chart for trapdoor stability (*H/W*=1)

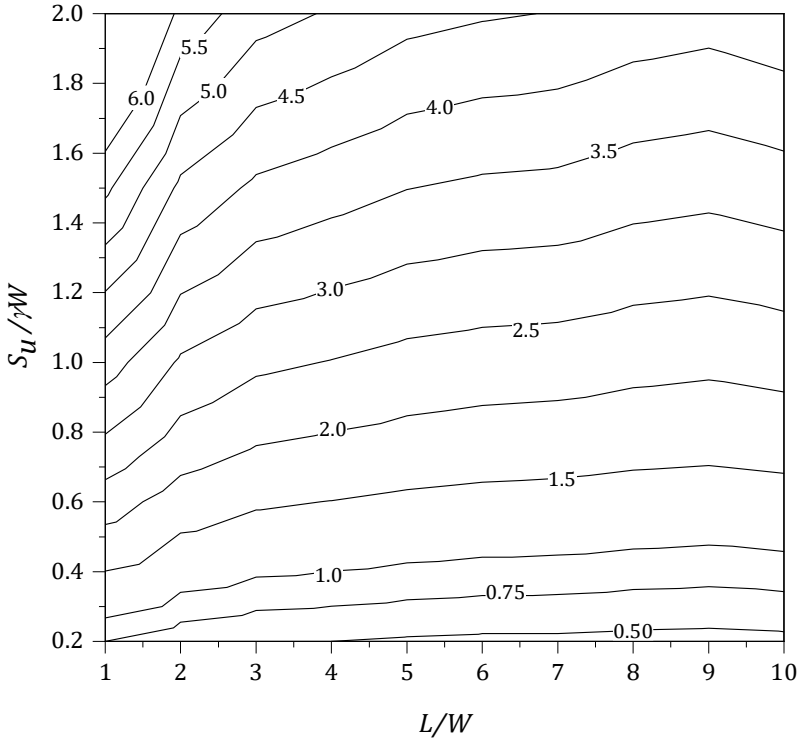

Figure 5. 14 Design chart for trapdoor stability (*H/W*=2)

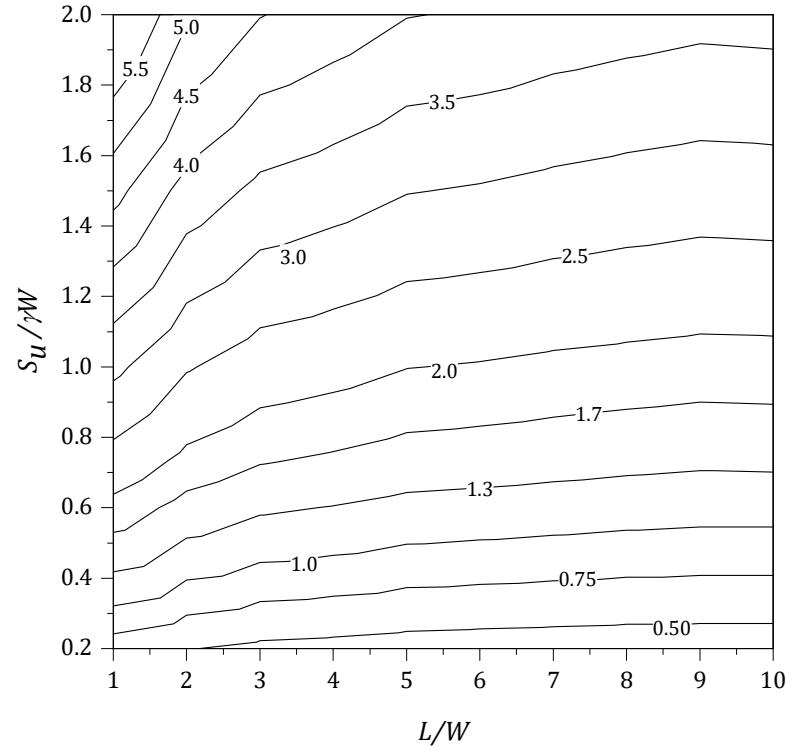

Figure 5. 15 Design chart for trapdoor stability (*H/W*=3)

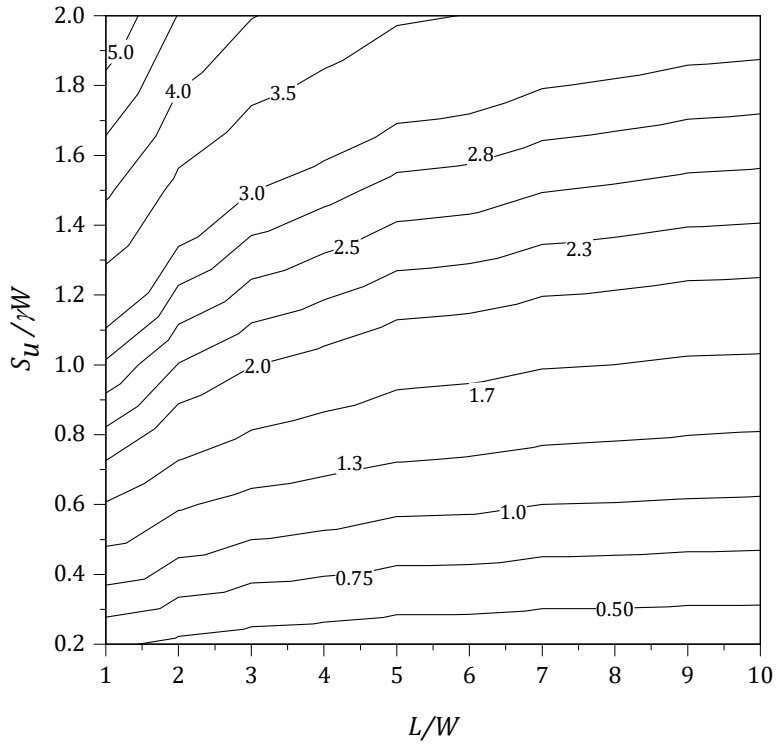

Figure 5. 16 Design chart for trapdoor stability (H/W=4)

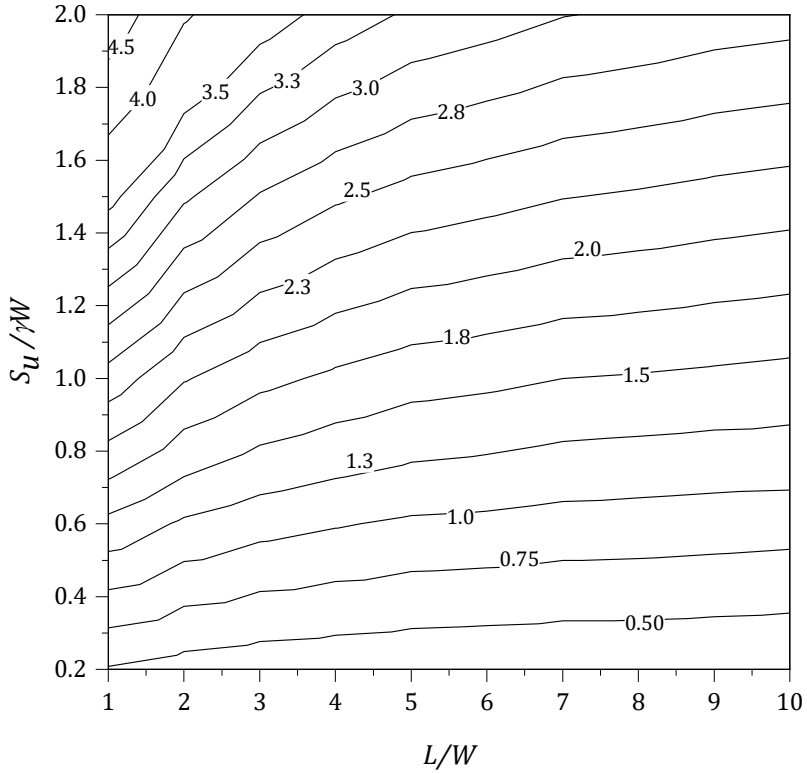

Figure 5. 17 Design chart for trapdoor stability (H/W=5)

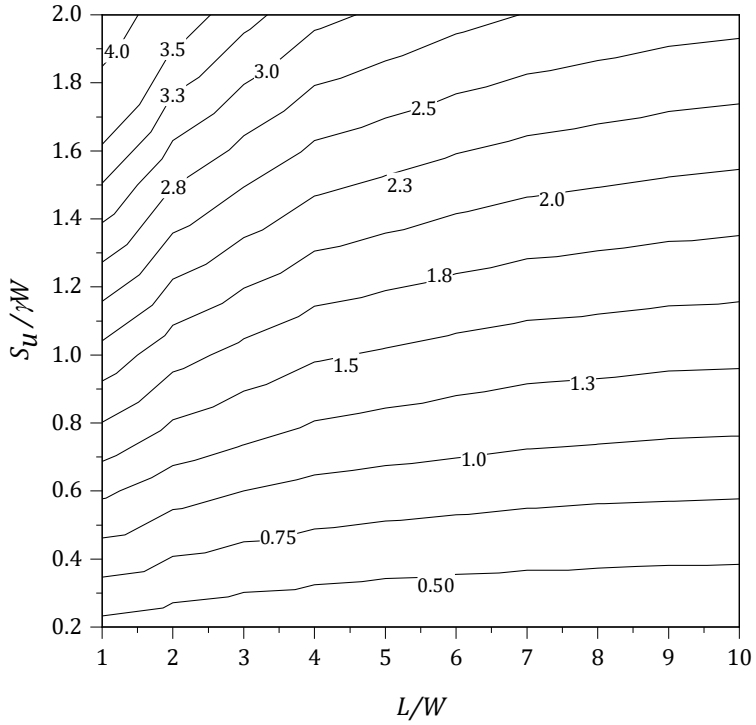

Figure 5. 18 Design chart for trapdoor stability (*H/W*=6)

The design charts can be represented by the general equation to cover all possible depth ratios. Equation 5.3 which introduced earlier can be further transformed into equation 5.6 to determine *FoS* for known design parameters such as *H/W, L/W* and $S_u/\gamma W$.

$$FoS = \frac{S_u / \gamma W}{\left[\left(\frac{0.045H}{W} + 0.191\right) + \left(\frac{0.012H}{W} + 0.064\right)\ln\frac{L}{W}\right]} \tag{5.6}$$

Equation 5.6 can be very useful in the early design stage for engineers because it allows them to determine the *FoS* when other parameters are available.

Practical Examples

Workability of the stability design charts and equations can best demonstrated through a number of examples, as follows.

Example 1 - determine the factor of safety (FoS)

An existing sinkhole has no internal pressure and no surcharge pressure, determine the factor of safety for the cavity. The following data has been provided:

H=12 m, W=4 m, L=12 m, γ= 18 kN/m^3 and S_u=72 kPa.

1. Given H/W=3 and $Su/\gamma W$ = 1, equation 5.6 returns a *FoS* value of approximately 2.29.

2. Using figure 5.12, a value of *FoS* estimated to range from 2.168 to 2.464.

2. Using figure 5.13, a value of *FoS* = 2.30 is obtained.

3. An actual computer analysis of this case using *FLAC* gives *FoS* = 2.33.

The results obtained by figures 5.12, 5.13, equation 5.6 and numerical analyse (*FLAC* 3D) shows a good agreement.

Example 2 - determine the critical depth ratio (H/W)

In the case of a deep sinkhole, what would be the critical depth (H) required maintaining a *FoS* of 1 for the following given parameters:

S_u= 162 kPa, W=30 m, L=30 m, γ= 18 kN/m^3.

1. Given the parameters, $S_u/\gamma WFoS$ =0.3.

2. Using equation 5.3, the depth (H) is calculated to be 72.67 m. Converting the results in terms of a dimensionless ratio, H/W = 2.42.

3. Using figure 5.5 with $S_u/\gamma WFoS$ =0.3, H/W is estimated to be 2.5.

Example 3 – to determine the failure extent (E) for shallow case

An abandoned mineshaft has been detected by using *GPR* in parkland with soft soil. The geotechnical engineer has been assigned to estimate the surface failure of the cavity if it collapses. The following parameters have been provided:

H = 12 m, L=4 m, W = 4m, S_u = 30 kPa and γ = 18 kN/m^3.

1. Using H/W = 3, equation 5.5 gives E/W=2.57.

2. Using H/W = 3, figure 5.8 gives an approximate value of E/W=2.7.

3. The actual analyse of z displacement of the problem gives approximately E = 10.5 m. Converting the value into dimensionless form, E/W=2.63.

5.9. Conclusion

A series of 3D numerical models were established to investigate the stability of trapdoors with various opening sizes in undrained cohesive soil. Numerical results were obtained by utilising the shear strength reduction method in the finite difference method software *FLAC* 3D. In order to efficiently perform parametric analyses, a *FISH* script was developed to enable auto mesh generation and solver. The following conclusions can be drawn based on the current study:

- The *FoS* study showed that the 3D square opening results were almost two times larger than 2D plane strain results.
- The study of surface failure extent showed the transformation from a perfect circle to an ellipse as the value of width ratio *L/W* increased i.e. changing the opening size from a square to a wide rectangle.
- Strong soil arching was developed for deep trapdoors ($H/W > 3$) in the 3D study, resulting in local failure mechanisms.

Although the study has successfully demonstrated the stability and surface failure extent of sinkhole, it has a certain limitation in term of implementation of the surcharge load. In spite of its limitation, this study certainly adds to our understanding of failure mechanism and arching development in 3D sinkhole analysis. More research is required to examine the impact of surcharge load (σ_s) and support load (σ_t) and propagation of trapdoor in undrained clay.

6. TWO-DIMENSIONAL ANALYSIS OF SINKHOLE PROBLEM USING BROMS & BENNERMARK'S APPROACH

6.1. Introduction

Following the previous study of sinkhole problems in unsupported greenfield (chapters 4 and 5), this chapter advanced the study by investigating the problem associated with the sinkhole in urbanised areas where there is surcharge load applies due to building and traffic loads. In addition to the traditional active trapdoor problem, this study also considered the passive trapdoor which represents a blowout condition. However, the passive condition is unlikely to occur in natural sinkholes. The problem has been defined following Broms and Bennermark's stability number and the results presented in forms of factor of safety and critical stability number. In addition to the finite difference method, this study also utilises the finite element limit analysis to validate the numerical results. These results are then used to produce dimensionless design charts to estimate the stability of the trapdoor problem. Furthermore, the study investigates the surface failure extent due to working condition. In addition to the dimensionless design charts and design

equation, a number of examples have been provided to assist those practical field technicians.

6.2. Problem definition

The development of cover-collapse sinkholes is a complex procedure due to the continuous expansion of the cavity size over the time. To simplify the problem, it is assumed that the cavity is in the critical stage where the failure is imminent. Figure 6.1 shows the problem definition of an idealised horizontal trapdoor underlying a homogeneous layer of cohesive soil.

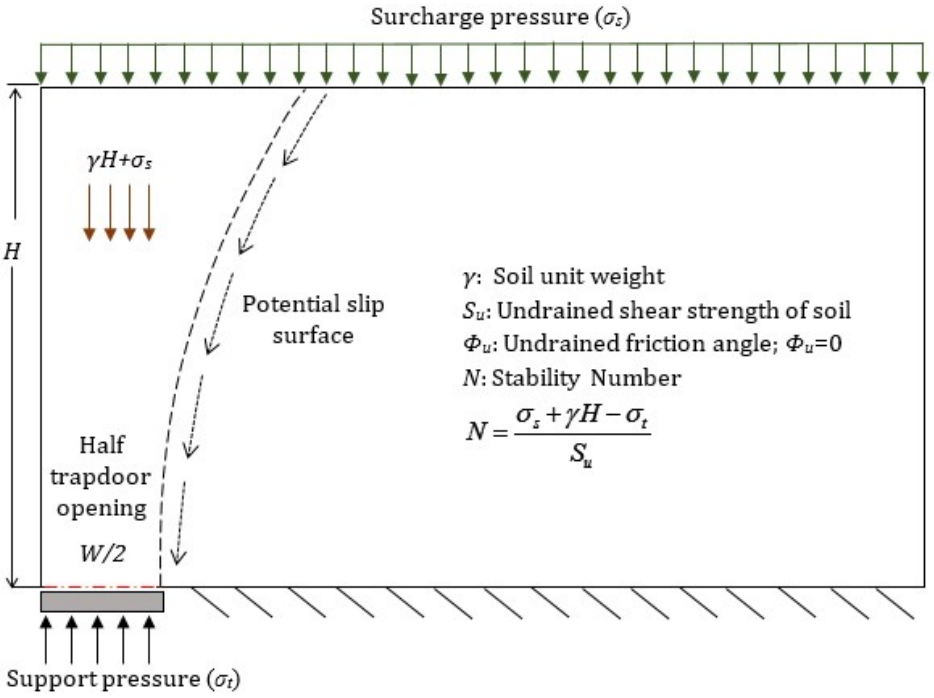

Figure 6. 1 Problem Definition

The undrained soil is modelled as uniform Mohr-Coulomb material with zero soil internal friction angle (Φ =0), the undrained shear strength (S_u) and the soil unit weight (γ). The trapdoor opening width is W and the depth from the surface to the trapdoor opening is notated by H. Note that the combination of surcharge pressure (σ_s), overburden pressure (γH) and support pressure (σ_t) can produce failure either in a collapse or blowout. For undrained clay without volume loss during plastic shearing, stability results are independent of loading directions and Broms and

Bennermark's original stability number is a suitable design parameter (Shiau and Al-Asadi, 2018). For drained soils, the original stability number is not applicable.

A broad range of stability numbers (N= -15 to 15) and depth ratios (H/W = 1 to 10) have been chosen to cover all possible investigations of collapse and blowout. The *SSRM* is adopted to solve for the *FoS*, which is a function of the stability number (N) and the depth ratio (H/W), as shown in equation 6.1. Note that the actual values of (σ_s), (σ_t), (γH), (S_u), and (H/W) used in the analyses are insignificant and are not to be reported here due to the nature of the dimensionless definition.

$$FoS = f\left(N, \frac{H}{W}\right) \tag{6.1}$$

It is important to validate the numerical solution of this study with the solutions of previous literatures obtained by finite element limit analysis (*FELA*) were selected to verify the *FDM* solutions.

6.3. Modelling technique

A typical grid for simulating the trapdoor stability problem in *FDM* is shown in figure 6.2.

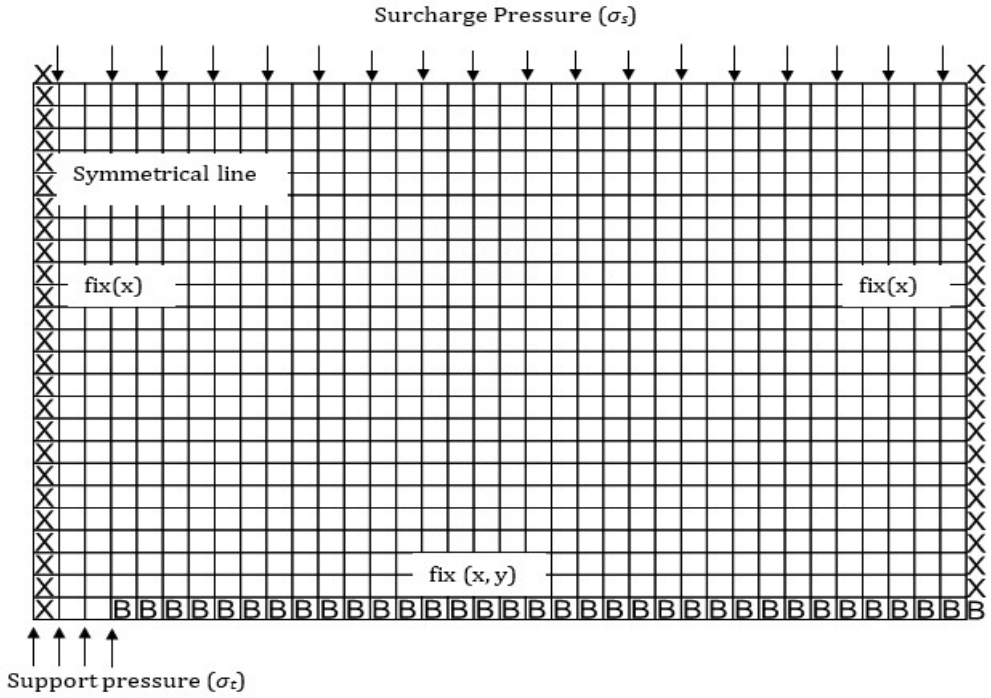

Figure 6. 2 Typical *FDM* mesh used for the problem

A *FISH* script was developed to assist in auto mesh generation and problem solving of the trapdoor problem. The *FISH* development was a particularly important tool in this study, as it allows parametric study to be conducted efficiently.

To improve computational efficiency, a symmetrical condition is considered. This symmetrical condition is particularly important for deep cases which normally require more *CPU* time. An effective domain should be such that it is large enough to present the entire velocity field. Both the left and the right boundaries of the mesh were fixed in the x-direction, allowing the soil to move in a vertical direction. The lower boundary of the mesh was restrained in both the x and y-direction except where the trapdoor opening is positioned. The trapdoor opening was not restrained so the soil body can freely move downward into the cavity.

In this chapter, the *SSRM* and *FoS* approach is adopted to analyse the stability of the trapdoor in collapse and blowout conditions. A total of 230 trapdoor cases were studied using *FDM*. Numerical results of the extensive investigation were presented in the form of design charts and equations.

6.4. Results and discussions:

Numerical results of the current *FDM* study for a broad range of stability numbers (N= -15 to 15) and depth ratios (H/W = 1 to 10) are presented in tables 6.1. In addition, the results of *FELA* obtained by Shiau et al. (2019) are also presented in tables 6.2 and 6.3 for the verification purpose.

Table 6. 1 *FoS* for various *N* and *H/W* (*FDM*)

N	*H/W*									
	1	2	3	4	5	6	7	8	9	10
-15.00	0.14	0.26	0.33	0.38	0.42	0.44	0.47	0.49	0.51	0.53
-12.50	0.17	0.31	0.39	0.45	0.50	0.53	0.56	0.59	0.62	0.63
-10.00	0.22	0.39	0.49	0.56	0.62	0.67	0.71	0.74	0.77	0.79
-7.50	0.29	0.52	0.66	0.76	0.83	0.89	0.94	0.99	1.02	1.06
-5.00	0.43	0.78	0.99	1.13	1.24	1.33	1.41	1.49	1.53	1.59
-3.00	0.72	1.30	1.65	1.89	2.08	2.23	2.35	2.46	2.56	2.65
-2.00	1.08	1.95	2.47	2.83	3.11	3.34	3.53	3.70	3.83	3.98
-1.00	2.16	3.90	4.94	5.67	6.24	6.70	7.09	7.42	7.67	7.98
-0.75	2.88	5.20	6.59	7.57	8.32	8.94	9.46	9.90	10.24	10.66
-0.50	4.32	7.80	9.89	11.35	12.49	13.40	14.17	14.83	15.42	15.95
-0.25	8.64	15.60	19.77	22.74	25.04	26.93	28.52	29.91	31.16	31.90
0.00	Infinity	Infinity	Infinity	Infinity	Infinity	Infinity	Infinity	Infinity	Infinity	Infinity
0.25	8.63	15.59	19.74	22.65	24.92	26.73	28.26	29.58	30.90	31.50
0.50	4.31	7.79	9.86	11.32	12.43	13.34	14.10	14.75	15.38	15.95
0.75	2.88	5.19	6.57	7.54	8.29	8.89	9.39	9.83	10.23	10.58
1.00	2.16	3.89	4.93	5.65	6.21	6.66	7.04	7.37	7.66	7.91
2.00	1.08	1.95	2.46	2.82	3.10	3.33	3.52	3.68	3.83	3.95
3.00	0.72	1.30	1.64	1.88	2.07	2.22	2.34	2.45	2.55	2.62
5.00	0.43	0.78	0.99	1.13	1.24	1.33	1.40	1.47	1.53	1.58
7.50	0.29	0.52	0.66	0.75	0.83	0.89	0.94	0.98	1.02	1.05
10.00	0.22	0.39	0.49	0.56	0.62	0.67	0.71	0.74	0.76	0.79
12.50	0.17	0.31	0.39	0.45	0.50	0.53	0.56	0.59	0.61	0.63
15.00	0.14	0.26	0.33	0.38	0.41	0.44	0.47	0.49	0.51	0.53

Table 6. 2 *FoS* for various *N* and *H/W* (*FELA UB*) (Shiau et al. 2019)

N	*H/W*									
	1	2	3	4	5	6	7	8	9	10
-15.00	0.13	0.25	0.32	0.37	0.41	0.44	0.46	0.48	0.50	0.52
-12.50	0.16	0.30	0.38	0.44	0.49	0.52	0.55	0.58	0.60	0.62
-10.00	0.20	0.37	0.48	0.55	0.61	0.65	0.69	0.73	0.75	0.78
-7.50	0.26	0.50	0.64	0.74	0.81	0.87	0.92	0.97	1.01	1.04
-5.00	0.40	0.74	0.96	1.10	1.22	1.31	1.38	1.45	1.51	1.56
-3.00	0.66	1.24	1.59	1.84	2.03	2.18	2.31	2.42	2.51	2.60
-2.00	0.99	1.85	2.38	2.76	3.04	3.27	3.46	3.62	3.78	3.90
-1.00	1.98	3.70	4.77	5.51	6.11	6.53	6.93	7.24	7.55	7.80
-0.75	2.64	4.95	6.34	7.36	8.11	8.72	9.22	9.66	10.06	10.40
-0.50	3.96	7.39	9.53	11.03	12.21	13.07	13.85	14.50	15.11	15.60
-0.25	7.92	14.79	19.06	22.05	24.30	26.13	27.71	28.99	30.22	31.20
0.00	Infinity	Infinity	Infinity	Infinity	Infinity	Infinity	Infinity	Infinity	Infinity	Infinity
0.25	7.92	14.79	19.06	22.05	24.32	26.13	27.71	28.99	30.22	31.20
0.50	3.96	7.42	9.53	11.03	12.16	13.07	13.85	14.50	15.11	15.60
0.75	2.64	4.95	6.34	7.36	8.11	8.72	9.22	9.67	10.06	10.40
1.00	1.98	3.70	4.77	5.51	6.08	6.53	6.93	7.25	7.55	7.80
2.00	0.99	1.85	2.38	2.76	3.04	3.27	3.46	3.62	3.78	3.90
3.00	0.66	1.24	1.59	1.84	2.03	2.18	2.31	2.42	2.51	2.60
5.00	0.40	0.74	0.96	1.10	1.22	1.31	1.38	1.45	1.51	1.56
7.50	0.26	0.50	0.64	0.74	0.81	0.87	0.92	0.97	1.01	1.04
10.00	0.20	0.37	0.48	0.74	0.61	0.65	0.69	0.73	0.75	0.78
12.50	0.16	0.30	0.38	0.44	0.49	0.52	0.55	0.58	0.60	0.63
15.00	0.13	0.25	0.37	0.37	0.41	0.44	0.46	0.48	0.50	0.52

Table 6. 3 *FoS* for various *N* and *H/W* (*FELA LB*) (Shiau et al. 2019)

N	*H/W*									
	1	2	3	4	5	6	7	8	9	10
-15.00	0.13	0.24	0.31	0.36	0.39	0.42	0.45	0.47	0.49	0.50
-12.50	0.16	0.29	0.37	0.43	0.47	0.51	0.54	0.56	0.58	0.60
-10.00	0.20	0.36	0.46	0.54	0.59	0.64	0.67	0.70	0.73	0.75
-7.50	0.26	0.48	0.61	0.72	0.79	0.85	0.90	0.94	0.97	0.75
-5.00	0.39	0.72	0.93	1.08	1.18	1.27	1.34	1.40	1.46	1.51
-3.00	0.65	1.20	1.54	1.78	1.97	2.12	2.24	2.35	2.43	2.51
-2.00	0.97	1.79	2.32	2.68	2.95	3.18	3.37	3.52	3.65	3.79
-1.00	1.94	3.58	4.65	5.36	5.92	6.34	6.74	7.03	7.30	7.57
-0.75	2.59	4.79	6.20	7.17	7.90	8.46	8.95	9.39	9.76	10.03
-0.50	3.89	7.21	9.28	10.73	11.77	12.72	13.49	14.05	14.60	15.10
-0.25	7.72	14.41	18.59	21.45	23.54	25.44	26.97	28.10	29.21	30.10
0.00	Infinity	Infinity	Infinity	Infinity	Infinity	Infinity	Infinity	Infinity	Infinity	Infinity
0.25	7.78	14.32	18.53	21.47	23.61	25.44	26.95	28.10	29.21	30.29
0.50	3.86	7.21	9.21	10.73	11.80	12.72	13.48	14.05	14.60	15.15
0.75	2.59	4.76	6.20	7.15	7.87	8.46	8.98	9.39	9.78	10.10
1.00	1.95	3.58	4.65	5.37	5.90	6.34	6.74	7.03	7.30	7.57
2.00	0.97	1.80	2.32	2.68	2.97	3.18	3.37	3.51	3.65	3.76
3.00	0.65	1.20	1.54	1.79	1.98	2.12	2.24	2.35	2.43	2.51
5.00	0.39	0.72	0.93	1.07	1.18	1.27	1.35	1.41	1.46	1.51
7.50	0.26	0.48	0.62	0.72	0.79	0.85	0.90	0.94	0.97	1.01
10.00	0.20	0.36	0.46	0.54	0.59	0.64	0.67	0.70	0.73	0.75
12.50	0.16	0.29	0.37	0.43	0.47	0.51	0.54	0.56	0.58	0.60
15.00	0.13	0.24	0.31	0.36	0.40	0.42	0.45	0.47	0.49	0.50

Using the data in the tables 6.1 to 6.3, figure 6.3 plots the *FoS* results of collapse and blowout from the analyses of lower bound, upper bound and finite differences for the depth ratio of *H/W*= 3.

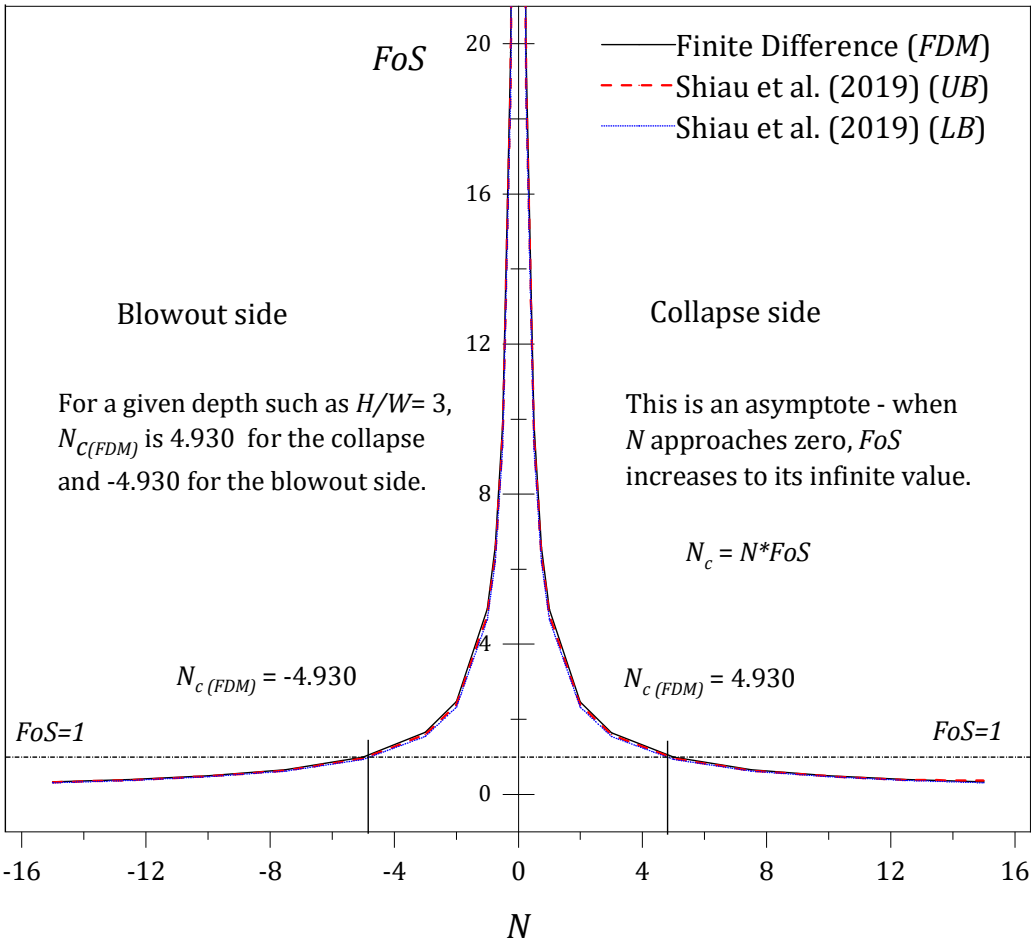

Figure 6. 3 *FoS vs. N (UB, LB and FDM)* for a depth ratio of *H/W* = 3

The results show that the curves are in hyperbolic form where *FoS* and *N* are the vertical and horizontal asymptote respectively. The general equation of the curve is presented in equation 6.2.

$$N_c = FoS \times N \tag{6.2}$$

Equation 6.2 suggests that for a given depth ratio (*H/W*= 3), any combination of *FoS* and *N* on the curve yields a unique value. This unique value is the critical stability number (N_c) with a *FoS* of one. By drawing a *FoS* = 1 horizontal line on figure 6.3,

graphically, the two intersection points give a N_c value of 4.925 for the collapse and -4.930 for the blowout.

When the supporting pressure ratio (σ_t/S_u) is greater than the overburden pressure ratio (($\sigma_s + \gamma H)/S_u$)), the negative value of N represents a blowout movement. Contrary to this, a positive value of N indicates that the soil moves in the collapse condition. This occurs when the overburden pressure ratio (($\sigma_s+\gamma H)/S_u$)) is greater than the supporting pressure ratio (σ_t/S_u). As N further increases, an incipient collapse is reached where FoS= 1 and the corresponding N is the critical N_c. When the supporting pressure ratio (σ_t/S_u) is equal to the overburden pressure ratio (($\sigma_s + \gamma H)/S_u$)), N is equal to zero, and FoS is at a maximum (infinite) where a 'stressless' scenario exists.

Equation 2.2 (Broms and Bennermark's original equation) can be re-arranged into a form that is more amenable to analysis, as shown in equation 6.3.

$$\sigma_t = \sigma_s + \gamma H - (N_c \times S_u) \tag{6.3}$$

Using equation 6.3, a critical supporting pressure σ_t (when FoS= 1) can be determined as long as N_c is known. Note that there is only one unique N_c (±) for a particular depth ratio and N_c is a function of the depth ratio H/W regardless of the undrained shear strength of the soil. It is therefore important to study the effect of H/W on the critical stability number N_c. Figure 6.4 shows such a relationship between N_c and H/W. Note that the critical stability number (N_c) increases nonlinearly as H/W increases, and the gradient of the curve decreases for large values of N_c.

The area bounded by the collapse and the blowout curves represents the safe zone where FoS > 1. As the stability number (N) approaches zero (when Over burden pressure ratio (OPR) is equal to Supporting pressure ratio $(SPR$), the factor of safety becomes infinite. Also, see the asymptote in figure 6.3.

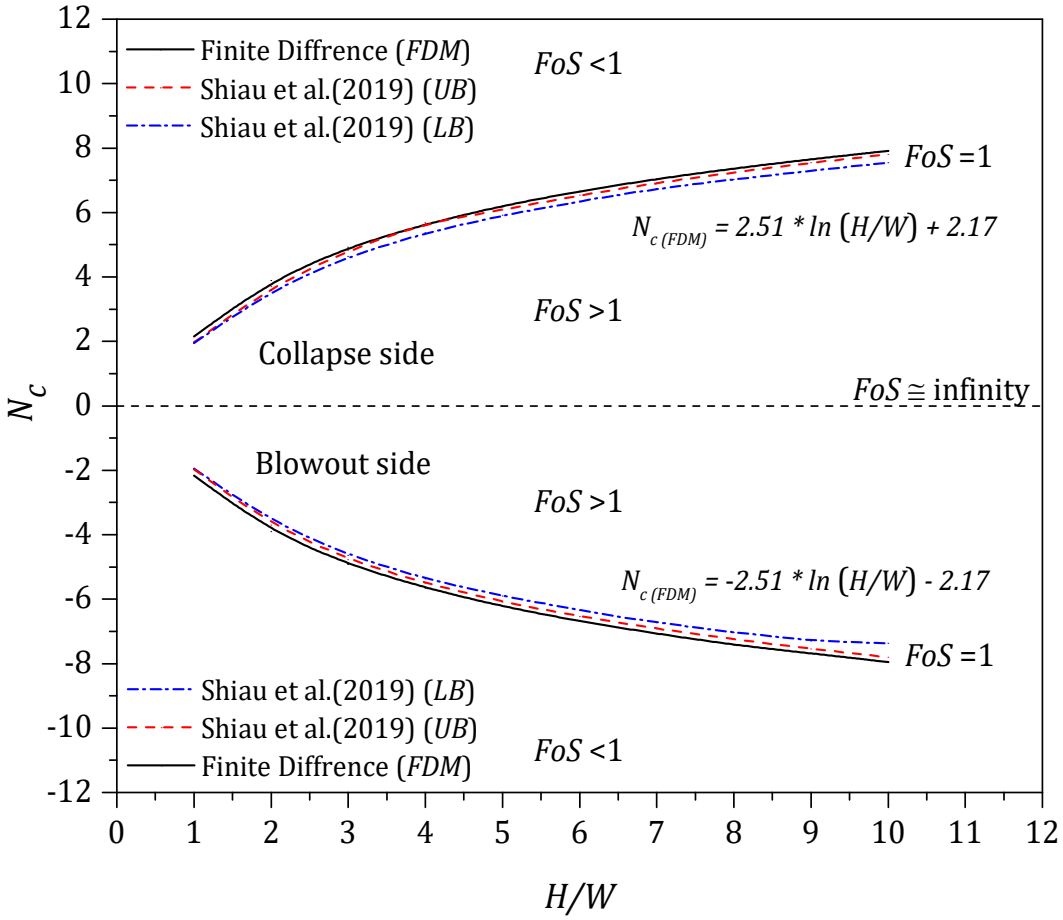

Figure 6. 4 N_c *vs. H/W (FDM, FELA UB and FELA LB*)

Note that the critical stability number (N_c) represents the "design" *N* value when *FoS* = 1. This is the failure envelope for *FoS* = 1. Also, note that *FoS* > 1 when a "design" *N* value is located within the failure envelope, and *FoS* < 1 when a "design" *N* value is located outside the failure envelope.

The finite difference results of N_c were chosen for the regression analysis. These are presented in equations 6.4 and 6.5 for collapse and blowout respectively. For these purpose the logarithmic function was chosen to yields an accurate curve-fitting of *FDM* with the high accuracy of r^2 = 0.998.

$$N_{c(FDM)} = 2.51 \times \ln\left(\frac{H}{W}\right) + 2.17 \tag{6.4}$$

$$N_{c(FDM)} = -2.51 \times \ln\left(\frac{H}{W}\right) - 2.17 \tag{6.5}$$

Using equations 2.2 and 6.2, the *FoS* can be determined with equation 6.6.

$$FoS = \frac{N_C}{N} = \frac{N_c \times S_u}{\sigma_s + \gamma H - \sigma_t} \tag{6.6}$$

Substituting equations 6.4 and 6.5 into equation 6.5, equation 6.7 can be used to determine the factor of safety (*FoS*) for known design parameters (σ_s , σ_t , γ, H, W and S_u).

$$FoS = \frac{N_C}{N} = \frac{(\pm 2.51 \times \ln(H/W) \pm 2.17) \times S_u}{\sigma_s + \gamma H - \sigma_t} \tag{6.7}$$

Equation 6.7 has also been presented graphically in figure 6.5. The design contour map of *FoS* was constructed based on the *FDM* numerical solutions.

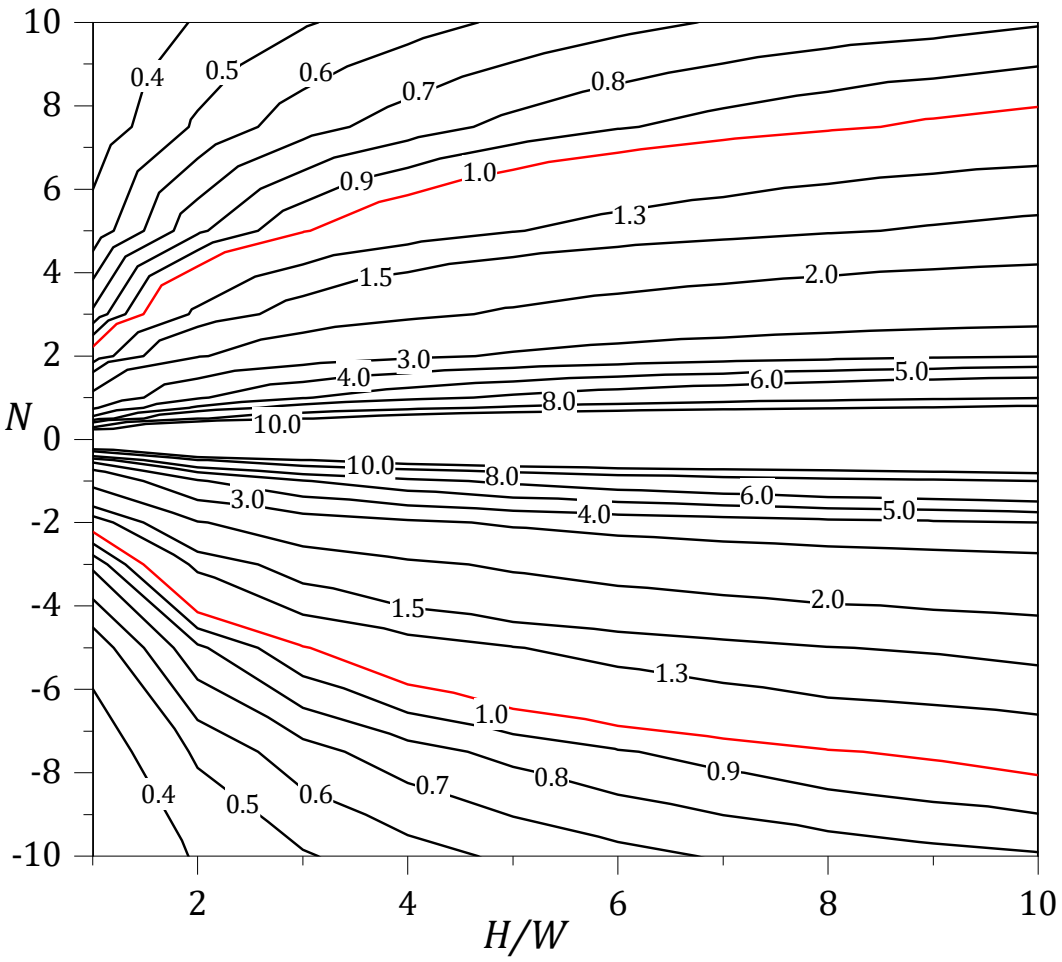

Figure 6. 5 *FoS* design chart for various *N* and *H/W*

By rearranging equation 6.6, one can determine the required support pressure σ_t and surchage load σ_s for a given FoS using equations 6.8 and 6.9 respectively.

$$\sigma_t = \sigma_s + \gamma H - \left(\frac{N_c \times S_u}{FoS} \right) \tag{6.8}$$

$$\sigma_s = \sigma_t + \left(\frac{N_c \times S_u}{FoS} \right) - \gamma H \tag{6.9}$$

Results Comparison

Figure 6.6 compares results of the N_c obtained in this study with those in published literature.

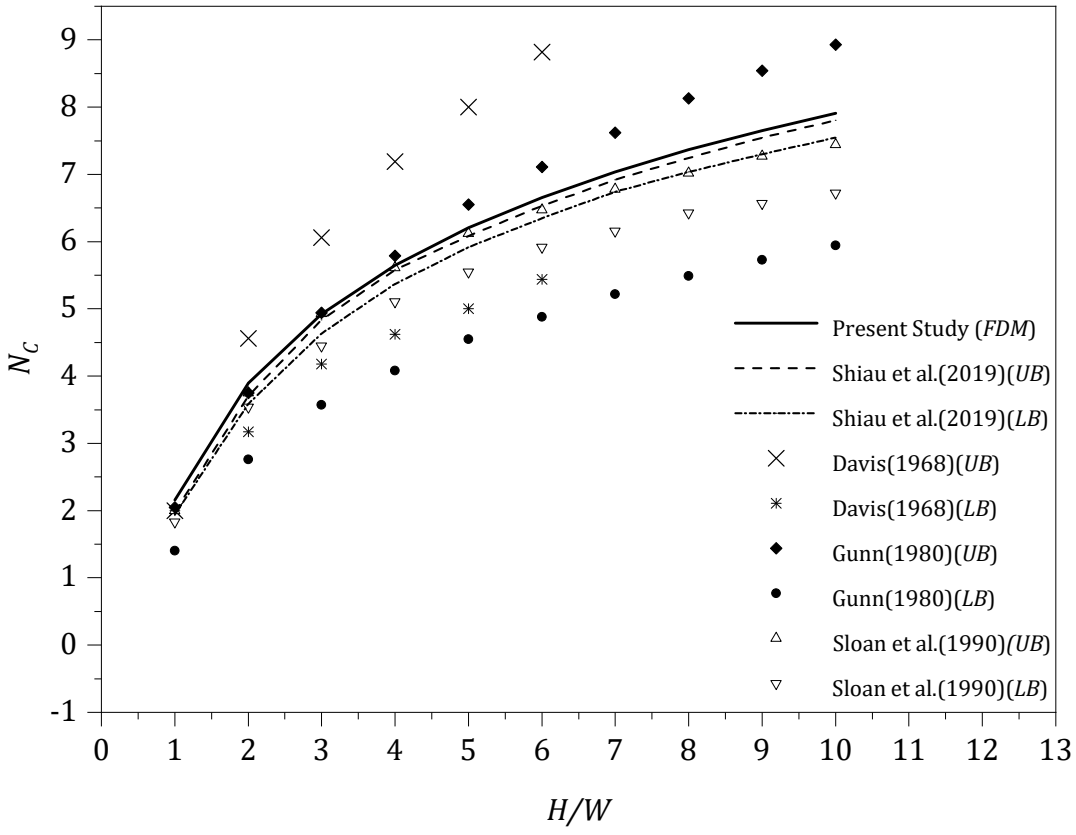

Figure 6. 6 Comparison of N_c values

In general, the *FDM* results are 0.6% to 8 % larger than the *FELA UB* solutions of Shiau et al. (2019). Overall, the predicted trend of *FDM* shows a good agreement with the *FELA LB* and *UB* solutions.

Table 6.4 shows that the *FDM* results of current the study are significantly different to Davis (1968) solutions, who considered a number of simple stress fields for lower bound solutions and vertical slip mechanisms for upper bound solutions.

Table 6. 4 Comparison of N_c values

H/W	Present study	Shiau et al. (2019)		Davis (1968)		Gunn (1980)		Sloan et al. (1990)	
	FDM	*LB*	*UB*	*LB*	*UB*	*LB*	*UB*	*LB*	*UB*
1	2.16	1.94	1.98	2	2	1.4	2.05	1.83	2
2	3.90	3.59	3.71	3.17	4.56	2.76	3.75	3.54	3.75
3	4.93	4.63	4.83	4.18	6.06	3.57	4.94	4.45	4.93
4	5.65	5.37	5.68	4.62	7.19	4.08	5.79	5.11	5.61
5	6.21	5.92	6.08	5	8	4.55	6.55	5.55	6.12
6	6.66	6.35	6.53	5.44	8.82	4.88	7.11	5.92	6.47
7	7.04	6.74	6.92	-	-	5.22	7.62	6.16	6.78
8	7.37	7.03	7.25	-	-	5.49	8.13	6.43	7.02
9	7.65	7.3	7.55	-	-	5.73	8.54	6.57	7.27
10	7.91	7.55	7.8	-	-	5.94	8.93	6.72	7.44

The results of Davis's investigation have been improved by Gunn (1980) using the three rigid blocks parameters. Despite the improvement, the upper bound solution of Gunn (1980) are still 4 to 12.9% larger than the current *FDM*.

Results show that there is about some 0.65% to 15% difference between this study (*FDM*) and Sloan et al. (1990). Although Sloan et al. (1990) carried out extensive research on trapdoor stability, the use of linear finite limit analysis software produced less accurate results.

In particular, the lower bound shows a large variation in comparison to *FDM*. In general, except for Davis (1968) and Gunn (1980), the assessment of the trapdoor critical stability number (N_c) shows a very good agreement with those of existing solutions.

6.5. Failure extent

Results of the failure extent investigation are shown in figure 6.7. The distance of failure extent was determined by inspection of the velocity vector plots produced in the program.

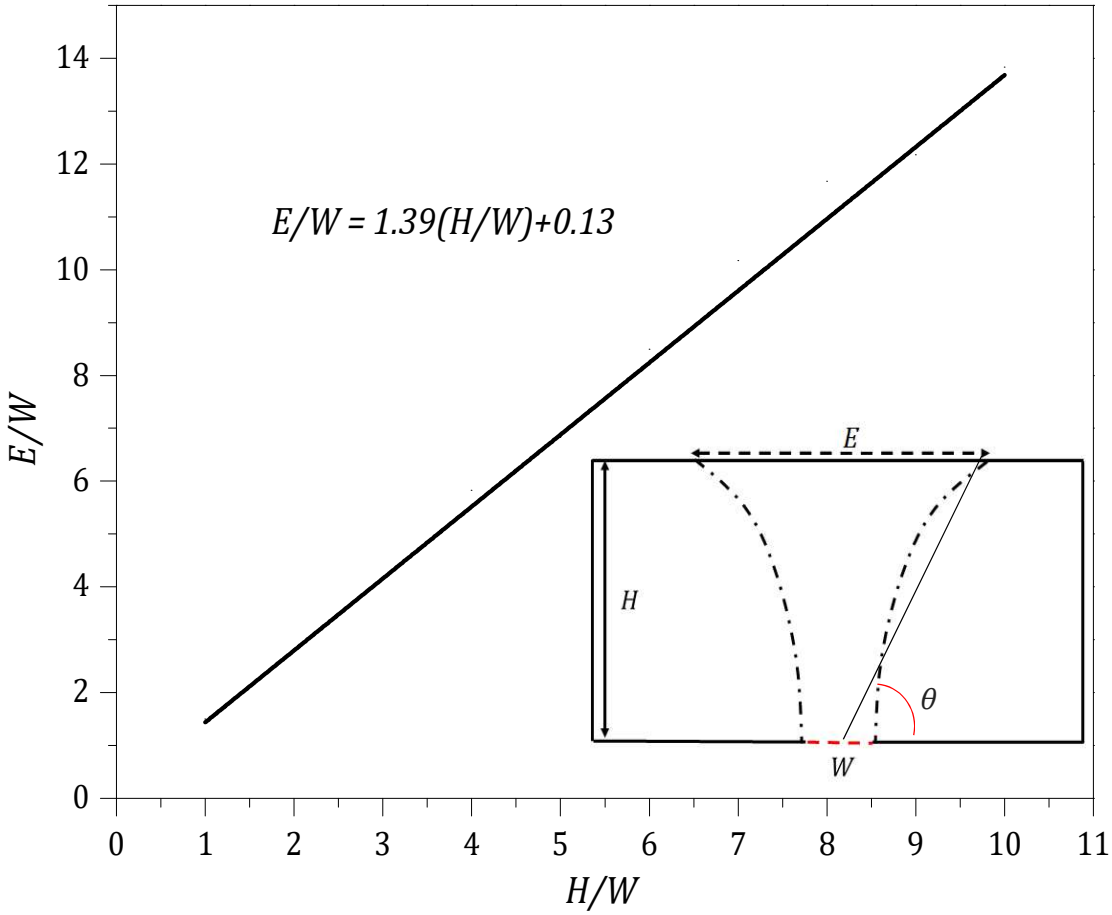

Figure 6. 7 Failure extent

Figure 6.7 suggests that the failure extent ratio (*E/W*) is linearly proportional to the depth ratio (*H/W*). The linear relationship is presented in equation 6.10.

$$\frac{E}{W} = 1.39\left(\frac{H}{W}\right) + 0.13 \qquad (6.10)$$

Table 6.5 shows the data used for plotting figure 6.7.

Table 6. 5 Determination of failure extent

Depth ratio (H/W)	Actual depth(H) in meter	Measured surface half failure extent ($E/2$) in meter	Angle $\theta=\tan^{-1}(H/(E/2))$ in degree	Ratio of failure extent to trapdoor width (E/W)
1	6	4.50	53.1	1.50
2	12	8.50	54.7	2.83
3	18	12.5	55.2	4.17
4	24	17.5	53.9	5.83
5	30	20.5	55.7	6.83
6	36	25.5	54.7	8.50
7	42	30.5	54.0	10.17
8	48	35.0	53.9	11.67
9	54	36.5	55.9	12.17
10	60	41.5	55.3	13.83

Half cavity size (W/2) = 3 meters

A practical conclusion can be drawn from table 6.5, showing that an approximate 55 degree line can be drawn from the centre of the trapdoor to the outer boundary of the failure surface to estimate the failure extent. Note that this investigation is valid for all values of stability numbers (N).

Worked examples

Example 1- Determine the FoS

An old vertical mining shaft has no internal pressure and no surcharge pressure. For the given parameters (S_u = 154 kPa, γ = 18 kN/m^3, H= 36 m, and W = 6 m), determine the *FoS*.

- Since there is no internal pressure, only the collapse failure should be considered.
- The stability number is $N = \gamma H/S_u = 4.21$.
- Using H/W = 6 and N = 4.21, equation 6.7 gives a *FoS* of 1.58 for the collapse.
- Using H/W = 6 and N = 4.21, figure 6.5 gives an approximate *FoS* of 1.6.
- An actual computer analysis of this case gives a *FoS* of 1.63.

What is the critical support pressure σ_t when σ_s =200 kPa and FoS = 1?

- Using equation 6.5, N_c =6.67 for collapse.
- From equation 6.8, $\sigma_t = \sigma_s + \gamma H - (N_c * S_u / FoS)$ = 200 + (18*36) - (6.67*154/1) = -179.18 kPa.

Example 2- Estimate the depth of a sinkhole (H)

An existing sinkhole has a diameter of 10 meters. Estimate the depth of the sinkhole using the following parameters for cohesive soil. S_u = 54 kPa and γ = 19 kN/m^3.

- Note that equation 6.10 is independent of the design parameter N. The only needed information is the E.
- From equation 6.10, $10/W = 1.39*(H/W) + 0.13$.
- By ignoring the small value of $(0.13W)$, the depth (H) is found to be 7.19 m.

Example 3- Design of a supported cavity (σ_t)

A FoS of 4 is required for the design of an underground military bunker where the surcharge pressure is given as σ_s = 50 kPa. The following parameters are known: S_u = 25 kPa, γ = 18 kN/m^3, H= 40 m and W = 30 m.

- Using equation 6.4, the critical stability number is N_c = 2.89. Note that figure 6.4 can also be used to find the N_c value.
- Substitute the N_c value into equation 6.8,
  $\sigma_t = \sigma_s + \gamma H - (N_c * S_u / FoS)$ = 50+(18*40)-(2.9*25/4) = 752 kPa.
- The required pressure to support the cavity for a factor of safety of 4 is 752 kPa.

6.6. Conclusion

A series of *2D* plane strain numerical models constructed and tested to investigate the stability of trapdoor with non-zero surcharge load (σ_s) and internal pressure (σ_t) with in undrained clay. The results of this study obtained by utilizing the shear strength reduction method (*SSRM*) in finite difference method. The results presented in the form of a factor of safety (*FoS*) for a broad range of stability number (N).

The *FoS* was found to be a function of the depth ratio (*H/W*) and stability number (*N*). The numerical results suggest that the *FoS* increases when the stability number (*N*) decreases. The *FoS* becomes very large when the stability *N* is very small. Further investigation on failure mechanisms indicates a linear relationship between the failure extent ratio (*E/W*) and the depth ratio (*H/W*). The failure angle (θ) measured from the centre of the opening (*W*) to the outer boundary of the failure surface is approximately equal to 55 degrees for all depth ratios (*H/W*).

This investigation has improved the understanding of trapdoor stability and associated surface failure extent. Further study is needed for a more realistic three-dimensional analysis of sinkhole failure. This is to be followed in the next chapter (chapter7).

7. THREE-DIMENSIONAL ANALYSIS OF SINKHOLE PROBLEM USING BROMS & BENNERMARK'S APROACH

7.1. Introduction

The stability of soil overlying the cavity is often a concern when it comes to the risk of sinkhole occurrences. Current sinkhole studies have been centred on the use of geophysical techniques to detect underground cavity sizes and associated depths. With the measured information, it is possible to theoretically predict the extent of a ground surface collapse.

This chapter studies the stability of 3D trapdoors and the associated extent of ground surface failure using Broms and Bennermark's approach. The shear strength reduction method is used to obtain factors of safety for various scenarios associated with the collapse of three-dimensional trapdoors underlying undrained clay. Numerical solutions are verified by using the 3D finite element limit analysis

technique with upper and lower bound theorems and other published results. A number of practical examples are provided to demonstrate the use of design charts and tables. These design tools can be used together with the application of geophysical tools to predict sinkhole occurrences.

7.2. Problem Definition

Figure 7.1 shows the cross-sectional of an idealised three-dimensional horizontal trapdoor problem.

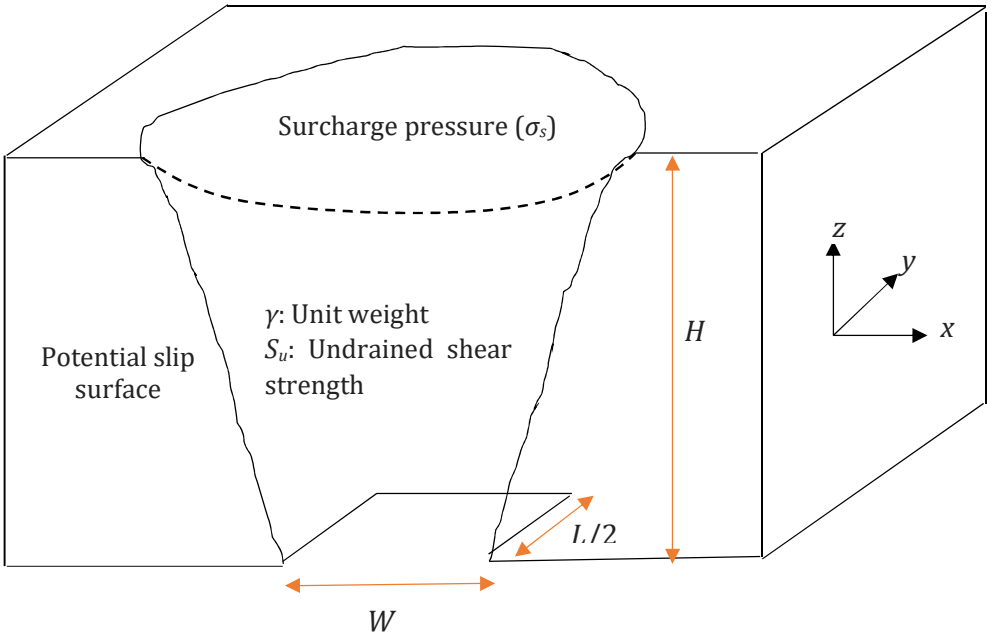

Figure 7. 1 Problem definition

The undrained soil medium is assumed to be homogeneous throughout and is modelled as a Tresca material with the undrained shear strength (S_u) and unit weight (γ). The cavity has a width (W) and an opening length represented by (L). The depth (H) represents the vertical distance from the ground surface to the opening of the cavity. An extensive range of depth ratios (H/W=1-6) and opening ratios (L/W=1-10) are selected for parametric studies using the stability number (N) introduced by Broms and Bennermark (1967).

Broms and Bennermark's stability number (N) consists of two parts; namely the overburden pressure ratio ($OPR = (\sigma_s + \gamma H)/S_u$) and the supporting pressure ratio ($SPR = \sigma_t / S_u$). The combination of these two factors would generate three different

cases. Firstly, if the overburden pressure ($\sigma_s + \gamma H/S_u$) is greater than the supporting pressure (σ_t/S_u), the cavity undergoes a collapse failure. Secondly, if the supporting pressure (*SPR*) and the overburden pressure (*OPR*) are equal, the cavity is in an idealised weightless condition. And finally, if the supporting pressure (*SPR*) is greater than the overburden pressure (*OPR*), a blowout failure occurs.

It should be noted that while in reality the natural trapdoor could be subjected to internal pressure (due to water pressure or even by vertical seismic forces), this study neglects the effect of such internal pressures and only considers the collapse failure i.e. positive *N* values (*OPR* > *SPR*). A wide range of stability number (*N*=1 to 15) have been selected to cover most collapse combinations. The finite difference software *FLAC3D and SSRM* are used to determine the *FoS,* which is a function of the depth ratio (*H/W*), the opening ratio (*L/W*) and the stability number (*N*), as shown in equation 7.1.

$$FoS = f\left(\frac{H}{W}, \frac{L}{W}, N\right) \tag{7.1}$$

7.3. Modelling Technique

The finite difference method (*FDM*) is one of the oldest techniques used in numerical studies and is a powerful method for analysing complex geotechnical stability problems involving nonlinear solutions. The *SSRM* is often implemented through the conventional Mohr-Coulomb model. This method is popular in geotechnical engineering and has been widely used in the analysis of slope stability, nevertheless, it has seldom been used in the analysis of underground stability problems (Shiau et al. 2018).

Internal model validation

Three different meshes have been developed for the purpose of model validation. The full mesh, half mesh, and quarter mesh produce identical *FoS* results, which have greatly improved the confidence in develping the models. For efficiency reasons, the quarter mesh was used in this study. It has significantly reduced the computational time whilst maintaining accuracy of the solutions. In addition, a *FISH*

script has been developed to automate mesh generation and solve for the solution, allowing parametric studies to be undertaken efficiently.

A typical 3D finite difference mesh used in this study is shown in figure 7.2. The domain size of the models were carefully chosen by observing the velocity fields to minimise boundary effects. Both the front and inner faces are fixed in the y-direction, representing the symmetrical faces. The outer face and back face are restrained in x and y directions while the lower face (except where the trapdoor is located) is restrained in x, y and z directions. The top face is free to displace in all directions. A total of 720 cases were analysed using the *FoS* approach. Numerical results of the *FoS* are validated by using the solutions obtained from 3D *FELA* (Shiau et al. 2019) and are then used to find the critical stability number (N_c) for each depth ratio (H/W). In addition, the vertical velocity contours of the *FDM* output are also examined to investigate the surface subsidence.

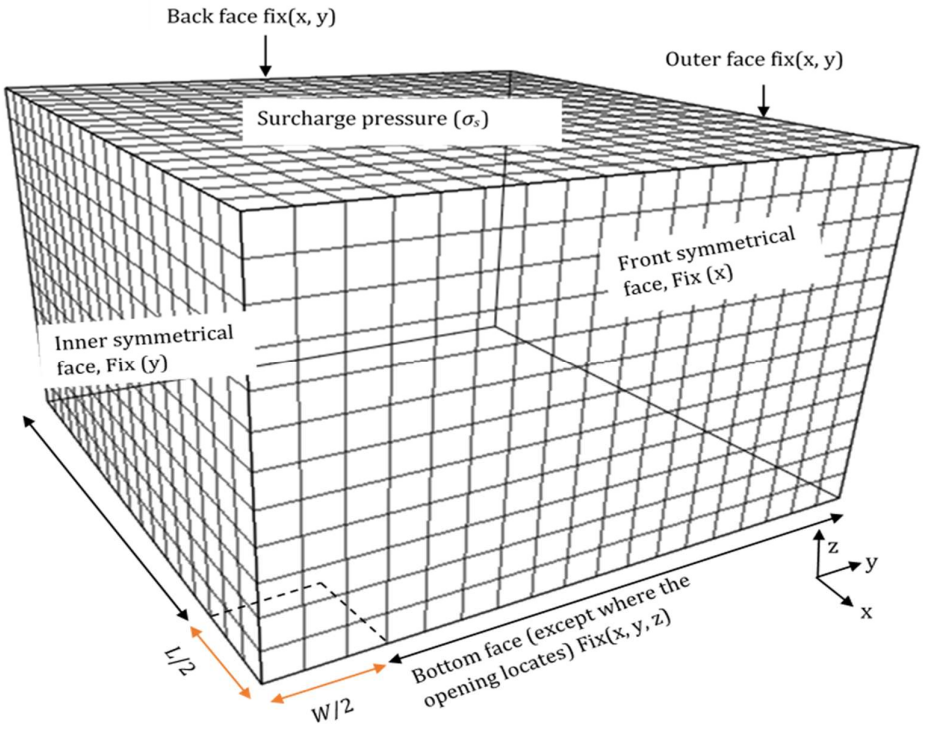

Figure 7. 2 Typical quarter mesh for *FLAC* 3D include boundary conditions

7.4. Results and discussions

To cover a wide range of practical parameters, an extensive range of stability numbers (N=0 to 15), depth ratios (H/W=1 to 6) and opening ratios (L/W=1 to 10),

were selected for the parametric studies. The comprehensive *FoS* results of this investigation are presented in tables 7.1 to 7.5.

Table 7. 1 *FoS* results for *H/W*=1-6 (*L/W*=1 and 2)

	N	*H/W*					
		1	2	3	4	5	6
		FoS					
L/W=1	0	Infinity	Infinity	Infinity	Infinity	Infinity	Infinity
	0.25	19.08	30.17	36.66	41.26	44.83	47.75
	0.5	9.54	15.09	18.33	20.63	22.42	23.87
	0.75	6.36	10.06	12.22	13.75	14.94	15.92
	1	4.77	7.54	9.16	10.32	11.21	11.94
	2	2.39	3.77	4.58	5.16	5.6	5.97
	3	1.59	2.51	3.05	3.44	3.74	3.98
	5	0.95	1.51	1.83	2.06	2.24	2.39
	7.5	*0.64*	*1.01*	*1.22*	*1.38*	*1.49*	*1.59*
	10	0.48	0.75	0.92	1.03	1.12	1.19
	12.5	0.38	0.6	0.73	0.83	0.9	0.95
	15	0.32	0.5	0.61	0.69	0.75	0.8
L/W=2	0	Infinity	Infinity	Infinity	Infinity	Infinity	Infinity
	0.25	16.83	26.1	31.51	35.36	38.34	40.77
	0.5	8.42	13.05	15.76	17.68	19.17	20.39
	0.75	5.61	8.7	10.5	11.79	12.78	13.59
	1	4.21	6.52	7.88	8.84	9.58	10.19
	2	2.1	3.26	3.94	4.42	4.79	5.1
	3	1.4	2.17	2.63	2.95	3.19	3.4
	5	0.84	1.3	1.58	1.77	1.92	2.04
	7.5	0.56	0.87	1.05	1.18	1.28	1.36
	10	0.42	0.65	0.79	0.88	0.96	1.02
	12.5	0.34	0.52	0.63	0.71	0.77	0.82
	15	0.28	0.43	0.53	0.59	0.64	0.68

Table 7. 2 *FoS* results for *H/W*=1-6 (*L/W*=3 and 4)

	N	*H/W*					
		1	2	3	4	5	6
		FoS					
L/W=3	0	Infinity	Infinity	Infinity	Infinity	Infinity	Infinity
	0.25	15.52	23.86	28.73	32.19	34.87	37.07
	0.5	7.76	11.93	14.37	16.1	17.44	18.53
	0.75	5.17	7.95	9.58	10.73	11.62	12.36
	1	3.88	5.96	7.18	8.05	8.72	9.27
	2	1.94	2.98	3.59	4.02	4.36	4.63
	3	1.29	1.99	2.39	2.68	2.91	3.09
	5	0.78	1.19	1.44	1.61	1.74	1.85
	7.5	0.52	0.8	0.96	1.07	1.16	1.24
	10	0.39	0.6	0.72	0.8	0.87	0.93
	12.5	0.31	0.48	0.57	0.64	0.7	0.74
	15	0.26	0.4	0.48	0.54	0.58	0.62
L/W=4	0	Infinity	Infinity	Infinity	Infinity	Infinity	Infinity
	0.25	14.59	22.32	26.85	30.06	32.55	34.58
	0.5	7.29	11.16	13.42	15.03	16.27	17.29
	0.75	4.86	7.44	8.95	10.02	10.85	11.53
	1	3.65	5.58	6.71	7.51	8.14	8.65
	2	1.82	2.79	3.36	3.76	4.07	4.32
	3	1.22	1.86	2.24	2.5	2.71	2.88
	5	0.73	1.12	1.34	1.5	1.63	1.73
	7.5	0.49	0.74	0.89	1	1.08	1.15
	10	0.36	0.56	0.67	0.75	0.81	0.86
	12.5	0.29	0.45	0.54	0.6	0.65	0.69
	15	0.24	0.37	0.45	0.5	0.54	0.58

Table 7. 3 *FoS* results for *H/W*=1-6 (*L/W*=5 and 6)

	N	*H/W*					
		1	2	3	4	5	6
		FoS					
L/W=5	0	Infinity	Infinity	Infinity	Infinity	Infinity	Infinity
	0.25	13.87	21.16	25.43	28.46	30.81	32.73
	0.5	6.93	10.58	12.72	14.23	15.41	16.37
	0.75	4.62	7.05	8.48	9.49	10.27	10.91
	1	3.47	5.29	6.36	7.12	7.7	8.18
	2	1.73	2.65	3.18	3.56	3.85	4.09
	3	1.16	1.76	2.12	2.37	2.57	2.73
	5	0.69	1.06	1.27	1.42	1.54	1.64
	7.5	0.46	0.71	0.85	0.95	1.03	1.09
	10	0.35	0.53	0.64	0.71	0.77	0.82
	12.5	0.28	0.42	0.51	0.57	0.62	0.65
	15	0.23	0.35	0.42	0.47	0.51	0.55
L/W=6	0	Infinity	Infinity	Infinity	Infinity	Infinity	Infinity
	0.25	13.27	20.23	24.31	27.2	29.44	31.27
	0.5	6.64	10.12	12.15	13.6	14.72	15.63
	0.75	4.42	6.74	8.1	9.07	9.81	10.42
	1	*3.32*	*5.06*	*6.08*	*6.8*	*7.36*	*7.82*
	2	1.66	2.53	3.04	3.4	3.68	3.91
	3	*1.11*	*1.69*	*2.03*	*2.27*	*2.45*	*2.61*
	5	0.66	1.01	1.22	1.36	1.47	1.56
	7.5	0.44	0.67	0.81	0.91	0.98	1.04
	10	0.33	0.51	0.61	0.68	0.74	0.78
	12.5	0.27	0.4	0.49	0.54	0.59	0.63
	15	0.22	0.34	0.41	0.45	0.49	0.52

Table 7. 4 *FoS* results for *H/W*=1-6 (*L/W*=7 and 8)

	N	*H/W*					
		1	2	3	4	5	6
		FoS					
L/W=7	0	Infinity	Infinity	Infinity	Infinity	Infinity	Infinity
	0.25	12.78	19.46	23.37	26.15	28.3	30.06
	0.5	6.39	9.73	11.69	13.07	14.15	15.03
	0.75	4.26	6.49	7.79	8.72	9.43	10.02
	1	3.19	4.87	5.84	6.54	7.08	7.52
	2	1.6	2.43	2.92	3.27	3.54	3.76
	3	1.06	1.62	1.95	2.18	2.36	2.51
	5	0.64	0.97	1.17	1.31	1.42	1.5
	7.5	0.43	0.65	0.78	0.87	0.94	1
	10	0.32	0.49	0.58	0.65	0.71	0.75
	12.5	0.26	0.39	0.47	0.52	0.57	0.6
	15	0.21	0.32	0.39	0.44	0.47	0.5
L/W=8	0	Infinity	Infinity	Infinity	Infinity	Infinity	Infinity
	0.25	12.34	18.8	22.58	25.26	27.34	29.04
	0.5	6.17	9.4	11.29	12.63	13.67	14.52
	0.75	4.11	6.27	7.53	8.42	9.11	9.68
	1	3.09	4.7	5.64	6.31	6.83	7.26
	2	1.54	2.35	2.82	3.16	3.42	3.63
	3	1.03	1.57	1.88	2.1	2.28	2.42
	5	0.62	0.94	1.13	1.26	1.37	1.45
	7.5	0.41	0.63	0.75	0.84	0.91	0.97
	10	0.31	0.47	0.56	0.63	0.68	0.73
	12.5	0.25	0.38	0.45	0.51	0.55	0.58
	15	0.21	0.31	0.38	0.42	0.46	0.48

Table 7. 5 *FoS* results for *H/W*=1-6 (*L/W*=9 and 10)

	N	*H/W*					
		1	2	3	4	5	6
		FoS					
L/W=9	0	Infinity	Infinity	Infinity	Infinity	Infinity	Infinity
	0.25	11.96	18.22	21.89	24.49	26.51	28.15
	0.5	5.98	9.11	10.94	12.24	13.25	14.08
	0.75	3.99	6.07	7.3	8.16	8.84	9.38
	1	2.99	4.56	5.47	6.12	6.63	7.04
	2	1.5	2.28	2.74	3.06	3.31	3.52
	3	1	1.52	1.82	2.04	2.21	2.35
	5	0.6	0.91	1.09	1.22	1.33	1.41
	7.5	0.4	0.61	0.73	0.82	0.88	0.94
	10	0.3	0.46	0.55	0.61	0.66	0.7
	12.5	0.24	0.36	0.44	0.49	0.53	0.56
	15	0.2	0.3	0.36	0.41	0.44	0.47
L/W=10	0	Infinity	Infinity	Infinity	Infinity	Infinity	Infinity
	0.25	11.62	17.71	21.28	23.81	25.77	27.37
	0.5	5.81	8.86	10.64	11.9	12.89	13.69
	0.75	3.87	5.9	7.09	7.94	8.59	9.12
	1	2.9	4.43	5.32	5.95	6.44	6.84
	2	1.45	2.21	2.66	2.98	3.22	3.42
	3	0.97	1.48	1.77	1.98	2.15	2.28
	5	0.58	0.89	1.06	1.19	1.29	1.37
	7.5	0.39	0.59	0.71	0.79	0.86	0.91
	10	0.29	0.44	0.53	0.6	0.64	0.68
	12.5	0.23	0.35	0.43	0.48	0.52	0.55
	15	0.19	0.3	0.35	0.4	0.43	0.46

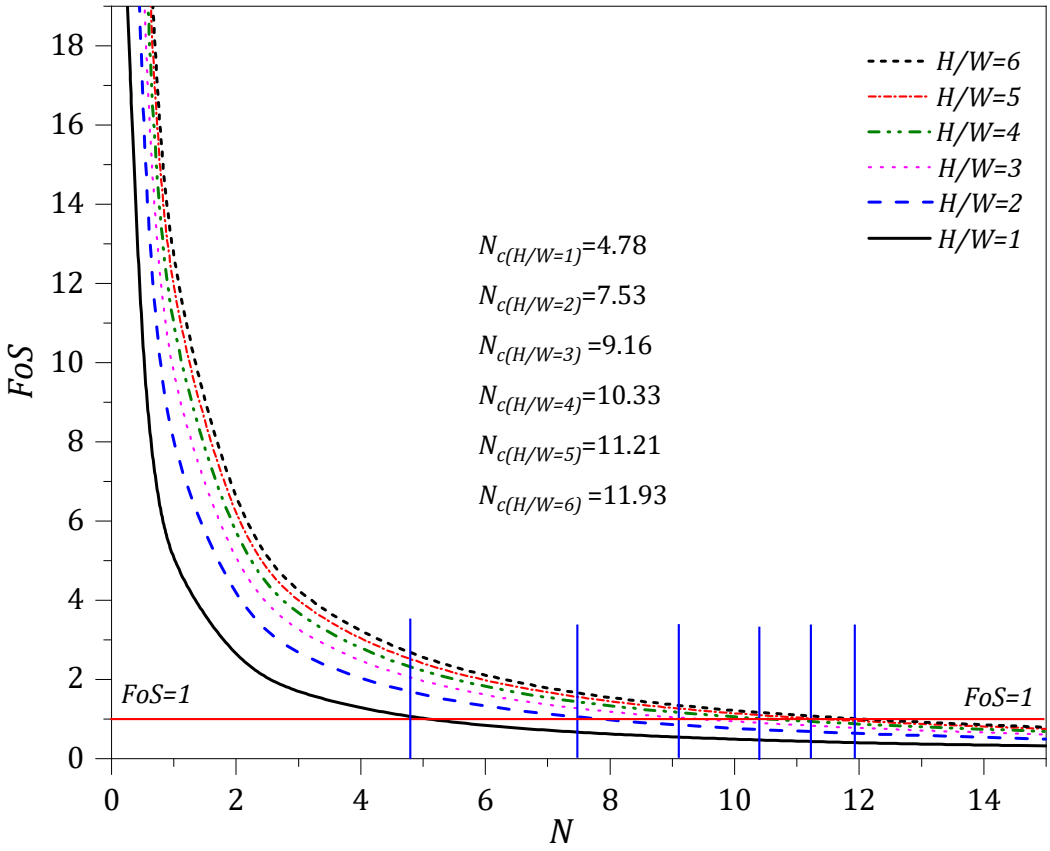

Figure 7. 3 *FoS* vs *N* for *L/W*=1

Figure 7.3 presents the *FDM* results of *FoS* versus *N* for *L/W*=1. The results show a hyperbolic curve, where *N* and *FoS* are considered as a horizontal and vertical asymptote respectively. The general equation for this graph can be defined as in equation 7.2, indicating that any combination of the *N* and *FoS* would result in a distinctive value of N_c.

$$N_c = N \times FoS \tag{7.2}$$

As shown in figure 7.3, this unique N_c value is constant for each *H/W*. Also, note that the value of N_c increases as *H/W* increases. A closer inspection of figure 7.3 reveals that, when *N* is equal to zero (i.e. overburden pressure ratio is equal to the supporting pressure ratio), the *FoS* is at a maximum (∞). This condition is considered as the 'weightless scenario'. As the stability number (*N*) increases, the *FoS* gradually decreases. When *FoS* is equal to 1, the corresponding stability number is the critical stability number (N_c). For such a critical condition, Broms and Bennermarks's equation 2.2 can be rearranged to estimate other critical parameters

such as the critical surcharge load as shown in equation 7.3. Note that the same process can be used to calculate other critical parameters using equation 2.2.

$$\sigma_s = \sigma_t + (N_c \times S_u) - \gamma H \tag{7.3}$$

Note that the same process can be repeated to calculate the critical supporting pressure but since the focus of this study is on collapse, therefore the critical supporting pressure relationship has not been presented.

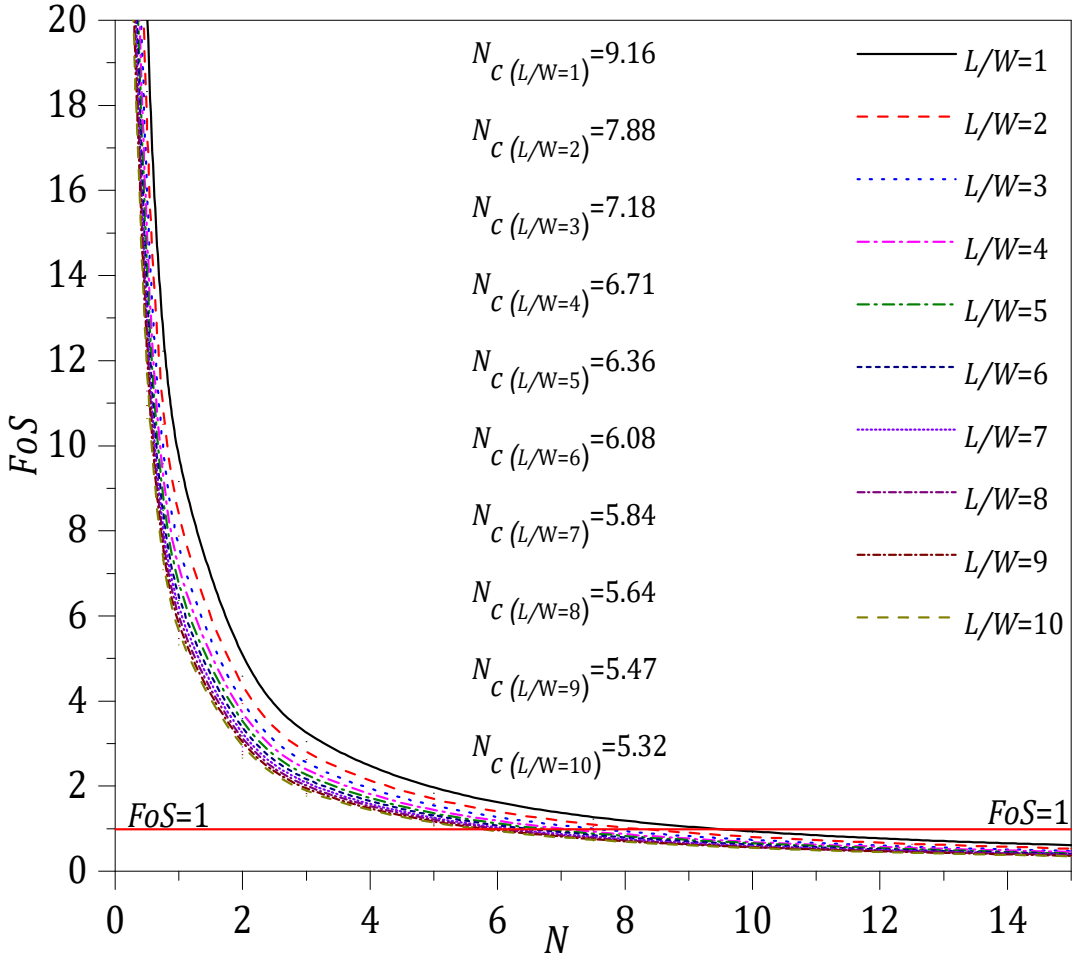

Figure 7. 4 *FoS* vs *N* for *H/W*=3

Figure 7.4 investigates the effect of the opening ratio (*L/W*) on the stability of the trapdoor for *H/W*=3. Similar to figure 7.3, the results form an asymptote and suggest that as *L/W* increases, N_c decreases. Based on the results in figures 7.3 and 7.4, the relationship between *H/W* and the critical stability number (N_c) is presented in figure 7.5.

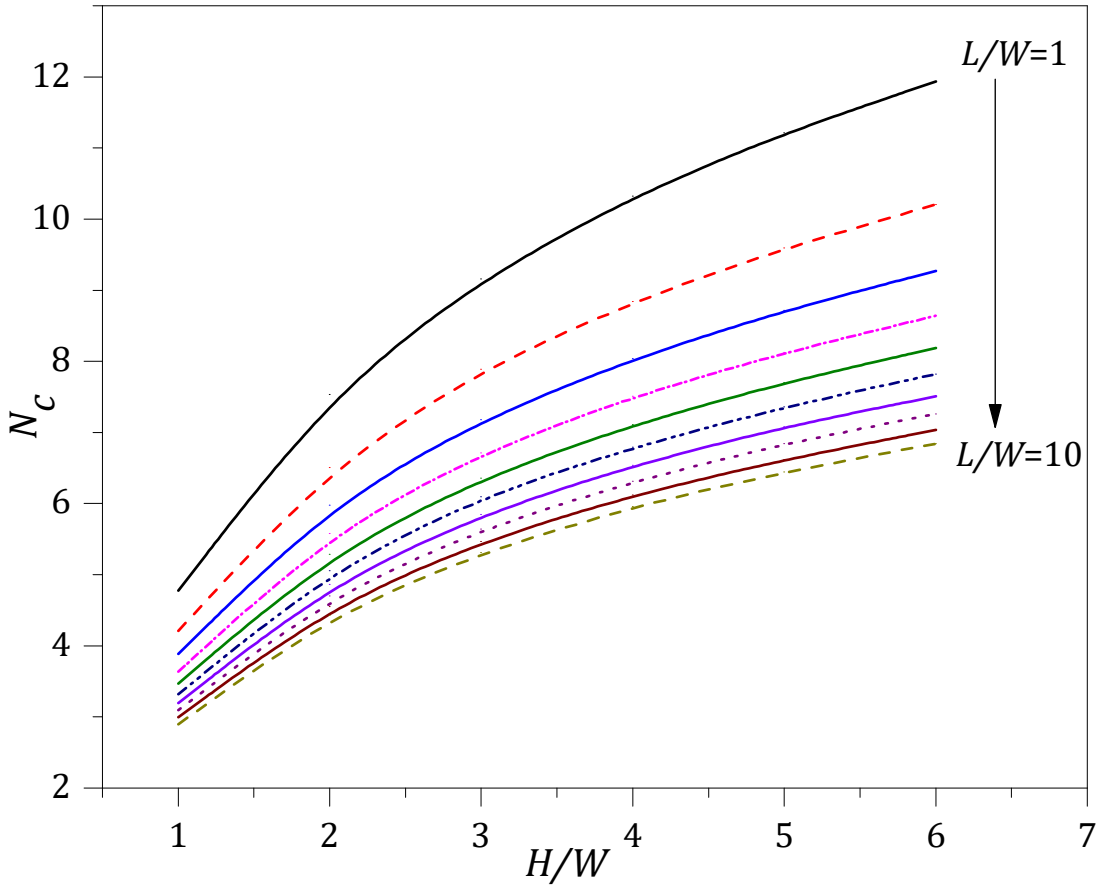

Figure 7. 5 N_c vs H/W for various opening ratios (L/W)

The numerical results used to plot figure 7.5 are presented in table 7.6.

Table 7. 6 N_c results for various opening ratios (L/W) and depth ratios (H/W=1-6)

L/W	H/W=1	H/W=2	H/W=3	H/W=4	H/W=5	H/W=6
1	4.78	7.53	9.16	10.33	11.21	11.93
2	4.21	6.51	7.88	8.84	9.59	10.20
3	3.89	5.98	7.18	8.04	8.72	9.27
4	3.64	5.58	6.71	7.51	8.13	8.64
5	3.47	5.29	6.36	7.11	7.70	8.19
6	3.32	5.06	6.08	6.79	7.36	7.82
7	3.20	4.86	5.84	6.54	7.08	7.51
8	3.10	4.70	5.64	6.31	6.84	7.26
9	3.00	4.55	5.47	6.12	6.62	7.04
10	2.90	4.43	5.32	5.96	6.45	6.85

The area bounded by each curve and x-axis (*H/W*) represents the safe zone where the *FoS* is greater than 1. On the other hand, the area above each curve represents the unsafe zone (*FoS* < 1). Figure 7.5 also shows that the difference in N_c values become smaller as the *L/W* becomes larger (i.e. approaches a 2D plane strain solution, *L/W*=∞).

Figure 7.5 is particularly important for designers because of the critical parameters presented. Note that N_c represents a *FoS* = 1 condition and is a function of both *H/W* and *L/W*, as shown in equation 7.4.

$$N_c = f(\frac{H}{W}, \frac{L}{W}) \tag{7.4}$$

The relationship of the critical stability number (N_c) can also be mathematically represented by equation 7.5.

$$N_c = [-0.81 \times \ln(L/W) + 4.77] + [4 \times (L/W)^{-0.26} \times \ln(H/W)] \tag{7.5}$$

Substituting equation 7.5 into equation 7.3, the critical surcharge load (σ_s) can be estimated by using equation 7.6.

$$\sigma_s = \sigma_t - \gamma H + [(-0.81 \times \ln(L/W) + 4.77) + ((4 \times (L/W)^{-0.26}) \times \ln(H/W))] \times S_u \tag{7.6}$$

Substituting equation 7.5 into equation 7.2.

$$(-0.81 \times \ln(L/W) + 4.77) + [4 \times (L/W)^{-0.26} \times \ln(H/W)] = N \times FoS \tag{7.7}$$

The *FoS* can be determined using equation 7.8.

$$FoS = \frac{[-0.81 \times \ln(L/W) + 4.77] + [4 \times (L/W)^{-0.26} \times \ln(H/W)]}{N} \tag{7.8}$$

Applying original Brom & Bennemark's equation (Eq. 2.2), equation 7.8 can also further expanded into equation 7.9.

$$FoS = \frac{[-0.81 \times \ln(L/W) + 4.77] + [4 \times (L/W)^{-0.26} \times \ln(H/W)] \times S_u}{\sigma_s + \gamma H - \sigma_t} \tag{7.9}$$

Given the design parameters σ_s, σ_t, γ, H, S_u, L/W, and H/W, equation 7.9 can be used to estimate a *FoS*.

7.4.1. Results verification

The numerical solutions of N_c for L/W=1 using *FDM* are compared with those using *FELA* (Shiau et al. 2019) and previous 2D investigations (Keawsawasvong et al. 2017). Figure 7.6 shows such a comparison.

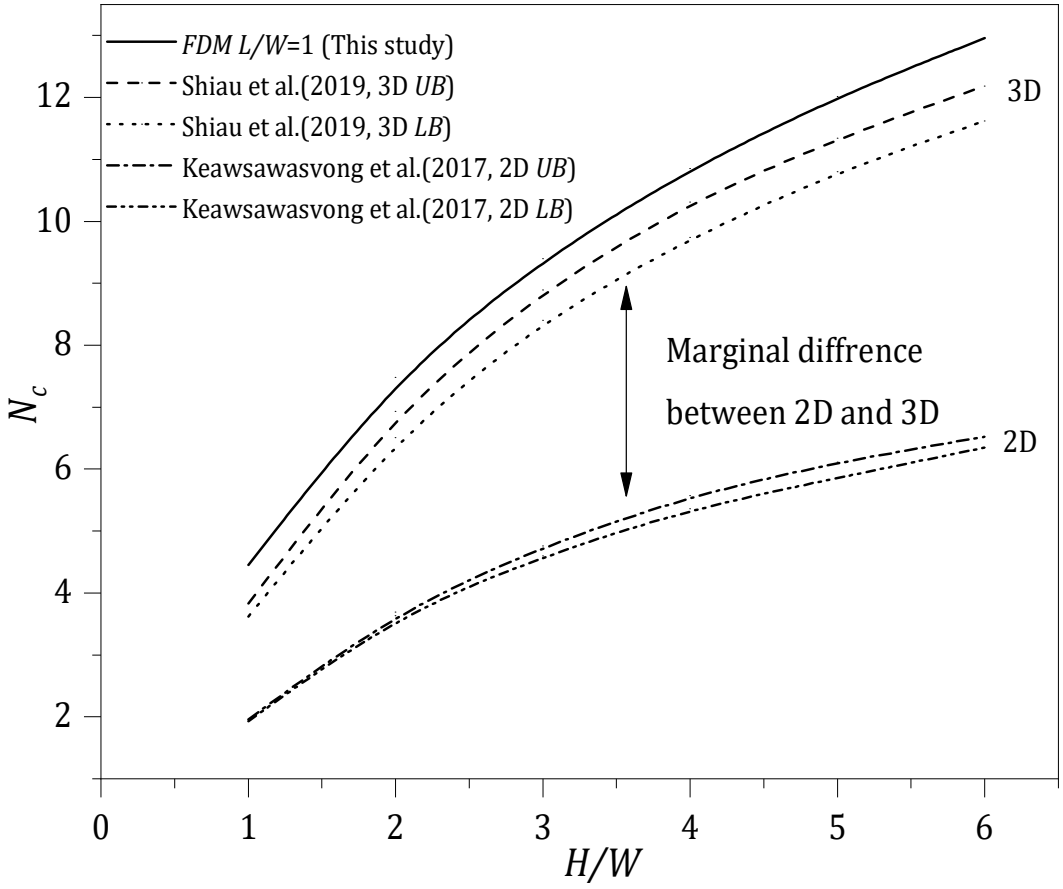

Figure 7. 6 2D (L/W=∞) and 3D (L/W=1) comparison of N_c

Two conclusions can be drawn from this comparison. Firstly, the 3D finite difference solutions are consistently higher than those obtained using 3D finite limit analysis (Shiau et al. 2019). This diffrence is found to be 5-12%. The possible explanation for this variation could be due to the novel use of adaptive mesh in finite limit analysis, which has significantly improved the accuracy of the results. Secondly, the 3D *FDM*

results are almost twice higher than those 2D results in Keawsawasvong et al. (2017).

Table 7. 7 N_c results comparison obtained by *FLAC* 3D, *FELA 3D and FELA 2D*

H/W	3D *FDM* *L/W*=1 (This study)	Shiau et al. (2019, 3D *LB*)	Shiau et al. (2019, 3D *UB*)	Keawsawasvong et al. (2017, 2D *LB*)	Keawsawasvong et al. (2017, 2D *UB*)
1	4.46	3.62	3.83	1.93	1.96
2	7.48	6.51	6.93	3.63	3.69
3	9.40	8.40	8.89	4.60	4.76
4	10.85	9.74	10.31	5.36	5.57
5	12.02	10.80	11.34	5.86	6.11
6	12.96	11.62	12.18	6.35	6.52

Table 7.7 shows the values used for plotting figure 7.6. Note that the marginal difference between 2D and 3D solutions are important for designers, as it provides useful information of the theoretical differences, thus enabling better engineering decisions.

7.4.2. Failure extent

Figure 7.7 presents results of the ground surface failure extent for *L/W=1.* The results are presented in dimensionless ratios where *E/W* is defined as the failure extent ratio and it is a function of the depth ratio *H/W.*

Note that *E* is the diameter of the circular failure surface and is obtained by measuring the distance of non-zero plastic shear strain rate in the output plot of *FDM*. The 3D surface failure extent can be estimated by using equation 7.10.

$$\left(\frac{E}{W}\right)_{L/W=1} = 0.35\frac{H}{W} + 1.12 \tag{7.10}$$

This equation is only applicable to a depth ratio of *H/W*=3. For *H/W* > 3, local failure mechanims are observed and failures do not extend to the ground surface. A possible explanation for this could be attributed to soil arching.

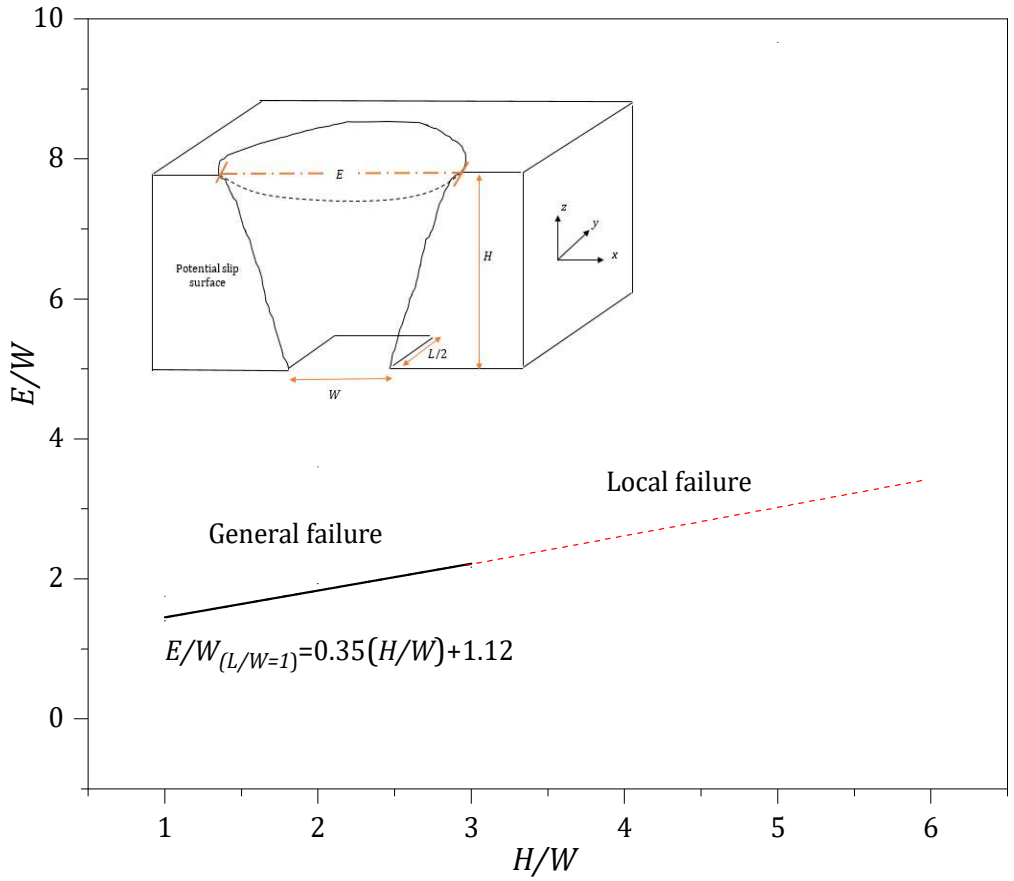

Figure 7. 7 Failure Extent

7.4.3. Arching effect

The arching phenomena was explained by Terzaghi (1936) as a redistribution of the stress from yielding soil particles into non-yielded adjacent soil portions. For trapdoors, when the soil above the opening moves downward, upward shear stress is created. This transfers all or part of the downward pressures to immobile soil particles. Due to this redistribution of stress, the vertical stress above the trapdoor decreases, while the stress on the immobile part of the soil increases (Terzaghi 1936). Figure 7.8 shows the major principal stress contour plots of square openings (L/W=1) for H/W= 1 to 4.

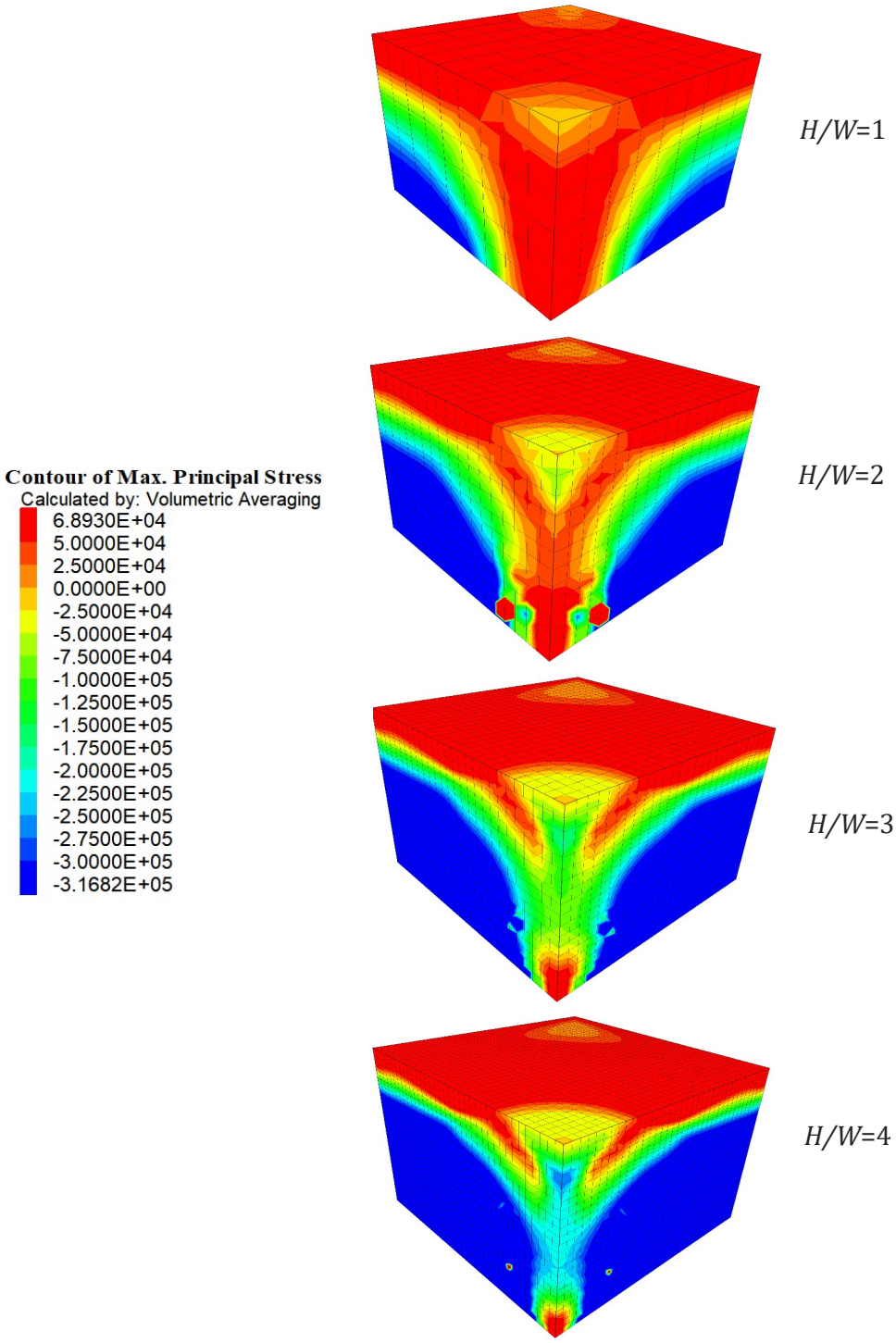

Figure 7. 8 Major principal stress contour for H/W=1 to 4 (L/W=1)

In the shallow cases (H/W= 1 to 3), the positive stresses remain throughout the depth from the surface to the trapdoor. In the case of H/W=4, numerical results show a change of stress sign from postive to negative at a certain depth above the trapdoor level. There is a stress discontinuiety across this region when the depth ratio increases from 3 to 4, indicating a possible formation of a local failure mechanism in deep cases. For these cases, failures do not extend to the ground surface.

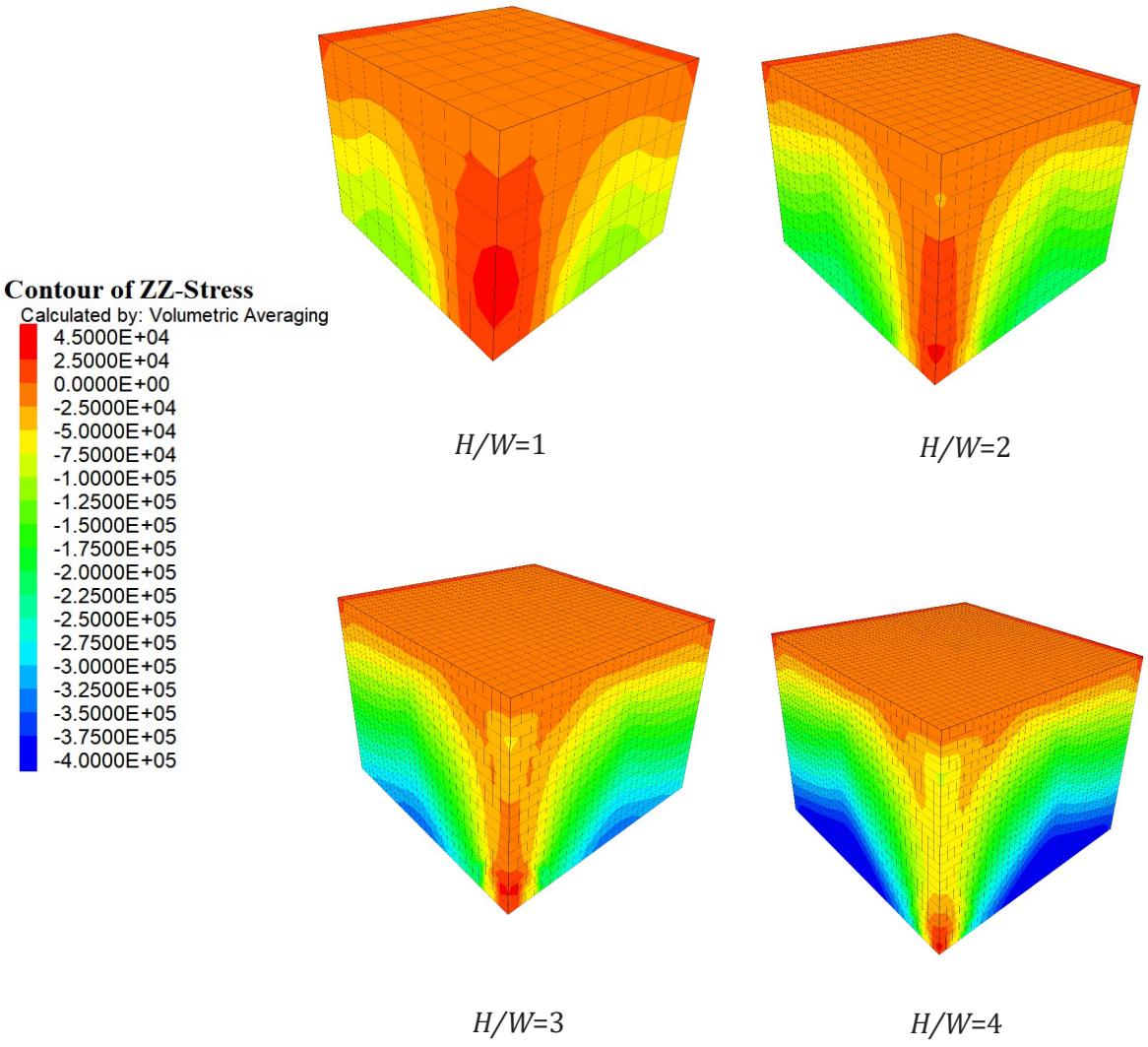

Figure 7. 9 Contour of vertical stress for H/W=1 to 4 (L/W=1)

This transition in vertical stress was reported earlier by Finn (1963). While the edges of the trapdoor experience compression stress, the tensile stress develops on

the soil above the trapdoor. The same observation can be made from the vertical stress plots in figure 7.9 as well as the velocity plots in figures 7.10 and 7.11. Note that for local failures, the vertical distance between the trapdoor and the edge of collapse zone (where there is a transition of stress sign from positive to negative) is an important parameter to be used in the evaluation of the volume of the collapse zone as well as the intensity of the soil arching effect.

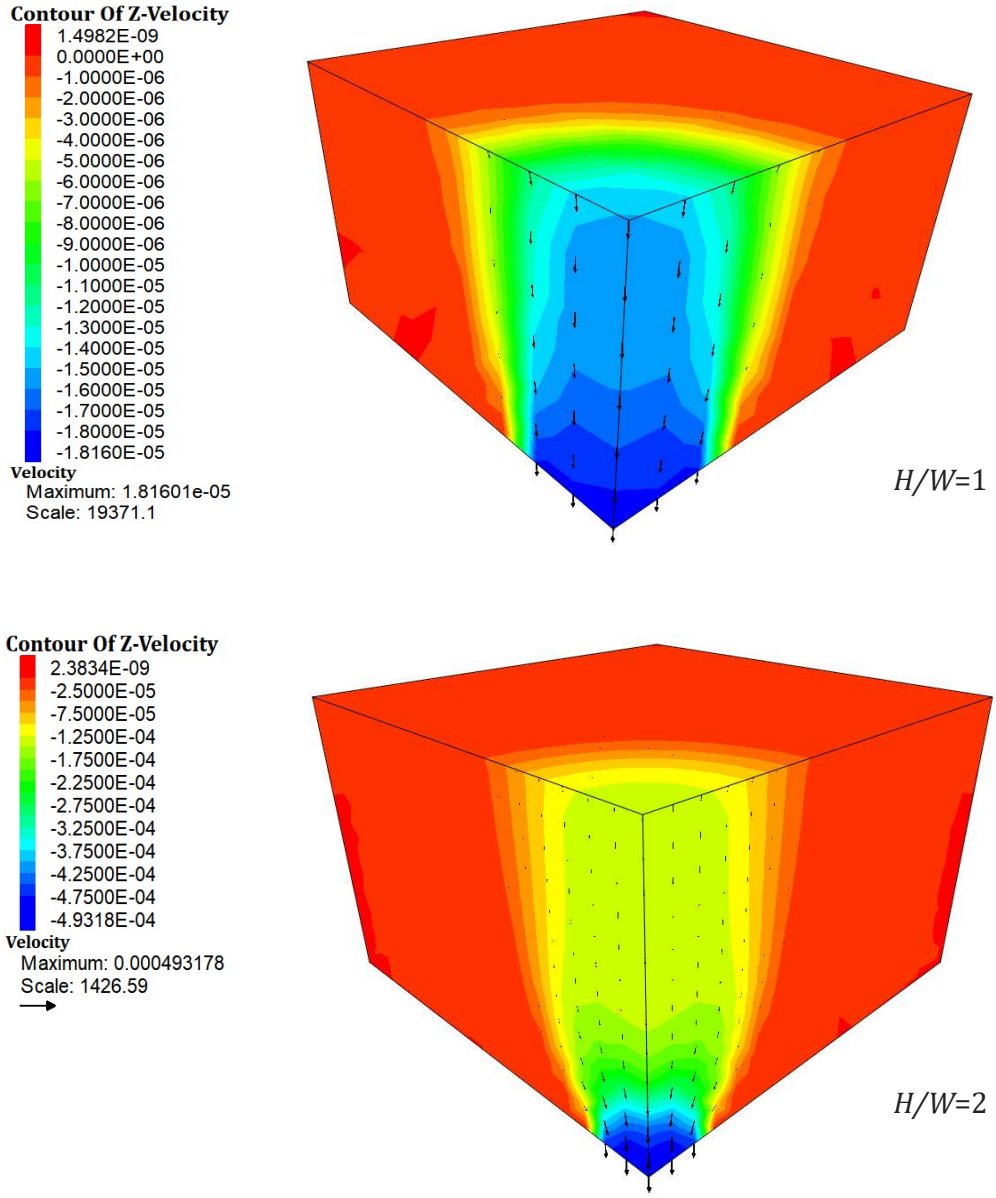

Figure 7. 10 Velocity vector and z velocity contour for H/W=1 and 2 (L/W=1)

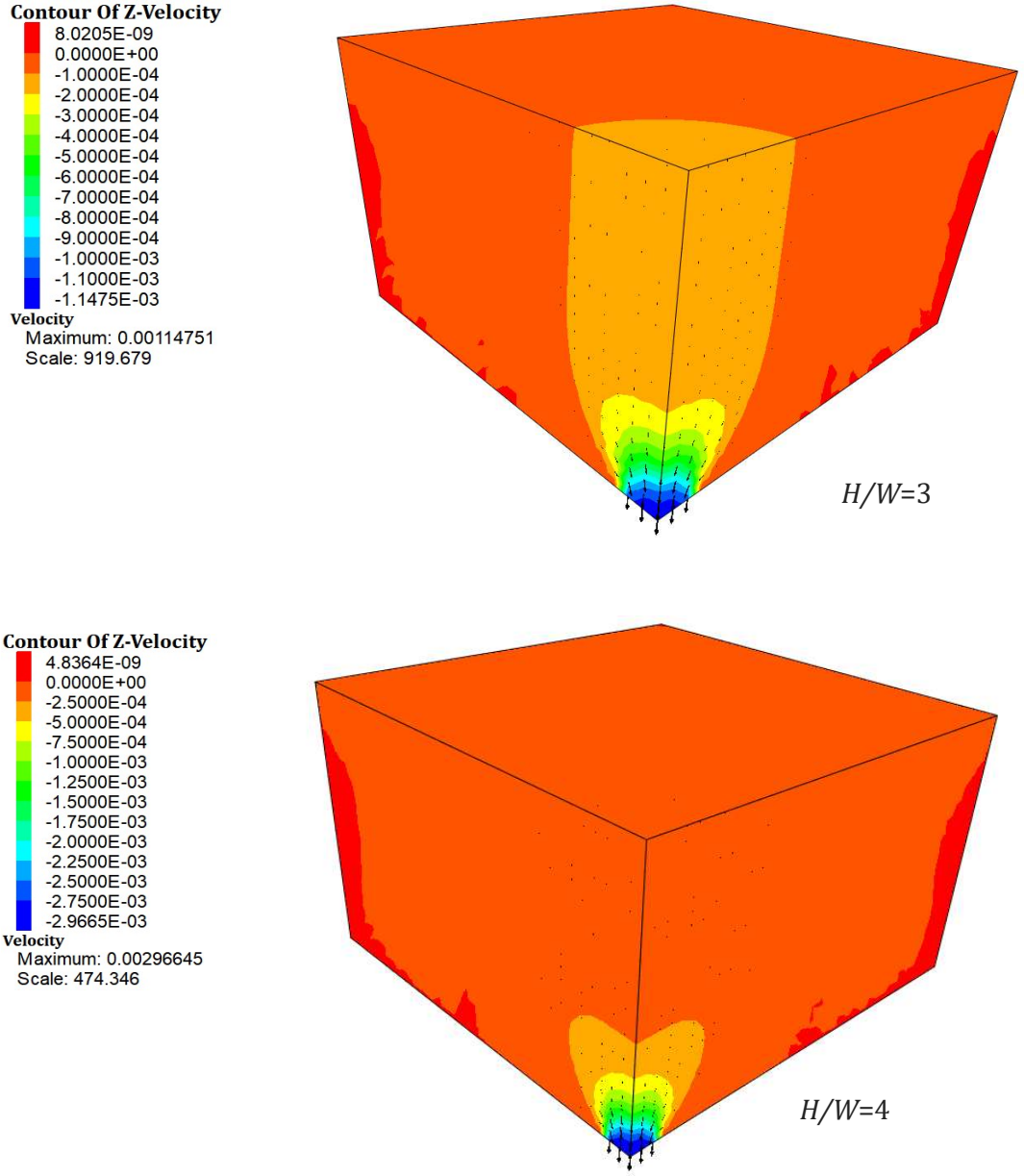

Figure 7. 11 Velocity vector and z velocity contour for H/W=3 and 4 (L/W=1)

Intrestingly in figure 7.10, for H/W= 1 and 2, the movment of soil particles are uniformly distributed across the depth while in figure 7.11, for H/W = 3 and 4, the soil movements are confined to the area at a certain depth above the trapdoor. The immobilisation of the soil under compression (due to self-weight and surcharge load) introduces supporting soil arches, therefore, resulting in the formation of a cavity as the soil starts to fall downward. For shallow cases such as H/W = 1 and 2,

the vertical distance from the soil surface to the trapdoor location is not large enough to allow the development of soil arching, and therefore the failure mechanism would extend to the ground surface.

7.4.4. Practical examples

The practicality of design charts and equations can be best demonstrated through a number of examples. For design purposes, the stability design charts can be used to estimate the depth ratio (H/W), critical stability number (N_c) and factor of safety (FoS). They can also be used to determine the safe working pressure to maintain soil stability.

Example 1- Determine the FoS

Determine the FoS for the problem with the following given parameters.

S_u = 108 kPa, σ_s= 60 kPa, γ = 20 kN/m^3, σ_t= 0 kPa, H= 6 m, L=6 m and W = 6 m.

1. Using H/W = 1 and L/W = 1, equation 7.9 gives a FoS of 2.86.
2. Using H/W = 1 and L/W = 1, table 7.6 gives a N_c value of 4.78. The design value of $N = (\sigma_s + \gamma H - \sigma_t)/S_u$ = 1.67. Therefore, $FoS = N_c/N$ = 2.86

Example 2 –Estimate the surface failure extent (E)

A review of Interferometric Synthetic Aperture Radar ($InSAR$) images discovered the surface ground subsidence in a populated residential area. Further inspection by using the Ground Penetration Radar (GPR) revealed that a sinkhole exists in the area. The geotechnical engineer has been assigned to estimate the possible ground surface failure extent should a sudden collapse occurs. The following parameters are provided:

H = 15 m, L= 6 m, W = 6 m, S_u = 30 kPa and γ = 18 kN/m^3.

1. Using equation 7.10, the failure surface extent would be E/W= 1.995. Given W = 6 m, E is estimated to be 12 m.
2. The actual observation of z velocity plot shows that the deformed surface is approximately E = 11 m. Converting this value into dimensionless form, E/W=1.83.

7.5. Conclusion

This study has investigated the soil stability and ground surface failure extent of 3D trapdoor problems in homogeneous undrained soil. Numerical results of *FoS* for a wide range of depth ratios (*H/W*) and opening ratios (*L/W*) were obtained by utilising the *SSRM* in *FDM*. The current 3D *FoS* solutions were used to estimate Broms & Bennermark's critical stability number (N_c) for various trapdoor problems. The following conclusions can be drawn from the present study.

- The dimensionless design charts, tables, and equations are useful for practical engineers. Examples have also been given to illustrate the usefulness of such charts.
- For each depth ratio (*H/W*), there exists a unique critical stability number (N_c). The comparison of critical stability numbers (N_c) between 3D and 2D showed that the 3D solutions (*L/W*=1) are almost twice as large as those in 2D plane strain solutions (*L/W*=∞).
- The results of failure extent investigations have shown that the failure extent ratio (*E/W*) increases linearly with the depth ratio (*H/W*) until a certain depth ratio where a transformation of general failures to local failures occur. In this study, the failure surface does not extend to the ground surface when *H/W* >3, suggesting a development of strong soil arching support in deep cases, and therefore resulting in local failure mechanisms.

The 3D study contributed to our understanding by offering valuable insight into the sinkhole failure mechanism and arching development. It will be of broad use to decision makers as it lays the ground for a scientist to combine this study with available Geophysics tools such as Interferometric Synthetic Aperture Radar (*InSAR*), Electrical Resistivity Imaging (*ERI*) and Ground Penetration Radar (*GPR*) to establish an early warning system. More research is required to examine the vertical distance between the trapdoor opening and the edge of collapse zone in deep cases with local failure mechanisms. In addition, the sinkhole propagation investigation maybe of greatest interest to researchers in future studies.

8. CONCLUSION

8.1. Summary

The thesis has successfully investigated the soil stability and its associated ground surface failure extent of an undrained cohesive cover over a collapsible sinkhole. The shear strength reduction method (*SSRM*) was utilised to explore two- and three-dimensional failure mechanisms of a horizontal trapdoor by using the finite difference programs *FLAC* 2D and *FLA*C 3D.

The study began with the idealised 2D greenfield condition, It was followed by a realistic 3D model to investigate the actual effect of soil arching. To consider both the surcharge and the supporting pressures, the study was further extended to the use of Broms and Bennermark's stability number to investigate both 2D and 3D problems. Stability results were presented in dimensionless forms for design purpose. Moreover, the velocity plots were used to determine the overall failure mechanism and the surface failure extent. The results through out of this study showed a good agreement with those published and those obtained by finite element limit analysis. Several practical examples are provided to demonstrate the use of design charts and tables by practical designers.

8.2. Key conclusions of Chapter 4

The following main conclusions were drawn based on the two-dimensional analysis of undrained sinkhole under greenfield condition.

- To assist practical designers, numerical results were presented in the form of the factor of safety that is a function of the depth ratio and the shear strength ratio. These results, presented following Taylor's slope stability design charts, compared favourably with the rigorous upper and lower bound solutions. Practical examples were used to demonstrate how to use the design charts and equations.
- It was found that the *FoS* value decreases nonlinearly as the depth ratio (*H/W*) increases, suggesting that none or very little arching support developed for the current study of homogeneous cohesive soil. The study of non-zero plastic shear strain rates and velocity vectors also suggested that soil arching has minimal effect in the current plane strain study of undrained clay.
- The study showed that the failure extent ratio increases linearly with the depth ratio. It was concluded that the total surface failure extent ratio (*E/W*) is approximately 1.35 times larger than the depth ratio (*H/W*).

8.3. Key conclusions of Chapter 5

The following main conclusions were drawn based on the three-dimensional analysis of undrained sinkhole under greenfield condition.

- To assist practical designers, numerical results were presented in the form of factor of safety that is a function of the depth ratio and the shear strength ratio. Examples were used to demonstrate how to use the design charts and equations in practice.
- The investigation of *FoS* suggested that the 3D square opening results are almost twice larger than those in 2D plain strain.
- The results showed that the failure extent ratio (*E/W*) increases linearly when the depth ratio (*H/W*) increases. The study of surface failure extent indicated a transformation from a perfect circle to an ellipse as the value of

width ratio L/W increases; i.e. changing the opening size from a square to a wide rectangle.

- It was noted that strong soil arching was developed in deep trapdoors, and the corresponding failure mechanisms do not propagate to the ground surface. Local failure was observed for these deep cases.

8.4. Key conclusions of Chapter 6

The following main conclusions were drawn based on the two-dimensional analysis of undrained sinkhole using Broms and Bennermark's stability number.

- The numerical results suggest that the FoS increases as the stability number (N) decreases. The FoS reaches toward the infinity when the stability N approaches zero. The relationship between FoS and N shows an asymptote which yields a unique critical stability number (N_c) for every depth ratio (H/W).
- The study on the ground failure surface extent concluded that the failure extent ratio (E/W) increases linearly as the depth ratio (H/W) increase. The failure angle (θ) measured from the centre of the opening (W) to the edge of failure surface is found to be 55 degrees for all depth ratios (H/W).
- Numerical results were used to produce equations and design contour map, and examples were provided to illustrate the practical use of the charts and equations.

8.5. Key conclusions of Chapter 7

The following main conclusions were drawn based on the three-dimensional analysis of undrained sinkhole using Broms and Bennermark's stability number.

- The dimensionless design charts, tables, and equations are useful for practical engineers. Examples have also been given to illustrate the usefulness of such charts.
- For each depth ratio (H/W), there exists a unique critical stability number (N_c). The comparison of critical stability numbers (N_c) between 3D and 2D

showed that the 3D solutions (L/W=1) are almost twice as large as those in 2D plane strain solutions (L/W=∞).

- The results of failure extent investigations have shown that the failure extent ratio (E/W) increases linearly with the depth ratio (H/W) until a certain depth ratio where a transformation of general failures to local failures occur. In this study, the failure surface does not extend to the ground surface when H/W >3, suggesting a development of strong soil arching support in deep cases, and therefore resulting in local failure mechanisms.

8.6. Recommendation

When it comes to the underground study, the complexity of the problem is very high. This is due to the number of the variables involved in the problem. This is especially true with the sinkhole problems, where the physical properties of the materials, the geology of the area, the loads such as building and traffic, and the underground structures such as pipelines are different for each problem. Note that sinkhole failure might occurs any time without sign and warning. This means that the design and equation of trapdoor stability and failure extent are much more challenging to use in practice. Having said that, the well-defined parametric study of the trapdoor are still important and useful in the evaluation of the stability and ground surface failure extent.

Based on the current investigation of the trapdoor stability, some important points have been identified for future study.

- The underground cavity grows over time, an investigation into 3D finite difference models considering the sinkhole size propagation mechanism and the associate prediction of the ground subside geometry would be useful.
- An investigation into the stability of other opening shapes, which better represents the internal dissolution of the cavity such as spherical or dome shape, would provide better understanding of the sinkhole failure problem.
- The thesis suggested that local failures would only occur for depth ratios greater the 3. A detailed investigation into the critical depth which transits the general failure into the local failure mechanism would be a promising future work.

- A comprehensive investigation into the failure zone for deep cases would be beneficial to mining industry in the determination of local collapse zone.

More broadly, to simulate more realistic situation, further studies need to be carried out to investigate the failure mechanism in increasing soil strength in homogeneous and layered soils.

REFERENCES

Abbasi, B, Russell, D & Taghavi, R 2013, 'FLAC 3D mesh and zone quality'. Proceedings of the 3rd International FLAC/DEM Symposium, China. http://www.itasca.com.au/proceedings-of-the-3rd-international-flacdem-symposium%E2%80%8F

Abdulla, WA & Goodings, DJ 1996, 'Modeling of sinkholes in weakly cemented sand', Journal of Geotechnical Engineering, vol. 122, no. 12, pp. 998-1005.

Alpha Geofisica 2017, 'Equipamentos para pesquisa Geofísica e Mineração', Brazil, viewed 10th September 2018, http://www.alphageofisica.com.br/gssi/gpr.htm.

Antes, H 2010, 'A short course on boundary element methods', Institute for Angewandte Mechanik, Technische Universität Braunschweig, Braunschweig, Germany.

Atkinson, J & Cairncross, AM 1973, 'Collapse of a shallow tunnel in a Mohr–Coulomb material', In Proceedings of the Symposium on the Role of Plasticity in Soil Mechanics, Cambridge, UK, 13–15 September 1973. Edited by A.C. Palmer. Cambridge University Engineering Department, University of Cambridge, Cambridge, UK. pp. 202–206.

Atkinson, J & Potts, D 1977, 'Stability of a shallow circular tunnel in cohesionless soil', Geotechnique, vol. 27, no. 2, pp. 203-15.

Attewell, PB, Yeates, J & Selby, AR 1986, 'Soil movements induced by tunnelling and their effects on pipelines and structures', Blackie and Son Ltd., London.

Augarde, CE, Lyamin, AV & Sloan, SW 2003, 'Prediction of undrained sinkhole collapse', Journal of Geotechnical and Geoenvironmental Engineering, vol. 129, no. 3, pp. 197-205.

Baker, R 2003, 'A second look at Taylor's stability chart', Journal of Geotechnical and Geoenvironmental Engineering, vol. 129, no. 12, pp. 1102-8.

Broms, BB & Bennermark, H 1967, 'Stability of clay at vertical openings', Journal of Soil Mechanics & Foundations Division, vol. 93, no. 1, pp. 71-94.

Benson, AK 1995, 'Applications of ground penetrating radar in assessing some geological hazards: examples of groundwater contamination, faults, cavities', Journal of Applied Geophysics, vol. 33, no. 1-3, pp. 177-93.

Buis, A & Harrington, J.D 2014, 'That Sinking Feeling'. viewed 9th August 2017, https://www.jpl.nasa.gov/news/news.php?feature=4071.

Chang,L, Hanseen. RF 2014, 'Detection of cavity migration and sinkhole risk using radar interferometric time series', Remote Sending Environment, vol.14, pp. 56-64.

Chelapati, CV 1964, 'Arching in soil due to the deflection of a rigid horizontal strip', in Proceeding of Symposium on Soil Structural Interaction, Arizona, US, pp.356-377.

Clough, GW & Schmidt, B 1981, 'Design and performance of excavations and tunnels in soft clay', Developments in Geotechnical Engineering, volume 20, 1981, Pages 567-634 vol 20, pp. 567-634

Chrzanowski, A, Szostak-Chrzanowski, A & Forrester, D 1998, '100 Years of Ground Subsidence Studies', in 100th General Meeting of CIM, Montreal, May, pp. 3-7.

Craig, W 1990, 'Collapse of cohesive overburden following removal of support', Canadian Geotechnical Journal, vol. 27, no. 3, pp. 355-64.

Davis, E, Gunn, M, Mair, R & Seneviratine, H 1980, 'The stability of shallow tunnels and underground openings in cohesive material', Geotechnique, vol. 30, no. 4, pp. 397-416.

Davis, E 1968, 'Theories of plasticity and the failure of soil masses, in soil mechanics-selected topics', Ch. 6, Ed. I. K. Lee. London, Butterworths.

Dhatt, G, LefranÃ, E & Touzot, G 2012, Finite element method, John Wiley & Sons.

Dimmock, PS & Mair, RJ 2007, 'Estimating volume loss for open-face tunnels in London Clay', Proceedings of the Institution of Civil Engineers-Geotechnical Engineering, vol. 160, no. 1, pp. 13-22.

Drucker, D, Prager, W & Greenberg, H 1952, 'Extended limit design theorems for continuous media', Quarterly of Applied Mathematics, vol. 9, no. 4, pp. 381-9.

Drumm, EC, Aktürk, Ö, Akgün, H & Tutluoğlu, L 2009, 'Stability charts for the collapse of residual soil in karst', Journal of Geotechnical and Geoenvironmental Engineering, vol. 135, no. 7, pp. 925-31.

Drumm, E, Kane, W & Yoon, C 1990, 'Application of limit plasticity to the stability of sinkholes', Engineering Geology, vol. 29, no. 3, pp. 213-25.

Fattah, MY, Shlash, KT & Salim, NM 2013, 'Prediction of settlement trough induced by tunneling in cohesive ground', Acta Geotechnica, vol. 8, no. 2, pp. 167-79.

Finn, W 1963, 'Boundary Values Problems of Soil Mechanics', Journal of the Soil Mechanics and Foundations Division, vol. 89, no. 5, pp. 39-72.

FLAC 3D 2002, Fast Lagrangian Analysis of Continua, Itasca Consulting Group, Minneapolis, Minnesota, USA.

FLAC 2D 2003, Fast Lagrangian Analysis of Continua, Itasca Consulting Group, Minneapolis, Minnesota, USA.

Ford, D & Williams, PD 2013, Karst hydrogeology and geomorphology, John Wiley & Sons.

Fraldi, M & Guarracino, F 2009, 'Limit analysis of collapse mechanisms in cavities and tunnels according to the Hoek–Brown failure criterion', International Journal of Rock Mechanics and Mining Sciences, vol. 46, no. 4, pp. 665-73.

Geological survey 2018, 'Karst landforms', Department of Communication Climate Action and Environment, Ireland, viewed 5th September 2018, https://www.gsi.ie/en-ie/programmes-and-projects/groundwater/activities/understanding-irish-karst/Pages/default.aspx

Geoscience 2018, 'Interferometric Synthetic Aperture Rada', Geoscience Australia, Australia, viewed 26th August 2018, http://www.ga.gov.au/scientific-topics/positioning-navigation/geodesy/geodetic-techniques/interferometric-synthetic-aperture-radar.

Griffiths, D & Lane, P 1999, 'Slope stability analysis by finite elements', Geotechnique, vol. 49, no. 3, pp. 387-403.

Griffin, S & Pippett, T 2002, 'Ground penetrating radar', Geophysical and Remote Sensing Methods for Regolith Exploration, CRC LEME Open File Report, vol. 144, pp. 80-9.

Gunn, M.J 1980, 'Limit analysis of undrained stability problems using a very small computer'. University of Cambridge, Department of Engineering.

Gutiérrez, F, Parise, M, De Waele, J & Jourde, H 2014, 'A review on natural and human-induced geohazards and impacts in karst.' Earth-Science Reviews, Vol 138, pp.61-88.

Guarino, PM, Santo, A, Forte, G, De Falco, M & Niceforo, DMA 2018, 'Analysis of a database for anthropogenic sinkhole triggering and zonation in the Naples hinterland (Southern Italy)', Natural Hazards, vol. 91, no. 1, pp. 173-92.

Guan, K, Zhu, W, Niu, L & Wang, Q 2017, 'Three-dimensional upper bound limit analysis of supported cavity roof with arbitrary profile in Hoek-Brown rock mass', Tunnelling and Underground Space Technology, vol. 69, pp. 147-54.

Heidari, M, Khanlari, G, Beydokhti, AT & Momeni, A 2011, 'The formation of cover collapse sinkholes in North of Hamedan, Iran', Geomorphology, vol. 132, no. 3-4, pp. 76-86.

Holzer, TL 1984, 'Ground failure induced by ground-water withdrawal from unconsolidated sediment', Reviews in Engineering Geology, vol. 6, pp. 67-105.

Ibrahim, E, Soubra, A-H, Mollon, G, Raphael, W, Dias, D & Reda, A 2015, 'Three-dimensional face stability analysis of pressurized tunnels driven in a multilayered purely frictional medium', Tunnelling and Underground Space Technology, vol. 49, pp. 18-34.

InSar (2017,'Interferometric Synthetic Aperture Radar', Geoscience Australia, Australia, viewed 4th July 2017, http://www.ga.gov.au/scientific-topics/positioning-navigation/geodesy/geodetic-techniques/interferometric-synthetic-aperture-radar.

Intrieri, E, Gigli, G, Nocentini, M, Lombardi, L, Mugnai, F, Fidolini, F & Casagli, N 2015, 'Sinkhole monitoring and early warning: an experimental and successful GB-InSAR application', Geomorphology, vol. 241, pp. 304-14.

ITASCA 2013, FLAC Fast Lagrangian Analysis of Continua, Itasca Consulting Group, Minneapolis, Minnesota, USA.

Jacobsz, S 2016, 'Trapdoor experiments studying cavity propagation', Proceedings of the 1st Southern African Geotechnical Conference, Durban, South Africa, 18-19 October 2016, CRC Press, pp. 159-65.

Jones, CE & Blom, R 2015, 'Pre-event and post-formation ground movment associated with the Bayou Corne sinkhole', Proceedings of the 14th Multidisciplinary Conference on Sinkholes and the Engineering and Environmental Impacts of Karst, pp.415-422.

Keawsawasvong, S & Ukritchon, B 2017, 'Undrained stability of an active planar trapdoor in non-homogeneous clays with a linear increase of strength with depth', Computers and Geotechnics, vol. 81, pp. 284-93.

Koutsabeloulis, N & Griffiths, D 1989, 'Numerical modelling of the trapdoor problem', Geotechnique, vol. 39, no. 1, pp. 77-89.

Krabbenhoft, K, Lyamin, AV, Hjiaj, M & Sloan, SW 2005, 'A new discontinuous upper bound limit analysis formulation', International Journal for Numerical Methods in Engineering, vol. 63, no. 7, pp. 1069-88.

Leca, E & Dormieux, L 1990, 'Upper and lower bound solutions for the face stability of shallow circular tunnels in frictional material', Geotechnique, vol. 40, no. 4, pp. 581-606.

Lei, MG, Jiang, X 2005, 'Experimental Study of Physical Models for Sinkhole Collapses in Wuhan, China', In Proceeding of 10th Multidisciplinary Conference on Sinkholes and the Engineering and Environmental Impacts of Karst, pp. 91-102.

Levy, M 2016 'Giant sinkhole in Fukuoka, Japan, repaired within days, Sydney, Australia, viewed 1st July 2017, http://www.smh.com.au/world/giant-sinkhole-in-fukuoka-japan-repaired-within-days-20161115-gsq5my.html.

Lyamin, A & Sloan, S 2002a, 'Lower bound limit analysis using non-linear programming', International Journal for Numerical Methods in Engineering, vol. 55, no. 5, pp. 573-611.

Lyamin, AV & Sloan, S 2002b, 'Upper bound limit analysis using linear finite elements and non-linear programming', International Journal for Numerical and Analytical Methods in Geomechanics, vol. 26, no. 2, pp. 181-216.

Mair, R 1979, 'Centrifuge modelling of tunnel construction in soft clay', Ph. D Thesis, University of Cambridge.

Mair, R 1983, 'Geotechnical aspects of soft ground tunnelling', Proceedings of International Symposium on Construction Problems in Soft Soils, Nanyang Technological Institute, Singapore.

Mansour, Z & Kalantari, B 2011, 'Traditional Methods vs. Finite Difference Method for Computing Safety Factors of Slope Stability', Electronic Journal of Geotechnical Engineering, vol. 16, pp. 1119–1130.

Martos, F 1958, 'Concerning an approximate equation of the subsidence trough and its time factors', in International Strata Control Congress, Leipzig, pp. 191-205.

Marti, J & Cundall, P 1982, 'Mixed discretization procedure for accurate modelling of plastic collapse', International Journal for Numerical and Analytical Methods in Geomechanics, vol. 6, no. 1, pp. 129-39.

Martin, C 2009, 'Undrained collapse of a shallow plane-strain trapdoor', Geotechnique, vol. 59, no. 10, pp. 855-63.

Matsui, T & San, K-C 1992, 'Finite element slope stability analysis by shear strength reduction technique', Soils and Foundations, vol. 32, no. 1, pp. 59-70.

McCarthy, DF 2002, 'Essentials of soil mechanics and foundations', Sixth edition, Prentice Hall, New Jersey, USA.

Michalowski, RL 2002, 'Stability charts for uniform slopes', Journal of Geotechnical and Geoenvironmental Engineering, vol. 128, no. 4, pp. 351-5.

Mollon, G, Dias, D & Soubra, A-H 2009, 'Face stability analysis of circular tunnels driven by a pressurized shield', Journal of Geotechnical and Geoenvironmental Engineering, vol. 136, no. 1, pp. 215-29.

Mühlhaus, HB 1985, 'Lower bound solutions for circular tunnels in two and three dimensions', Rock Mechanics and Rock Engineering, vol. 18, no. 1, pp. 37-52.

Murayama, S 1969, 'Model experiments on land subsidence', in proceedings of the Tokyo Symposium on Land Subsidence, vol.2, pp. 431-49.

Nagtegaal, JC, Parks, DM & Rice, J 1974, 'On numerically accurate finite element solutions in the fully plastic range', Computer Methods in Applied Mechanics and Engineering, vol. 4, no. 2, pp. 153-77.

Narasimhan, T & Witherspoon, P 1976, 'An integrated finite difference method for analyzing fluid flow in porous media', Water Resources Research, vol. 12, no. 1, pp. 57-64.

Naylor, D 1982, 'Finite elements and slope stability', Numerical Methods in Geomechanics: Proceedings of the NATO Advanced Study Institute, Portugal, vol. 92, p. 229-44.

Newton, J 1976, 'Induced sinkholes-a continuing problem along Alabama highways', in Proceedings of the Anaheim Symposium. Alabama, US, pp.453-463.

Oh, D, Kong, S, Lee, D, Yoo, Y & Lee, Y 2015, 'Effects of reinforced pseudo-plastic backfill on the behavior of ground around cavity developed due to sewer leakage', Journal of the Korean Geoenvironmental Society, vol. 16, no. 12, pp. 13-22.

Olick, D 2013, 'Sinkhole Damage Insurance Claims Are Increasing Significantly In Florida', Business Insider, viewed 19th June 2017, http://www.businessinsider.com/sinkhole-damage-insurance-claims-are-increasing-significantly-in-florida-2013-8/?r=AU&IR=T.

O'reilly, M & New, B 1982, 'Settlements above tunnels in the United Kingdom-their magnitude and prediction', Proc. Tunnelling '82. London (UK), Institute of Mining and Metallurgy, p.p 310–29.

OptumG2 2018, Optum Computational Engineering, https://optumce.com/

Plaxis, B.V. 2011, PLAXIS 2D Finite element software, https://www.plaxis.com

Point, H 2017, 'Umpherston Sinkhole', viewed 4th July 2018, http://www.ga.gov.au/scientific-topics/positioning-navigation/geodesy/geodetic-techniques/interferometric-synthetic-aperture-radar.

Poyiadji, E, Nikolaou, N & Karmis, P 2010, 'Ground failure due to gypsum dissolution', Bulletin of the Geological Society of Greece, vol. 43, no. 3, pp. 1393-1405.

Peck, RB 1969, 'Deep excavations and tunnelling in soft ground', Proc. 7th ICSMFE, 1969, pp. 225-90.

Satarugsa, P 2011, 'The Lessons Learnt from Geophysical Investigation of Sinkholes in Rock Salt in Thailand ', In proceeding of International Conference on Geology, Geotechnology and Mineral Resources of Indochina, Khon Kaen, Thailand, pp.445-455.

Sheorey, P, Loui, J, Singh, K & Singh, SK 2000, 'Ground subsidence observations and a modified influence function method for complete subsidence prediction', International Journal of Rock Mechanics and Mining Sciences, vol. 37, no. 5, pp. 801-18.

Shen, S-L, Xu, Y-S & Hong, Z-S 2006, 'Estimation of land subsidence based on groundwater flow model', Marine Georesources and Geotechnology, vol. 24, no. 2, pp. 149-67.

Shiau, J, Sams, M & Lamb, B 2016, 'Introducing advanced topics in geotechnical engineering teaching–Tunnel modelling', International Journal of Geomate, vol. 10, no. 1, pp. 1698-1705.

Shiau, J, Lamb, B & Sams, M 2016, 'The use of sinkhole models in advanced geotechnical engineering teaching', International Journal of Geomate, vol. 10, no. 2, pp. 1718-24.

Shiau, J, Lamb, B, Sams, M & Lobwein, J 2017, 'Stability charts for unsupported circular tunnels in cohesive soils', International Journal of Geomate, 13 (39), 95-102.

Shiau, J & Sams, M 2017, 'Estimation of tunneling induced ground settlement using pressure relaxation method', International Journal of Geomate, 13 (39), 132-139.

Shiau, J, Hassan, MM & Hossein, Z 2018, 'Stability charts for unsupported square tunnels in homogeneous undrained clay', International Journal of Geomate, vol. 15, no. 48, pp. 195-201.

Shiau, J , Sams, M , Al-Asadi, F & Hassan, MM 2018, 'Stability charts for unsupported plane strain tunnel headings in homogeneous undrained clay', International Journal of Geomate, vol. 14, no. 41, pp. 19-26.

Shiau, J & Al-Asadi, F 2018, 'Revisiting Broms and Bennermarks' original stability number for tunnel headings'. Geotechnique Letters, vol.8, no 4, pp. 310-315.

Shiau, J & Sams, M 2019, 'Relating volume loss and greenfield settlement'. Tunnelling and Underground Space Technology, vol.83. pp. 145-152.

Shiau, J, Asadi, F & Hassan, MM 2019, 'Finite element limit analysis of undrained trapdoor stability', International Journal of Geomechanics (to submit).

Sloan, S, Assadi, A, Purushothaman, N 1990, 'Undrained stability of a trapdoor', Geotechnique, vol. 40, no. 1, pp. 45-62.

Sloan, S 1988, 'Lower bound limit analysis using finite elements and linear programming', International Journal for Numerical and Analytical Methods in Geomechanics, vol. 12, no. 1, pp. 61-77.

Sloan, S 1989, 'Upper bound limit analysis using finite elements and linear programming', International Journal for Numerical and Analytical Methods in Geomechanics, vol. 13, no. 3, pp. 263-82.

Sloan, S 2013, 'Geotechnical stability analysis', Geotechnique, vol. 63, no. 7, p. 531.

Sowers, GF 1996, 'Building on sinkholes: design and construction of foundations in karst terrain', American Society of Civil Engineers, New York.

Subrin, D & Wong, H 2002, 'Tunnel face stability in frictional material: a new 3D failure mechanism', Comptes Rendus Mecanique, vol. 330, no. 7, pp. 513-9.

Taylor, DW 1937, 'Stability of earth slopes', Journal of Boston Society Civil Engineers, vol. 24, no. 3, pp. 197-247.

TEC 2007, 'Impacts of longwall coal mining on the environment in New South Wales, Total Environment Centre', Sydney, Australia, viewed 10th December 2017, https://d3n8a8pro7vhmx.cloudfront.net/boomerangalliance/pages/606/attachments/original/1486609983/tec_report_final.pdf?1486609983.

Terzaghi, K 1936, 'Stress distribution in dry and saturated sand above a yielding trap-door', in Proceedings of The International Conference of Soil Mechanic, Harvard university Press, Cambridge , vol. 1, no. 4, pp. 307-311.

Tharp, T 1999, 'Mechanics of upward propagation of cover-collapse sinkholes'. Engineering Geology, Vol 52, no 1-2, pp. 23-33.

Tharp, T 2002, 'Poroelastic analysis of cover-collapse sinkhole formation by piezometric surface drawdown'. Environmental Geology, Vol 42, no. 5, pp.447-456.

Tharp, T 2003, 'Cover-collapse sinkhole formation and soil plasticity', Proceedings of the Ninth Multidisciplinary Conference of Sinkholes and the Engineering and Environmental Impacts of Karst, Alabama, United States, pp. 110-23.

Thongprapha, T, Fuenkajorn, K & Daemen, J.K 2015,' Study of surface subsidence above an underground opening using a trap door apparatus'. Tunnelling and Underground Space Technology, Vol 46, pp.94-103.

Tuckwell, G 2017,A references for geophysical techniques and applications, RSK Group , Hertfordshire, UK, viewed 10th July 2018, http://www.environmental-geophysics.co.uk/documentation/handbook/handbook.pdf.

Ugai, K & Leshchinsky, D 1995, 'Three-dimensional limit equilibrium and finite element analyses: a comparison of results', Soils and Foundations, vol. 35, no. 4, pp. 1-7.

Ural, O 1973, 'Finite Element Method: Basic Concepts and Applications', Intext Educational Publishers, New York.

USGS 2018a, 'How much does sinkhole damage cost each year in the United States?', US Department of The Interior , US, viewed 12th September 2018, https://www.usgs.gov/faqs/how-much-does-sinkhole-damage-cost-each-year-united-states?qt-news_science_products=3#qt-news_science_products.

USGS 2018b, 'Sinkholes', US Department of the Interior, US, viewed 8th August 2018, https://water.usgs.gov/edu/sinkholes.html.

Van Schoor, M 2002, 'Detection of sinkholes using 2D electrical resistivity imaging', Journal of Applied Geophysics, vol. 50, no. 4, pp. 393-9.

Vardoulakis, I, Graf, B & Gudehus, G 1981, 'Trap-door problem with dry sand: A statical approach based upon model test kinematics', International Journal for Numerical and Analytical Methods in Geomechanics, vol. 5, no. 1, pp. 57-78.

Vaziri, HH, Jalali, JS & Islam, R 2001, 'An analytical model for stability analysis of rock layers over a circular opening', International Journal of Solids and Structures, vol. 38, no. 21, pp. 3735-57.

Vermeer, P, Bonnier, P & Möller, S 2002, 'On a smart use of 3D-FEM in tunnelling', in Proceeding of Eighth International Symposium on Numerical Models in Geomechanics, pp. 361-6.

Vermeer, P, Möller, S & Ruse, N 2003, 'On the application of numerical analysis in tunnelling', 12th Asian Regional Conference on Soil Mechanics and Geotechnical Engineering (12 ARC), Singapore, pp. 4-8.

Vermeer, PA, Ruse, N & Marcher, T 2002, 'Tunnel heading stability in drained ground', Felsbau, vol. 20, no. 6, pp. 8-18.

Wang, T, Lv, Q, Zhou, Y, Li, Y, Jiang, C & Yang, F 2011, 'Analysis on deformation and failure of surface borehole and casing due to coal extraction', in The Second International FLAC/DEM Symposium on Numerical Modeling, 14–16 February 2011, Melborne, Victoria, Australia.

Wilson, W.L & Garman. M 2016,'Identification and delineation of sinkhole collapse hazards in florida ground penetrating radar and electrical resistivity imaging', Subsurface Evaluations, Inc., Florida, USA.

Yang, MZ & Drumm, EC 2002, 'Stability evaluation for the siting of municipal landfills in karst', Engineering Geology, vol. 65, no. 2-3, pp. 185-95.

Yang, X & Huang, F 2013, 'Three-dimensional failure mechanism of a rectangular cavity in a Hoek–Brown rock medium', International Journal of Rock Mechanics and Mining Sciences, no. 61, pp. 189-95.

Zheng, Y-R, Zhao, S-Y, Kong, W-X & Deng, C-J 2005, 'Geotechnical engineering limit analysis using finite element method', Yantu Lixue (Rock Soil Mech.), vol. 26, no. 1, pp. 163-8.

Zienkiewicz, O, Humpheson, C & Lewis, R 1975, 'Associated and non-associated visco-plasticity in soil mechanics' , Geotechnique, vol. 25, no. 4, pp. 671-89.